

INFORMATION TO USERS

This manuscript has been reproduced from the microfilm master. UMI films the text directly from the original or copy submitted. Thus, some thesis and dissertation copies are in typewriter face, while others may be from any type of computer printer.

The quality of this reproduction is dependent upon the quality of the copy submitted. Broken or indistinct print, colored or poor quality illustrations and photographs, print bleedthrough, substandard margins, and improper alignment can adversely affect reproduction.

In the unlikely event that the author did not send UMI a complete manuscript and there are missing pages, these will be noted. Also, if unauthorized copyright material had to be removed, a note will indicate the deletion.

Oversize materials (e.g., maps, drawings, charts) are reproduced by sectioning the original, beginning at the upper left-hand corner and continuing from left to right in equal sections with small overlaps. Each original is also photographed in one exposure and is included in reduced form at the back of the book.

Photographs included in the original manuscript have been reproduced xerographically in this copy. Higher quality 6" x 9" black and white photographic prints are available for any photographs or illustrations appearing in this copy for an additional charge. Contact UMI directly to order.

UMI

A Bell & Howell Information Company
300 North Zeeb Road, Ann Arbor MI 48106-1346 USA
313/761-4700 800/521-0600

RICE UNIVERSITY

**Probabilistic Analysis of the Stability of Imperfection
Sensitive Arch and Shell Structures**

by

Khaled S. Hussain


A THESIS SUBMITTED
IN PARTIAL FULFILLMENT OF THE
REQUIREMENTS FOR THE DEGREE

Doctor of Philosophy

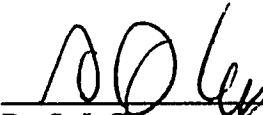
APPROVED, THESIS COMMITTEE:



Dr. R. P. Nordgren, Chairman
Herman and George R. Brown Professor of
Civil Engineering



Dr. J. P. Conte
Associate Professor of Civil Engineering



Dr. S. J. Cox
Associate Professor of Computational and
Applied Mathematics

Houston, Texas

April, 1996

UMI Number: 9631081

UMI Microform 9631081
Copyright 1996, by UMI Company. All rights reserved.

**This microform edition is protected against unauthorized
copying under Title 17, United States Code.**

UMI
300 North Zeeb Road
Ann Arbor, MI 48103

**PROBABILISTIC ANALYSIS OF THE STABILITY OF IMPERFECTION
SENSITIVE ARCH AND SHELL STRUCTURES**

by

Khaled S. Hussain

Abstract

The stability of arch and shell structures with random imperfections subjected to random loading is investigated. Arches are analyzed under different types of transverse loads while axial and/or pressure loading are considered for cylindrical shells. A probabilistic analysis of the randomness in the geometric imperfections along with the uncertainty in both loading and material properties is presented. The study investigates the effect of spatial variability of the different random parameters in the problem on the buckling load and the associated displacements. The imperfection sensitivity is studied for several geometrical configurations of the arches and shells and for various values of the statistical parameters for the random shape imperfections.

One- and two-dimensional random fields are introduced with different types of autocorrelation functions to characterize the structures and the imperfections. A sufficient number of terms is considered using two series expansion methods to express the field in

terms of its spectral decomposition. The first employs the Karhunen-Loeve theorem where the autocorrelation coefficient function is expanded in terms of its eigenvalues and eigenfunctions, while the second method utilizes any complete set of orthogonal functions. These techniques are compared with both the midpoint and local averaging methods for random field discretization and prove to be more computationally efficient within a given level of accuracy.

Both first- and second-order reliability methods (FORM/SORM) along with Monte Carlo simulation are used to evaluate different modes of instability based on the buckling load or the associated displacements. The probability density and the cumulative distribution functions of the buckling load are presented for various distributions of the imperfections. The sensitivity of the buckling load and the postbuckling displacements to different parameters is also presented. An extensive parametric study through many numerical examples is performed to establish a better understanding of the effects of the spatially variable imperfections on the buckling of arches and shells.

Acknowledgments

First and foremost, I would like to express my heartfelt gratitude to my advisor, Dr. Ronald Nordgren. I thank him for his constant help, encouragement and able advice throughout the different stages of this work. His precious instructions made this study both possible and enjoyable at the same time. Sincere thanks are expressed to Dr. Joel Conte for his guidance and his support in various aspects of the field of structural reliability. Special thanks also for Dr. Steve Cox for giving his time and showing his interest as a member of the thesis committee.

Special thanks are expressed to all my professors, friends and colleagues in the Civil Engineering Department at Rice University for their help and encouragement.

I would like to acknowledge the financial support provided through the Department of Civil Engineering and the Research Assistantship at Rice University.

Finally, I wish to express my gratitude to my wife, Hala, for her encouragement and support during all times and to my newly born daughter, Mahy, for giving me new goals in life.

Table of Contents

Abstract	ii
Acknowledgments	iv
Table of Contents	v
List of Figures	ix
List of Tables	xviii
1 Introduction	1
1.1 Motivation and Scope	1
1.2 Research Objectives	2
1.3 Review of Stability and Reliability Theories	2
1.4 Outline of the Thesis	8
2 Reliability Theory	12
2.1 Introduction	12
2.2 Concepts of Component Reliability	12
2.3 Probability of Failure	14
2.4 First- and Second-Order Reliability Methods	16
2.5 Design Point	18

2.6	Sensitivity Measures	20
2.7	Monte Carlo Simulation Methods	23
2.8	System Reliability	25
2.8.1	Unimodal Bounds	26
2.8.2	Bimodal Bounds	26
2.8.3	Reliability Index for Bounds	27
2.9	Random Field Discretization	27
2.10	Boundary Conditions	32
3	Stability of Shallow Arches	38
3.1	Introduction	38
3.2	Deterministic Stability Analysis	39
3.3	Exact Stability Solution	41
3.3.1	Uniform Radial Loading	43
3.3.2	Center Point Normal Loading	44
3.3.3	Linearly Varying Radial Loading	45
3.3.4	Limit-load vs. Bifurcation Buckling	45
3.3.5	Numerical Results	47
3.4	Series Stability Solution	50
3.5	Random Field Discretization	53
3.5.1	First Degree Exponential Autocorrelation Coefficient Function	54
3.5.2	Triangular Autocorrelation Coefficient Function	55

3.5.3	Second Degree Exponential Autocorrelation Coefficient Function	56
3.5.4	Sinusoidal Autocorrelation Coefficient Function	56
3.6	Numerical Results	57
4	Stability of Cylindrical Shells	103
4.1	Introduction	103
4.2	Deterministic Stability Analysis	105
4.3	Analysis Based on Flugge's Equations	105
4.4	Analysis Based on Donnell's Equations	110
4.4.1	Imperfection Modeling	113
4.5	Random Field Discretization	115
4.5.1	First Degree Exponential Autocorrelation Coefficient Function	116
4.5.2	Triangular Autocorrelation Coefficient Function	116
4.6	Numerical Examples	117
4.6.1	Pressure Loading	119
4.6.2	Axial Loading	124
4.6.3	Combined Loading	128
5	Summary and Conclusions	166
5.1	Stability of Shallow Arches	167
5.2	Stability of Cylindrical Shells	168
5.3	General Conclusions	169

5.4 Applications and Future Research	170
Bibliography	172
Appendix 1: Notation	180

List of Figures

2.1	Nonlinear transformation of the physical space into the standard normal space	35
2.2	FORM and SORM approximations to the failure surface in the standard normal space	36
2.3	Random field mesh	37
3.1	Coordinate system	64
3.2	Example load-deflection curves illustrating buckling loads for different magnitudes of imperfection in the case	65
3.3	Relation between the uniform pressure and the deflection at the middle of a shallow circular arch for different degrees of shallowness	66
3.4	Relation between the uniform pressure and the axial membrane force in a shallow circular arch for different degrees of shallowness.	67
3.5	Relation between the uniform pressure and the deflection at the middle of a shallow circular arch for different degrees of loading imperfection. ...	68
3.6	Relation between the uniform pressure and the axial membrane force in a shallow circular arch for different degrees of loading imperfection. ...	69
3.7	Cumulative distribution function for the unsymmetric buckling load of the arch under imperfect uniformly distributed loading.	70

3.8	Probability density function for the symmetric buckling load of the arch under imperfect uniformly distributed loading using the gradient of the CDF.	71
3.9	Probability density function for the symmetric buckling load of the arch under imperfect uniformly distributed loading using the FORM sensitivity.	72
3.10	Cumulative distribution function for the symmetric buckling load of the arch under uniformly distributed loading with random E and loading.	73
3.11	Cumulative distribution function for the symmetric buckling load of the arch under uniformly distributed loading for different mean values of the load imperfection.	74
3.12	Cumulative distribution function for the symmetric buckling load of the arch under uniformly distributed loading for different variances of the load imperfection	75
3.13	Cumulative distribution functions for the symmetric buckling load for both pinned and clamped ends arches under uniformly distributed loading	76
3.14	Cumulative distribution function for the symmetric buckling load and for both symmetric and antisymmetric modes of the arch under uniformly distributed loading	77
3.15	Relation between the uniform pressure and the deflection at the middle of a shallow perfect circular arch with clamped ends for different degrees of shallowness.	78
3.16	Values of the mean functions for three different fields of symmetric geometric imperfection along the arch with clamped ends.	79
3.17	Relation between the uniform pressure and the deflection at the middle of a clamped shallow circular arch with $\lambda = 7.31$ for different degrees of symmetric imperfection W.	80

3.18	Relation between the uniform pressure and the deflection at the middle of a clamped shallow circular arch with $\lambda = 5.74$ for different degrees of symmetric imperfection W.	81
3.19	Relation between the uniform pressure and the deflection at the middle of a clamped shallow circular arch with $\lambda = 5.19$ for different degrees of symmetric imperfection W.	82
3.20	Cumulative distribution function for the buckling pressure of a clamped arch with $\lambda = 7.31$, for different symmetric geometric imperfection configurations (Straight lines represent the deterministic cases with imperfection functions equal to the mean imperfections).	83
3.21	Cumulative distribution function for the buckling pressure of a clamped arch with $\lambda = 5.74$ for different symmetric geometric imperfection configurations (Straight lines represent the deterministic cases with imperfections equal to the mean of imperfection functions).	84
3.22	Cumulative distribution function for the buckling pressure of a clamped arch with $\lambda = 5.19$ for different symmetric geometric imperfection configurations (Straight lines represent the deterministic cases with imperfections equal to the mean of imperfection functions).	85
3.23	Cumulative distribution function for the symmetric buckling load of the clamped arch under uniformly distributed loading for different variances of the symmetric shape imperfection.	86
3.24	Probability density function for the unsymmetric buckling load of the clamped arch under uniformly distributed loading for different variances of the symmetric shape imperfection.	87
3.25	Values of the mean functions for three different fields of antisymmetric geometric imperfection along the arch with clamped ends.	88

3.26	Relation between the uniform pressure and the deflection at the middle of a clamped shallow circular arch with $\lambda = 7.31$ for different degrees of antisymmetric imperfection W.	89
3.27	Relation between the uniform pressure and the deflection at the middle of a clamped shallow circular arch with $\lambda = 5.74$ for different degrees of antisymmetric imperfection W.	90
3.28	Relation between the uniform pressure and the deflection at the middle of a clamped shallow circular arch with $\lambda = 5.19$ for different degrees of symmetric imperfection W.	91
3.29	Cumulative distribution function for the buckling pressure of a clamped arch with $\lambda = 7.31$, for different antisymmetric geometric imperfection configurations (Straight lines represent the deterministic cases with imperfections equal to the mean of imperfection functions).	92
3.30	Cumulative distribution function for the buckling pressure of a clamped arch with $\lambda = 5.74$ for different antisymmetric geometric imperfection configurations (Straight lines represent the deterministic cases with imperfections equal to the mean of imperfection functions).	93
3.31	Cumulative distribution function for the buckling pressure of a clamped arch with $\lambda = 5.19$ for different antisymmetric geometric imperfection configurations (Straight lines represent the deterministic cases with imperfections equal to the mean of imperfection functions).	94
3.32	Cumulative distribution function for the buckling pressure of a clamped arch with $\lambda = 7.31$ (solid lines) and $\lambda = 5.19$ (dashed lines), for different antisymmetric geometric imperfection configurations.	95
3.33	Rate of convergence of the reliability index for different discretizations methods for clamped ends arch under pressure loading	96

3.34	Rate of convergence of the reliability index for different discretizations methods for clamped ends arch under pressure loading using a sinusoidal autocorrelation coefficient function	97
3.35	Effect of the reliability method used on the reliability index for a clamped ends arch under pressure loading using SE method.	98
3.36	Rate of convergence of the reliability index for different correlation lengths for a clamped ends arch under pressure loading using a triangular autocorrelation coefficient function	99
3.37	The effect of the non-stationarity of the autocorrelation coefficient function on the reliability index for a clamped ends arch under pressure loading using KL method	100
3.38	The effect of the non-stationarity of the autocorrelation coefficient function on the reliability index for a pinned ends arch under pressure loading using KL method	101
3.39	Cumulative distribution functions for the unsymmetric buckling load for both pinned and clamped ends arches under uniformly distributed loading. .	102
4.1	Coordinate system	129
4.2	An example of the buckling diagram for a clamped perfect cylindrical shell under hydrostatic pressure using linear Flugge's equations for different values of $k = t^2 / 12 R^2$	130
4.3	An example of the buckling diagram for a clamped perfect cylindrical shell under axial compression using linear Flugge's equations ($k = t^2 / 12 R^2 = 10^{-5}$).	131
4.4	Series coefficients of the Fourier expansion of the mean function for the geometric imperfection configuration number 1 ($W_1 = 0.2t$) of a clamped cylindrical shell.	132

4.5	Series coefficients of the Fourier expansion of the mean function for the geometric imperfection configuration number 2 ($W_1 = 0.4t$) of a clamped cylindrical shell.	133
4.6	Series coefficients of the Fourier expansion of the mean function for the geometric imperfection configuration number 3 ($W_1 = 0.6t$) of a clamped cylindrical shell.	134
4.7	Effect of deterministic initial geometric imperfections on the typical postbuckling behavior of a clamped cylindrical shell under pressure loading for $z = 500$	135
4.8	Effect of deterministic initial geometric imperfections on the typical postbuckling behavior of a clamped cylindrical shell under pressure loading for $z = 100$	136
4.9	Effect of deterministic initial geometric imperfections on the typical postbuckling behavior of a clamped cylindrical shell under pressure loading for $z = 50$	137
4.10	Cumulative distribution function for the buckling pressure of a clamped cylindrical shell for different geometric configurations under imperfection field $W_1 = 0.2t$	138
4.11	Cumulative distribution function for the buckling pressure of a clamped cylindrical shell for different amplitudes of the geometric imperfection configuration W_1	139
4.12	Cumulative distribution function for the buckling pressure of a clamped cylindrical shell for different amplitudes of the geometric imperfection configuration W_2 ($N = 13$).	140
4.13	Cumulative distribution function for the buckling pressure of a clamped cylindrical shell for different amplitudes of the geometric imperfection configuration W_3 ($N = 15$).	141

4.14	Rate of convergence of the reliability index for different discretizations methods for clamped ends cylindrical shell under pressure loading. . .	142
4.15	Effect of the reliability method used on the CDF for a clamped ends cylindrical shell under pressure using SE method.	143
4.16	The effect of the non-stationarity of the autocorrelation coefficient function on the CDF for a clamped ends cylindrical shell under pressure using KL method.	144
4.17	Cumulative distribution function for the buckling pressure of a clamped cylindrical shell for different autocorrelation coefficient functions. ...	145
4.18	Cumulative distribution function for the buckling pressure of a clamped cylindrical shell for different values of the exponential correlation length in the axial direction.	146
4.19	Cumulative distribution function for the buckling pressure of a clamped cylindrical shell for different values of the exponential correlation length in the circumferential direction.	147
4.20	Effect of deterministic initial geometric imperfections on the typical postbuckling behavior of a clamped cylindrical shell under axial loading for $z = 500$	148
4.21	Effect of deterministic initial geometric imperfections on the typical postbuckling behavior of a clamped cylindrical shell under axial loading for $z = 100$	149
4.22	Effect of deterministic initial geometric imperfections on the typical postbuckling behavior of a clamped cylindrical shell under axial loading for $z = 50$	150
4.23	Cumulative distribution function for the buckling axial load of a clamped cylindrical shell for different geometric configurations under imperfection field $W_1 = 0.4t$	151

4.24	Cumulative distribution function for the buckling axial load of a clamped cylindrical shell for different amplitudes of the geometric imperfection configuration W_1	152
4.25	Cumulative distribution function for the buckling axial load of a clamped cylindrical shell for different methods of deterministic stability analysis.	153
4.26	Cumulative distribution function for the buckling axial load of a clamped cylindrical shell for different values of N and for a series system.	154
4.27	Rate of convergence of the reliability index for different discretizations methods for clamped ends cylindrical shell under axial loading.	155
4.28	Effect of the reliability method used on the CDF for a clamped ends cylindrical shell under axial loading using SE method.	156
4.29	The effect of the non-stationarity of the autocorrelation coefficient function on the CDF for a clamped ends cylindrical shell under axial loading using KL method.	157
4.30	Cumulative distribution function for the buckling pressure of a clamped cylindrical shell for different autocorrelation coefficient functions.	158
4.31	Cumulative distribution function for the buckling axial load of a clamped cylindrical shell for different values of the absolute exponential correlation length.	159
4.32	Cumulative distribution function for the buckling axial load of a clamped cylindrical shell for different values of the exponential correlation length in the circumferential direction.	160
4.33	Cumulative distribution function for the buckling axial load of a clamped cylindrical shell for different values of the exponential correlation length in the axial direction.	161

- 4.34 Effect of the randomness in the modulus of elasticity of the material of a clamped cylindrical shell on the buckling under axial loading. 162
- 4.35 Cumulative distribution function for the buckling axial load of both clamped and hinged cylindrical shells under imperfection field $W_1 = 0.4t$ 163
- 4.36 Effect of initial geometric imperfection field $W_1 = 0.2t$ on the typical postbuckling behavior of a clamped cylindrical shell under combined axial and pressure loading for $z = 500$ 164
- 4.37 Cumulative distribution functions for the buckling axial load of a clamped cylindrical shell under various values of the hydrostatic pressure ratio. 165

List of Tables

3.1	Arch properties	47
3.2	Random variables	48
3.3	Values of P_f for the buckling load of the clamped arch under uniformly distributed loading for different correlation lengths ($C_t = 6.35$)	62
4.1	Values of N for the lowest buckling loads.	120

To my Parents, and my Wife

Chapter 1

Introduction

1.1 Motivation and Scope

The buckling resistance of arch and shell structures has become one of the major areas of current interest in structural mechanics. This is due to the fact that buckling represents a critical mode of failure for this wide category of structures. In many arch and shell problems, the theoretical buckled form is in a condition of unstable equilibrium, and a new position of equilibrium can exist at a greatly reduced buckling load. Thus, the theoretical bifurcation or limit buckling load calculated by classical theory is rarely attained in experiments or practical structures. Furthermore, imperfections in shell geometry, material properties and applied loads reduce the buckling load significantly below the classical value.

The present investigation is concerned with improving the characterization of buckling loads and their imperfection sensitivity by treating imperfections as random fields. Then, the methods of reliability theory can be used to calculate the statistical distributions of buckling loads. Before elaborating on the methods of analysis, a brief review of both arches and shells stability methods and of reliability theories will be presented.

1.2 Research Objectives

The goal of this research is to develop a rigorous, versatile and efficient method of stability analysis of arch and shell structures with random geometric, material and loading imperfections. The structures considered are:

- a- Shallow circular arches under concentrated or distributed loads.
- b- Circular cylindrical shells under pressure and/or axial loads.

To conduct this study, a theoretical analysis combined with powerful numerical tools is developed for studying the response of the structures both in the deterministic and probabilistic senses. The proposed methods are capable of treating the shell stability problem accurately and efficiently, considering spatially variable imperfections and taking into account the nonlinear behavior. The methods are capable of analyzing the postbuckling behavior and determining the sensitivity of the solutions to each single parameter.

1.3 Review of Stability and Reliability Theories

The stability of arch and shell structures received considerable attention after Koiter proposed his theory in 1945 concerning the general initial postbuckling behavior of elastic bodies under static conservative loads. In this theory, the stability of equilibrium at the bifurcation point is thoroughly clarified on the basis of the energy criterion and then the initial postbuckling behavior is asymptotically analyzed. This analysis leads to the classification of bifurcation points into three types, that is, asymmetric, unstable symmetric, and stable symmetric forms. Further, the effect of initial imperfection is taken

into consideration, clarifying the imperfection sensitivity of the structure in connection with the type of the bifurcation point.

In the early 1960's the interest in a general theory sprang up almost simultaneously in the United States and in England. In the United States, the Koiter theory was reconstructed by Budiansky (1974) and Hutchinson and Koiter (1970) in a form more suitable for application to elastic continua. They conducted numerous researches on the initial postbuckling behavior as well as the imperfection sensitivity of a variety of shell structures. In England, on the other hand, another general theory of elastic stability was initiated by Thompson (1967) in terms of generalized coordinates of the discrete elastic system, which has been extensively developed by Thompson and Hunt (1973) and their associates at University College, London. Based on a similar theory, a comprehensive study was performed by Britvec (1973) on the buckling behavior of various frame structures, while the Thompson theory has been further refined and extended by Huseyin (1975).

The stability of thin, shallow arches has received extensive treatment in the literature. While the behavior can be modeled by reasonably straightforward and uncomplicated equations, arches are capable of exhibiting both limit-point and bifurcation-type buckling. The bifurcation buckling behavior is strongly affected by imperfections in the shape of the arch and the material properties.

Analysis of buckling and postbuckling behavior of shallow arches dates back to Biezeno and Grammel (1939) where they considered the stability of arches under a central concentrated load. More recent work on the same problem was done by Fung and Kaplan

(1952) and Dickie and Broughton (1971). The deterministic analyses of Gjelsvik and Bodner (1962) and Schreyer and Masur (1966) are of particular relevance to the work presented herein. The former investigated the clamped shallow circular arch under center point loading using the energy method, while the latter obtained and solved the governing differential equations for the same problem.

The circular cylindrical shell constitutes a fundamental element in light-weight structures, thus making the determination of the buckling load one of the most crucial problems for the design and development of these structures. Hence, numerous researches have been conducted on this subject. The first complete presentation of shell analysis was done by Love (1888). Love also had major contributions to shell theory in his book on the theory of elasticity (Love, 1927). Following that, the basic equations for shell analysis were established by Flugge (1932) and Donnell (1933). Early work by Karman and Tsien (1941) studied the postbuckling behavior of cylindrical shells under compression by applying the Ritz procedure to the Donnell nonlinear equations.

The buckling load of imperfect cylindrical shell highly depends on the extent and shape of the initial imperfections. For shells with different boundary and loading conditions, various responses and behaviors are obtained. The nonlinear analysis of imperfect cylindrical shells represents one of the best known examples of the very complicated stability behavior for thin-walled structures.

A central decision in buckling analyses of imperfection sensitive structures is the choice of an appropriate imperfection form. In particular, either deterministic or probabilistic approaches can be employed. Deterministic methods furnish a precise

technique in the exploration of the mechanisms involved in the imperfection sensitivity, whereas probabilistic methods may provide the key to acceptable design criteria.

The effect of random imperfections and loads on the buckling behavior of shallow arches has been studied by many researchers. They recognized that if imperfections are random quantities, then the buckling load must be expressed in statistical terms. These studies include the work done by Sankar and Ariaratnam (1971) who obtained analytical expressions for calculating the probability of the snapping of an arch in a specified time interval under lateral loading that varies randomly with time. A recent study by Palassopoulos (1995) presents a method for incorporating stochastic imperfections in the Finite Element Method formulation for evaluating the buckling strength of imperfection-sensitive arches. However, the previous work does not provide a complete statistical distribution for the buckling load or extend the analysis to postbuckling deflections.

Probabilistic methods of analysis of cylindrical shells were initiated by Bolotin (1962), who recognized that both applied loads and initial geometry imperfections should be treated as random variables. His work was followed by a number of general analyses for single-mode systems by Roorda (1969) and Hansen and Roorda (1974). These papers investigated critical load and initial imperfection statistics as well as rudimentary reliability theory concepts. In addition, Amazigo (1969) considered the influence of axisymmetric random imperfections in an infinite cylindrical shell.

Many different approaches were suggested for methods used to model the existing imperfections. Tennyson, et. al., (1971) proposed the measurement of a number of axial imperfection profiles of cylindrical shells and the use of measured quantities in the

asymptotic results given by Amazigo (1969). On the other hand, based on an examination of a great deal of experimental work, Roorda (1971) has suggested that the statistics of the initial imperfections depend on the radius to thickness ratio R/t of the shell. Both of these design concepts assume that the design imperfections are axisymmetric. This assumption is based on the hypothesis that axisymmetric imperfections are of primary importance. Furthermore, it has been suggested that it is impractical for a designer either to determine the statistics of a complete mapping of a shell surface or even to use such information if it was obtained. The extent of accuracy of such suggestion is investigated in the current study.

Reliability theory provides a useful framework for modeling probabilistic structural problems. The application of probability-based methods to structural analysis was first developed by Ang and Cornell (1974). At the same time Ravindra et al. (1974) used the safety index method for the design of structural members. In these analyses, the physical variables are taken to be random variables and the reliability with respect to a given failure mode is simply defined as the probability that the set of these random variables lies in the safe region. Different methods of probabilistic simulations, mainly Monte Carlo simulation, can be used to evaluate the failure probability. However, simulation methods are limited to small one-dimensional stability problems, e.g., beam-columns and frames, because of the computational complexity associated with analyzing larger problem.

The theory and methods of structural reliability have developed significantly during the last decade. In this period research on both philosophical and conceptual issues, as well as reliability and sensitivity computation methods has taken place. Extensive

developments in the reliability methods (Madsen et al. 1986, Melchers 1987, Der Kiureghian et al. 1986, 1987) enabled the use of versatile and efficient algorithms to estimate the probability of failure replacing simulations methods. The field now has reached a stage where the use of the developed methodology is becoming widespread.

The early studies were based on the mean-value first-order second-moment (MVFOSM) method which had the basic disadvantage of lacking invariance with respect to the formulation of the limit-state function. Elishakoff, et. al., (1987) applied the first-order second-moment (FOSM) reliability method to the buckling of cylindrical shells. However, they considered the effect of imperfections on the buckling load only, without extending to postbuckling behavior or studying the complete statistical distribution. Arbocz and Hol (1991) combined the same FOSM method with a finite element analysis of the stability problem of axially loaded cylindrical shells. The FOSM method had the advantage of being invariant to the formulation of the limit-state function but, on the other hand, lacked both comparativeness properties and completeness where it could not account for information beyond second moments.

First- and second-order reliability methods, commonly referred to as FORM and SORM, were introduced recently by Augusti et al. (1984) and Madsen et al. (1986) and were used by Der Kiureghian and Liu (1986) to approximately evaluate the probability of failure for any general problem. Either one of these methods can be briefly described as a transformation from the basic set of random variables into a standard normal vector where the limit state surface is approximated. Then the probability of failure is computed according to the approximating failure surfaces; a plane in FORM and a quadratic surface

in SORM. These methods showed wide acceptance in different fields of stability problems as they have a more analytical basis and require less computational time than simulation methods.

However, the application of FORM/SORM along with Monte Carlo simulation to get a complete description of the response of imperfect shells and arches under buckling loads is yet to receive the needed attention. System reliability analysis is another important issue to be considered when a structure has more than one potential mode of failure which is the case for the stability problem of shallow arches and shells as will be shown in this study.

1.4 Outline of the Thesis

The present research is focused on developing a general method that can provide information on the reliability against instability of arch and shell structures with random imperfections and random loads. The cases under study employ a variety of theoretical formulations and solution techniques. This allows the treatment of a large class of shells and arches for buckling loads under general imperfections in geometry, material and loading.

The first part of this dissertation, presented in Chapter 2, deals with the definitions and the methods of analysis used in the reliability theory. The formulation of the limit-state functions defining the failure of the structures is discussed along with the different techniques to evaluate and analyze the failure criteria. The use of random fields to represent the continuous imperfect properties of the structures is introduced. Different methods for the discretization of the random fields are presented.

The second part of this dissertation, presented in Chapter 3, deals with the buckling of

shallow circular arches. First, the deterministic buckling loads for different modes of instability are obtained using a nonlinear analysis. The arches are analyzed for different degrees of shallowness under various loads and boundary conditions. The postbuckling behavior for arch is studied for both symmetric or asymmetric responses using series expansions to obtain closed-form solutions by energy minimization.

The third part of this dissertation, presented in Chapter 4, deals with the buckling of cylindrical shells. They are first analyzed using the general shell theory based on the equations given by Flugge, then, nonlinear Donnell's theory is applied because of its relative simplicity and practical accuracy. The analysis in each case is based on the minimization of the total potential energy of the shell with respect to the virtual displacement consistent with the geometrical constraints along the boundaries.

In both second and third parts of this dissertation, the analysis starts by considering the behavior of the structures under deterministic loads and with deterministic geometrical and material imperfections. After reviewing the stability analysis methods, reliability theory is introduced into the problem by considering random fields to model the imperfections and various techniques to discretize the continuous fields. As a result, the buckling load is a random variable with statistical properties that depend on the statistical distribution of the imperfections. Different autocorrelation functions are employed to describe the spatial variability of the imperfections. An interface technique is established between the algorithms developed to analyze the shells and the general reliability code CALREL (Liu et al., 1989).

Both first- and second-order reliability methods (FORM/SORM) are used to evaluate

different modes of failure for the cylindrical shell and the arch based on the buckling load or the associated displacements. Monte Carlo simulation (MCS) is used for comparison matters in some of the smaller problems. Both the probability density and the cumulative distribution functions of the buckling load are presented for different distribution inputs. The sensitivity of the buckling load and the postbuckling displacements to different parameters are also presented.

Throughout the analysis, different types of loading are presented along with a parametric comparison between the different cases. For the arch case, various possibilities of a concentrated load at the apex of the arch or a radial varying or uniform loads are presented. Cylindrical shells under either pressure or axial loading or both of them are analyzed for different types of boundary conditions.

For the case of the cylindrical shells, the effects of the imperfections on the stability behavior are included in the analytic formulation and treated by the Galerkin method. The geometric imperfections are modeled in a general form by a two dimensional Fourier series. Complete solutions first are developed for the deterministic case by considering the coefficients of the series representing the imperfection to be known parameters and solving for the coefficients of the response of the shell under end loads and pressure.

An extensive parametric study is performed in the form of numerical examples to establish a better understanding of the effects of the spatially variable imperfections on the buckling of arch and shell structures. The different aspects of the responses are discussed and compared with results from other methods. This shows how the reliability theory can be used as a versatile tool in identifying realistically the behavior of almost any shell

structure under buckling.

The imperfection sensitivity of the arch is evaluated from consideration of the distribution of the buckling load for various values of the shallowness parameter. Different height to thickness ratios are considered for the cylindrical shell. In both cases, the effect of different fields on imperfections are considered with special emphasis on the sensitivity of the buckling loads with respect to the various parameters identifying the imperfection configuration and distribution.

Some of the practical applications of the theory are discussed. These include the techniques proposed for the measurement and characterization of the initial imperfections and their statistical distribution. Suggested methods of experimental verification are presented. And finally, some proposed methods for specifying the allowed imperfections in design code are considered.

Chapter 2

Reliability Theory

2.1 Introduction

The methodology used in the probabilistic analysis in this research is reviewed herein to the extent necessary to understand the formulation. Three reliability methods are discussed namely, first- and second-order reliability methods (FORM and SORM, respectively) and Monte Carlo simulation (MCS). FORM and SORM were developed in the past decade to assess the safety of structural components and structural systems while MCS has been widely used for more than 50 years. A complete discussion of the development and history of reliability methods can be found in Der Kiureghian and Liu (1986), Madsen et al. (1986) and Melchers (1987).

2.2 Concepts of Component Reliability

The structural reliability problem is often formulated in terms of a vector of *basic random variables* $X = (X_1, X_2, \dots, X_n)$, describing the uncertain components of interests in the problem. These include quantities such as loads, environmental factors, material properties, structural dimensions, and variables introduced in the problem to account for modeling and prediction errors. A *limit-state function* $g(X)$ (also known as the

performance function) is a scalar function describing the limiting state of the structure in terms of X .

The limit-state function is, by convention, formulated such that $g(X) \leq 0$ denotes the failure of the structure whereas $g(X) \geq 0$ denotes its survival. The boundary between the failure and safe sets

$$g(X) = 0 \quad (2.1)$$

is an n -dimensional hypersurface and is termed as the *limit-state surface*.

In order to illustrate the introduction of a limit state function in the stability problem, we will start by discussing the classic example of the *load-resistance* problem. In this case, the limit-state function is formulated as

$$g = R - S \quad (2.2)$$

in which R is the resistance of a given structure and S is the load applied to the structure. Both the resistance and the load are assumed random due to any uncertainty in the problem. For each realization, the g -function can be either negative, indicating that the structure failed to resist the load, or positive, indicating that the structure survived the applied load. A general assumption in this classic example is the uncoupling of the random variables since each of them usually depends on certain parameters different from the other.

In arches and shells stability problems, various kinds of imperfections are inherent in the analysis. These can be categorized into geometric, material and loading imperfections. All of them have different levels of uncertainties, hence can be modeled as random quantities. Uncoupling two quantities defining the load and resistance is not a straight

forward task in this case. The instability (failure) of structures can be formulated in terms of excess deflection or excess loading capacity as given by the limit-state function

$$g(X) = C_t - C(X) \quad (2.3)$$

where C_t is a specified target value of a certain parameter C , which may be the buckling load or the maximum deflection (at buckling), and $C(X)$ is the value of this same parameter evaluated for the state X . Thus P_f from reliability analysis expresses the probability that the random variable C exceeds C_t . In other words, the failure is equivalent to the failing of the structure to meet the design standards regarding the load or the deflection.

2.3 Probability of Failure

By definition, reliability is based on estimating the *probability of failure*, which is given by the n -fold integral

$$P_f = P[g(X) \leq 0] = P[C_t \leq C(X)] = \int_{g(X) \leq 0} f_X(x) dx \quad (2.4)$$

in which $P[\dots]$ is the probability operator, the vector x is any realization of the random vector X , and $f_X(x)$ is the joint probability density function (PDF) of X .

By varying the value of C_t in Eq. 2.3 and repeating the reliability calculation, one obtains $P_f(C_t)$ and the cumulative distribution function (CDF) for the failure load or deflection. The probability density function (PDF) can then be obtained either by differentiating the CDF or (better) by using the sensitivity output that is easily computed during the FORM analysis as will be discussed later in this chapter.

A number of problems exists in the process of evaluating the integral in Eq. 2.4 for

continuous structural problems. The first difficulty is the existence of many random variables which increase the number of the dimensions in the problem space making the integration process very time consuming. A second problem results from the boundaries defined by the g -function which usually have a complex formulation. Problems arise when for each realization of the random variables corresponding to a single point in the domain, a very lengthy numerical routine needs to be evaluated as in the case of cylindrical shells analysis. Other difficulties are due to the magnification of numerical inaccuracies because of the small numbers for the probability of failure in structural problems together with the lack of complete information concerning the probabilistic distribution of the random variables.

Many approximation methods have been used over the years to overcome most of these difficulties. This includes first-order and mean-value first-order second-moment (MVFOSM) reliability methods. However FORM and SORM have shown in recent years to be good approximation methods for evaluating the failure probability. They have an advantage over previous methods which lacked invariance with respect to the formulation of the limit-state function, where different formulations of the same problem would lead to different failure probabilities. Some of the previous methods also lacked comparativeness properties and many lacked completeness where they could not account for information beyond second moments. Compared with simulation techniques, FORM and SORM have the advantage of obtaining good approximations in a tiny fraction of the time required with simulation methods such as MCS.

2.4 First- and Second-Order Reliability Methods

The primary purpose of reliability methods is to evaluate the n -fold integral in Eq. (2.4). The use of FORM and SORM as approximation methods was discussed by Augusti et al. (1984), Madsen et al. (1986) and Bjerager (1990).

A number of steps are included in the use of FORM and SORM. First, the vector of the random variables \mathbf{X} is transformed into the vector of uncorrelated standard normal variates \mathbf{U} (zero mean, unit variance and zero correlation) as illustrated in Fig. 2.1. The transformation $\mathbf{U} = \mathbf{T}(\mathbf{X})$ is generally a non-linear one-to-one mapping existing for random variables having continuous strictly increasing joint cumulative distribution function (CDF). In other words, the original joint PDF is transformed from the physical space (x -space) to the standard normal space (u -space). Then Eq. (2.4) becomes

$$P_f = \int_{G(\mathbf{U}) \leq 0} (2\pi)^{-n/2} \exp\left(-\frac{1}{2}\mathbf{u}^T\mathbf{u}\right) d\mathbf{u} \quad (2.5)$$

in which $G(\mathbf{U})$ is the limit-state function in the standard normal space. This transformation depends on the distribution of the vector \mathbf{X} and on the correlation between the variables. For statistically independent Gaussian variables, the transformation reduces to a linear mapping of the random variables. On the other hand, for non-Gaussian variables, the distributions are assumed to be of the Nataf type as discussed later in this chapter.

The transformation to the u -space has a number of advantages including that the PDF is rotationally symmetric. Also the PDF decays exponentially with the square of the distance from the origin so that integrating at the design point, defined in the next paragraph, should give good accuracy.

The second step is finding the point u^* , called the *design point*, which is the nearest point on the limit state surface $G(U) = 0$ to the origin. The design point is considered to have the highest likelihood of failure amongst all points in the failure region. The next step is to approximate the nonlinear limit-state surface in the u -space by a tangent surface at the design point. The distance (in space) between the origin and the design point is called the *reliability index*, β since it turns out to be a basis for estimating the failure probability.

The design point has a practical significance. Since the probability density in the u -space decays exponentially with u , the primary contribution to the probability integral in Eq. (2.5) comes from the part of the failure region closest to the origin. Therefore, the design point is an optimum point to approximate the surface $G(U) = 0$.

In the FORM approximation, the tangent surface at the design point is a hyper-plane as shown in Fig. 2.2, and the corresponding first-order approximation is

$$P_f \cong P_{f_{FORM}} = \Phi(-\beta) \quad (2.6)$$

where $\Phi(\dots)$ is the standard normal cumulative distribution function.

The SORM approximation is obtained by replacing the limit-state surface by a hyper-parabolic surface at u^* . The corresponding second-order approximation of the failure probability is obtained in terms of the reliability index and the principal curvatures of the hyper-parabolic surface. Several exact and approximate schemes are available to fit the approximating surface to the original one based on point or curvature fitting. In the current study, two methods are used. First, the asymptotic exact formula given by Breitung (1984)

$$P_f \cong P_{f_{SORM}} \cong \Phi(-\beta) \prod_{i=1}^{m-1} \{1 + \beta \kappa_i\}^{-1/2} \quad (2.7)$$

Where κ_i , $i = 1, 2, \dots, m-1$ are the principal curvatures of the fitting paraboloid at the design point in the u -space with the sign convention that curvatures are positive when the surface curves away from the origin.

The second formula used is given by Tvedt (1988) which is an exact and numerically feasible than Eq. 2.7. Here the failure probability is approximated by

$$P_f \equiv P_{f_{SORM}} = \phi(\beta) \operatorname{Re} \left[i \left(\frac{2}{\pi} \right)^{1/2} \int_0^\infty \frac{\exp \{ (t + \beta)^2 / 2 \}}{t} \left\{ \prod_{j=1}^{m-1} (1 - t \kappa_j)^{-1/2} \right\} dt \right] \quad (2.8)$$

in which $\phi(\dots)$ is the standard normal probability density function, κ_i defined as before, and i is the imaginary unit. During the study, results calculated based on Breitung formula were in a better agreement with results obtained by simulation methods.

The computational effort encountered in SORM is higher than that in FORM. However, the results of the latter can significantly depart from the true solution for cases where the limit-state surface has a significant curvature around the design point. Such cases occur for highly nonlinear structures as for the case of the buckling of shells making it important to obtain the second-order approximation. However, in either of the two methods, usually much of the computational effort is in finding the design point. Thus, the relative increase in the total processing time for using SORM instead of FORM is generally small.

2.5 Design Point

The most time consuming aspect of the reliability analysis based on FORM or SORM is the determination of the design point. This especially happens for higher dimensions

problems and when long algorithms are included in the formulation of the g -function. The design point determination is the solution of a nonlinear constrained optimization problem in the form of

$$\begin{aligned} &\text{Minimize} \quad |u| \\ &\text{Subject to} \quad G(u) = 0 \end{aligned} \quad (2.9)$$

Many algorithms exist for this problems, including the HL-RF method, which was originally developed by Hasofer and Lind (1974) and later modified by Rackwitz and Fiessler (1978). Other methods include the feasible direction method, the gradient projection method and the modified HL-RF which was later developed by Liu and Der Kiureghian (1986).

A comparison between different optimization algorithms was done by Liu and Der Kiureghian (1991), based on the generality, robustness, accuracy, efficiency and capacity of the methods. They concluded that the HL-RF required the least amount of computation and storage in each iteration and it converges in a few cycles. Hence it will be used throughout this analysis.

The algorithm starts by selecting an initial point, x_1 , in the x -space, which may be the mean point, then transform it to the u -space using the aforementioned one-to-one mapping. A sequence of points is constructed based on the following procedure

$$u_{i+1} = \left[\alpha_i u_i + \frac{G(u_i)}{|\nabla_u G(u_i)|} \right] \alpha_i^T \quad (2.10)$$

in which

$$\alpha_i = -\frac{\nabla_u G(u_i)}{|\nabla_u G(u_i)|} \quad (2.11)$$

is a unit vector pointing in the negative gradient direction, and

$$\nabla_u G(u) = \left(\frac{\partial}{\partial u_1} G(u), \dots, \frac{\partial}{\partial u_n} G(u) \right) \quad (2.12)$$

is the gradient vector which can be estimated in terms of the gradient vector in the x -space, $\nabla_x g(x)$, as follows

$$\nabla_u G(u) = \{ \nabla_x g(x) \} J_{u,x}^{-1} \quad (2.13)$$

in which $J_{u,x}$ is the Jacobian of the transformation from the physical to the standard-normal space. The algorithm usually converges to the design point in a few iterations. The reliability index is then evaluated as

$$\beta = \alpha^* \cdot u^* \quad (2.14)$$

in which α^* is a unit normal vector at the design point directed towards the failure region as shown in Fig. 2.2.

Care should be taken in choosing the initial point because of the possibility of the existence of a number of local minima. In such cases, more than one initial point should be tried in order to reach the global minimum. For extremely noisy or complex limit-state surfaces, using a number of starting points or the use of a smoothing algorithm usually improves the optimization process. Converging to a local minimum value and evaluating the failure probability on this basis would result in incorrect information regarding the behavior or safety of the structure under consideration.

2.6 Sensitivity Measures

Measures of sensitivity are easily obtained as a part of the FORM analysis.

Sensitivities are in the form of first-order derivatives of the reliability index and the first-order approximation of the probability of failure with respect to the input random variables, as well as to the deterministic parameters included in the g -function. The sensitivity measures show the relative importance of each random variable or deterministic parameter on the behavior of the structure.

One measure of sensitivity is the partial derivative of β which can be obtained either in the standard-normal space as

$$\nabla_{u^*}\beta = \left[\frac{\partial\beta}{\partial u_1}, \dots, \frac{\partial\beta}{\partial u_n} \right] = \alpha^* \quad (2.15)$$

where

$$\alpha^* = -\frac{\nabla_u G(u^*)}{|\nabla_u G(u^*)|} \quad (2.16)$$

or in the physical space as

$$\nabla_{x^*}\beta = (\nabla_{u^*}\beta)J_{u^*, x^*} = \alpha^* J_{u^*, x^*} \quad (2.17)$$

in which J_{u^*, x^*} is the Jacobian of the transformation from the physical to the standard-normal space evaluated at the design point.

The aforementioned sensitivity in the u -space is evaluated with no additional computational effort since α^* is readily available during the obtaining of the design point. However, the sensitivity in the x -space would be more physically meaningful. Der Kiureghian and Ke (1985) normalized the sensitivity measure in Eq. 2.17 in order not to be dependent on the units of x^* . This is known as the unit gamma sensitivity vector

$$\gamma = \frac{(\nabla_{x^*}\beta)D}{|(\nabla_{x^*}\beta)D|} \quad (2.18)$$

in which D is the diagonal matrix of the standard deviations of X .

Since choosing the appropriate probabilistic distribution plays an important role in the reliability results, a good measure of sensitivity is with respect to the parameters of the distribution function. This include the mean, standard deviation, and correlation coefficients of the random variables. Writing the joint PDF of the basic random variables as $f_X(x) = f_X(x, \theta)$, where θ is the vector of distribution parameters, then the sensitivity can be given as (Madsen et al. 1986)

$$\nabla_{\theta}\beta = \alpha^* J_{u^*, \theta} \Big|_{x^*} \quad (2.19)$$

and by applying the chain rule

$$\nabla_{\theta}P_f = -\phi(-\beta(\theta))\nabla_{\theta}\beta \quad (2.20)$$

where $J_{u^*, \theta} \Big|_{x^*}$ is the matrix containing the partial derivatives of the transformation with respect to θ evaluated at the design point. This particular equation is sometimes difficult to evaluate for certain distributions.

The other important set of sensitivities which can be obtained is with respect to the deterministic parameters in the g -function. This include C_r defined in Eq. (2.3) which shows the sensitivity of the reliability index with respect to variations in the chosen target load. Information about the sensitivity with respect to the correlation length of the used autocorrelation function is also important. Writing the limit-state function as $g(x) = g(x, \omega)$, where ω is the vector of deterministic parameters, then the sensitivity can be written as (Madsen et al. 1986)

$$\nabla_{\omega}\beta = \frac{1}{|\nabla_{u^*} G(u^*)|} \nabla_{\omega} g(x^*, \omega) \quad (2.21)$$

and by applying the chain rule

$$\nabla_{\omega} P_f = -\phi(-\beta(\omega)) \nabla_{\omega}\beta \quad (2.22)$$

Applying Eq. (2.21) to Eq. (2.3) to evaluate the sensitivity with respect to C_i gives the simplified formula

$$\nabla_{C_i} \beta = \frac{1}{|\nabla_{u^*} G(u^*)|} \quad (2.23)$$

2.7 Monte Carlo Simulation Methods

During this study, comparisons and verifications of the reliability results using FORM and SORM are accomplished based on Monte Carlo simulation (MCS) method. The comparison is usually done for smaller dimension problems because of the length of the computation time associated with MCS.

The method used is the so-called zero-one indicator-based Monte Carlo simulation which works by defining an *indicator function*, $I(x)$, such that

$$I(x) = \begin{cases} 1 & \text{if } g(X) \leq 0 \text{ (Fail)} \\ 0 & \text{if } g(X) > 0 \text{ (Safe)} \end{cases} \quad (2.24)$$

Then, the probability of failure is estimated based on the indicator function according to the following expression

$$P_f = \int_{g(X) \leq 0} f_X(x) dx = \int_x I(x) f_X(x) dx = E[I(x)] \quad (2.25)$$

in which $E[...]$ is the expectation operator.

By performing N Monte Carlo simulations by random selection of the prescribed joint probability density of the vector X , an *estimate* of the probability of failure \hat{P}_f is given as follows

$$P_f = E[\hat{P}_f] = \frac{1}{N} \sum_{i=1}^N p_i \quad (2.26)$$

where

$$p_i = I(x_i) \quad (2.27)$$

in which x_i denotes the i^{th} simulation.

An unbiased estimate of the variance of \hat{P}_f can be given by

$$\hat{\sigma}^2[\hat{P}_f] \equiv \frac{1}{N(N-1)} \sum_{i=1}^N (p_i - \hat{P}_f)^2 \quad (2.28)$$

By increasing the number of simulations, higher accuracy is reached in evaluating the probability of failure. A threshold is considered for the value of the coefficient of variation of the estimate of P_f in order to determine the stopping criterion for MCS procedure. The coefficient of variation is given by

$$\text{c.o.v.}[\hat{P}_f] \equiv \frac{\sigma[\hat{P}_f]}{P_f} \quad (2.29)$$

where

$$\sigma^2[\hat{P}_f] = \frac{P_f(1 - P_f)}{N} \equiv \frac{P_f}{N} \quad \text{if } P_f \text{ is small} \quad (2.30)$$

Thus for small P_f , the number of Monte Carlo simulations required can be calculated as

$$N = \frac{1}{P_f(\text{c.o.v.}[\hat{P}_f])^2} \quad (2.31)$$

For an assumed example threshold of a c.o.v. of 0.1, the number of simulations required is about $100/P_f$.

2.8 System Reliability

When a structure may fail partly or totally in more than one mode, the reliability problem is said to be a system reliability problem. If the structure has such properties that it always fails totally according to its weakest mode, the reliability will be smaller than calculated for each single mode. This is a so-called series system effect, and this is the difference between *component* reliability, where only one failure mode is considered, and *system* reliability, where more than one mode are considered.

System reliability is considered in the analysis of the buckling of shallow arches and cylindrical shells. For the arch, both symmetric (limit-load) and antisymmetric (snap-through) buckling can occur in the structure. Similarly, for cylindrical shells, more than one mode of failure is possible based on the number of circumferential waves in the critical buckling load. The initial geometric configuration and the amount of imperfection are the factors determining which mode will occur, and since the geometric imperfections are treated as random variables, the same arch or shell may buckle in more than one mode. For this case, the state of the system is described by the state of its components as Eq. (2.3) becomes

$$g_i(X) = C_i - C_i(X) \quad (2.32)$$

where $g_i(X)$, $i=1, \dots, n$, defines each mode of failure. The threshold C_i can be the same if the

failure mode is assumed to be the exceeding of a certain deflection or stress, or more than one threshold can be used for the case of combining failure modes based on deflections along with stresses. The failure, F , for a series systems can then be given as

$$F = \bigcup_i g_i(X) \leq 0 \quad (2.33)$$

The failure probability of series systems is calculated in terms of upper and lower bounds. First-order bounds make use of the individual component failure probabilities only, while second-order bounds make use of individual probabilities along with the intersection probabilities defined as

$$P_{f_{ij}} = P[g_i(X) \leq 0 \cap g_j(X) \leq 0] \quad (2.34)$$

2.8.1 Unimodal Bounds

This is the simplest case where first-order lower P_L and upper P_U bounds are obtained as

$$P_L = \max_{i=1}^n (P_{f_i})$$

$$P_U = \min \left[\sum_{i=1}^n P_{f_i}, 1 \right] \quad (2.35)$$

2.8.2 Bimodal Bounds

One formula for the second-order bounds is given by Ditlevsen (1979) as

$$\begin{aligned}
P_L &= P_{f_1} + \sum_{i=2}^n \max \left\{ 0, \left(P_{f_i} - \sum_{j=1}^{i-1} P_{f_{ij}} \right) \right\} \\
P_U &= P_{f_1} + \sum_{i=2}^n \left\{ P_{f_i} - \max_{j=1}^{i-1} P_{f_{ij}} \right\}
\end{aligned} \tag{2.36}$$

2.8.3 Reliability Index for Bounds

Reliability indices for the lower β_L and upper β_U bounds are given as

$$\begin{aligned}
\beta_L &= -\Phi^{-1}(P_U) \\
\beta_U &= -\Phi^{-1}(P_L)
\end{aligned} \tag{2.37}$$

2.9 Random Field Discretization

Analysis based on the aforementioned reliability theory is founded on introducing randomness into structural problems in the form of discrete random variables. However, description of structure geometry, loading, and material properties usually involves continuous functions for which uncertainties may be specified in terms of random fields. Thus, before undertaking reliability analysis, the random fields must be transformed into sets of discrete random variables.

The proposed discretization approach is based on the use of mean, variance and autocorrelation coefficient functions of a given random field. The dimension of the vector X of random variables for reliability analysis depends on the number of random variables used in the selected discretization technique. Thus, the number of random variables required for accurate discretization affects the computational effort in the reliability analysis.

Following the notation of Li and Der Kiureghian (1993), we consider a multidimensional Gaussian random field $v(z)$ defined on the domain Ω of physical space where $z \in \Omega$ as shown in Fig. 2.3. One of the most common and convenient ways to represent the field is through its mean function $\mu(z)$, variance function $\sigma^2(z)$, and the autocorrelation coefficient function $\rho(z, z')$. Also let v , $[v=v_1, v_2, \dots, v_n]$, denote a vector of Gaussian random variables with a mean vector μ and a covariance matrix Σ_{vv} through which the random field is to be described.

Four methods of discretization for the random field are considered within the scope of this study. The simplest of the four is the midpoint (MP) method (Der Kiureghian and Ke, 1988) where the field within the domain Ω_k of element k is described by a single random variable representing the value of the field at a central point z_k of the element. The field value within the element is assumed to be a constant, i.e.,

$$\hat{v}(z) = v(z_k); \quad z \in \Omega_k \quad (2.38)$$

where $\hat{v}(z)$ is an approximating vector consisting of a set of random variables which represent the discretized random field $v(z)$. The mean vector μ and the covariance matrix Σ_{vv} of $\hat{v}(z)$ are readily available from the mean, variance, and autocorrelation coefficient functions of the field evaluated at the element central points.

The second method considered is the local averaging (LA) method (Vanmarcke and Grigoriu, 1983) where the approximating field within each element is described in terms of the local average of the field over the element, \bar{v}_e , i.e.,

$$\hat{v}(z) = \int_{\Omega_k} v(z) d\Omega / \int_{\Omega_k} d\Omega = \bar{v}_e; \quad z \in \Omega_k \quad (2.39)$$

The mean vector μ and the covariance matrix Σ_{vv} of $\hat{v}(z)$ in this case are obtained in terms of integrals of the moment functions of the random field over the elements (Vanmarcke 1983).

The realization of the random field based on both MP and LA methods is a stepwise function with discontinuity along the element boundaries. One might expect a somewhat smaller discontinuity in the latter method because of the averaging process. However, a relatively fine mesh is required in both methods for accurate representation of the field.

The third method of random field discretization is the series expansion method based on the Karhunen-Loeve (KL) theorem (Lawrence, 1987, and Spanos and Ghanem, 1989). In this method the random field is expressed in terms of its spectral decomposition as

$$\hat{v}(z) = \mu(z) + \sigma(z) \sum_{i=1}^r \xi_i \sqrt{\lambda_i} f_i(z) ; \quad z \in \Omega \quad (2.40)$$

where ξ_i is a set of independent standard normal variates (zero mean, unit variance, zero correlation) and λ_i and $f_i(z)$ are the eigenvalues and eigenfunctions of the correlation function obtained from the integral equation

$$\int_{\Omega} \rho(z, z') f_i(z') dz' = \lambda_i f_i(z) \quad (2.41)$$

where the eigenfunctions are normalized to satisfy

$$\int_{\Omega} f_i(z) f_j(z) dz = \delta_{ij} \quad (2.42)$$

where

$$\delta_{ij} = \begin{cases} 1 & \text{if } i = j \\ 0 & \text{if } i \neq j \end{cases} \quad (2.43)$$

Theoretically, an infinite series ($r \rightarrow \infty$) is required for the complete representation of the random field in Eq. 2.40. However, usually only a few of the terms with the largest eigenvalues are enough to represent the field. The KL method requires the numerical evaluation of the eigenfunctions of the autocorrelation coefficient kernel in general. However, if the exact eigenfunctions are available, the KL method does not require a discretization of the domain Ω , and it is found to be the most efficient method of the four techniques considered here for discretizing the random field, i.e., it requires the smallest number of random variables to describe the field within a given level of accuracy as will be seen in the numerical analysis. The normal distribution for ξ_i is only valid if the random field is Gaussian. For other distributions of the random field, the distribution of ξ_i is very complicated and unknown. Analysis based only on the distribution moments is feasible in this case.

The final method, proposed by Zhang and Ellingwood (1994), uses a series expansion (SE) similar to that of Eq. 2.40 but with $f_i(z)$ replaced by any set of orthogonal functions in the generalized Fourier-type series form

$$\hat{v}(z) = \mu(z) + \sum_{i=1}^r \eta_i c_i h_i(z) ; \quad z \in \Omega \quad (2.44)$$

where η_i is a vector of zero-mean random variables, c_i is a vector of constant deterministic variables to be determined, and $h_i(z)$ is a given complete set of orthonormal functions. Using the definition of the covariance function $C(z, z')$ of the random field $v(z)$, along with the orthonormality of $h_i(z)$, it follows that

$$C_{mn} = \int_{\Omega} \int_{\Omega} C(z, z') h_m(z) h_n(z') dz dz' = c_m c_n E[\eta_m \eta_n] \quad (2.45)$$

Thus, Eq. 2.45 provides a set of equations for the variables c_i and the covariances $E[\eta_i \eta_j]$. The use of the SE method has an advantage over the KL method in general, in that no integral equation need to be solved. For simplicity, η_i can be taken to have unit variance and then C_m is given by Eq. 2.45 for $m = n$.

All existing methods of discretization relate $v(z)$ to $\hat{v}(z)$ through a linear transformation, thus assuming \hat{v} is Gaussian preserves the Gaussianity of $v(z)$. Many non-Gaussian random fields are transformable to Gaussian fields through nonlinear marginal transformations such as Nataf-type model (Nataf, 1962). Basically, the Nataf model uses the values of the marginal distributions and the correlation coefficients between the non-Gaussian variables in the x -space to obtain the distribution and the correlation of the variables in the u -space. For a simple case of statistically independent variables, the transformation takes the form

$$u_i = \Phi^{-1}[F_X(x_i)] \quad (2.46)$$

where $\Phi^{-1}(\dots)$ is the inverse of the standard normal cumulative distribution function and $F_X(x_i)$ is the cumulative distribution function (CDF) of the variable x_i . The application of this model was explained by Der Kiureghian and Liu (1986). This model makes use of the first two moments only of the probability distribution.

However, probabilities in structural reliability problems are often very small, making results sensitive to the tail regions of the probability distributions which are more affected by higher moments of the distribution. Therefore, for a non-Gaussian random field, a

direct application of these nonlinear transformations may not provide sufficient accuracy in tail probabilities, even if the first two moments are accurately represented. However, in most cases, the distribution of $\hat{v}(z)$ would be nearly Gaussian due to the central limit theory, regardless of the distribution of $v(z)$ (see Li and Der Kiureghian, 1993).

2.10 Boundary Conditions

If the value of the random field is restricted at the boundary of the domain Ω , then the random field is inhomogenous and this must be taken account of in the discretization. The SE method discretizes the random field using a set of complete orthogonal basis functions which satisfy the boundary conditions. Therefore, the SE method requires no further consideration. However, for the arch under study, when using the MP, LA or KL methods to discretize the field, special considerations are necessary.

The random field representing the imperfections is considered to have a known mean function and a known autocorrelation function for random variations about the mean. This way the random field can be considered, strictly speaking, homogenous in the second moments only, i.e, the variance function is taken to be a constant while the mean function can vary from a point to another. This can be considered as a superposition of a homogenous random field, with a zero mean, representing the imperfection and a deterministic function specifying the mean imperfection along the arch. The autocorrelation coefficient function for the random field can be described by

$$\rho(z, z') = \rho_o(z, z') + \frac{\mu(z)\mu(z')}{\sigma^2} \quad (2.47)$$

where $\rho_o(z, z')$ is a homogenous autocorrelation function for the random field with zero

mean, while $\rho(z, z')$ is inhomogenous because of its dependence on the mean values at z, z' . However, if boundary conditions are enforced on the random field, then $\rho_o(z, z')$ need not to be homogenous.

For cylindrical shells, the two-dimensional random fields defining the geometrical imperfection is strictly homogenous in the circumferential direction as the cylindrical shell is continuous. However, in the axial direction, we are faced with problem of considering the effect of the boundary conditions on the homogeneity of the random field. Thus, the boundary conditions effects are analyzed in a one-dimension only for both the arch and the cylindrical shell.

For the arch, one possible approximation is to ignore the effect of the boundaries entirely in the discretization process. In another approach, (believed to be novel), we postulate that the small initial curvature $\mathbf{K}(\theta)$ of the imperfection is a homogenous random field. Then, by integrating twice, the imperfection in the arch is given by the inhomogenous function

$$\bar{w}(\theta) = \int_{-\beta}^{\theta} \int_{-\beta}^{\theta'} \mathbf{K}(\theta'') d\theta' d\theta'' + C_1 \theta + C_2 \quad (2.48)$$

where θ is the polar angle measured from the center of the arch and C_1 and C_2 are random coefficients computed for each realization of the imperfections so as to satisfy the boundary conditions, e.g., $\bar{w}(\pm\beta) = 0$ where β is one-half the included angle of the arch. The relation between the autocorrelation functions for $\mathbf{K}(\theta)$ and $\bar{w}(\theta)$ can be determined by a differential equation. A similar relation for the imperfections \bar{W} in the cylindrical shell in the axial direction x can be given by

$$\overline{W}(x) = \int_0^x \int_0^{x'} \mathbf{K}(x'') dx'' dx' + C_1 x + C_2 \quad (2.49)$$

Comparison of results will determine the magnitude of error from neglecting the inhomogeneity in the first approach. The use of Eq. 2.48 or Eq. 2.49 is not required in the SE method if the expansion functions $h_i(z)$ satisfy the boundary conditions.

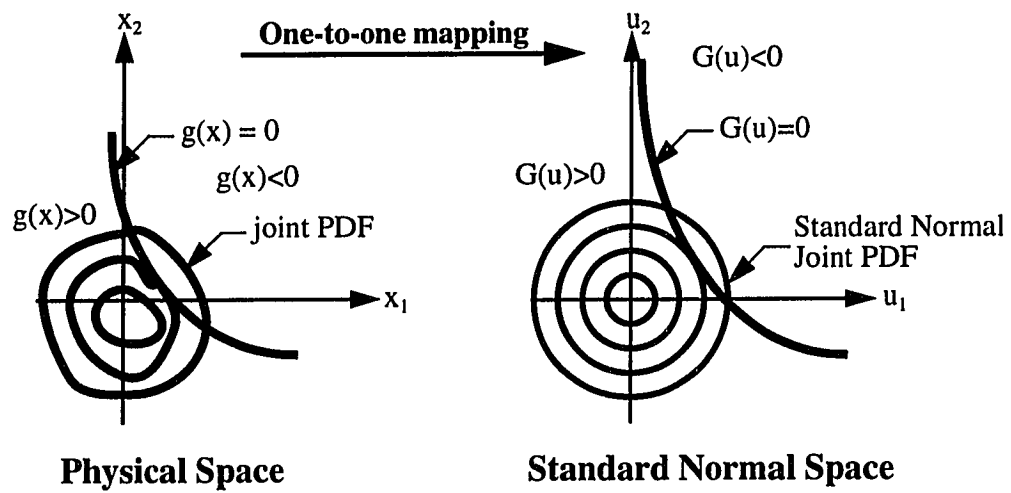


Figure 2.1 Nonlinear transformation of the physical space into the standard normal space

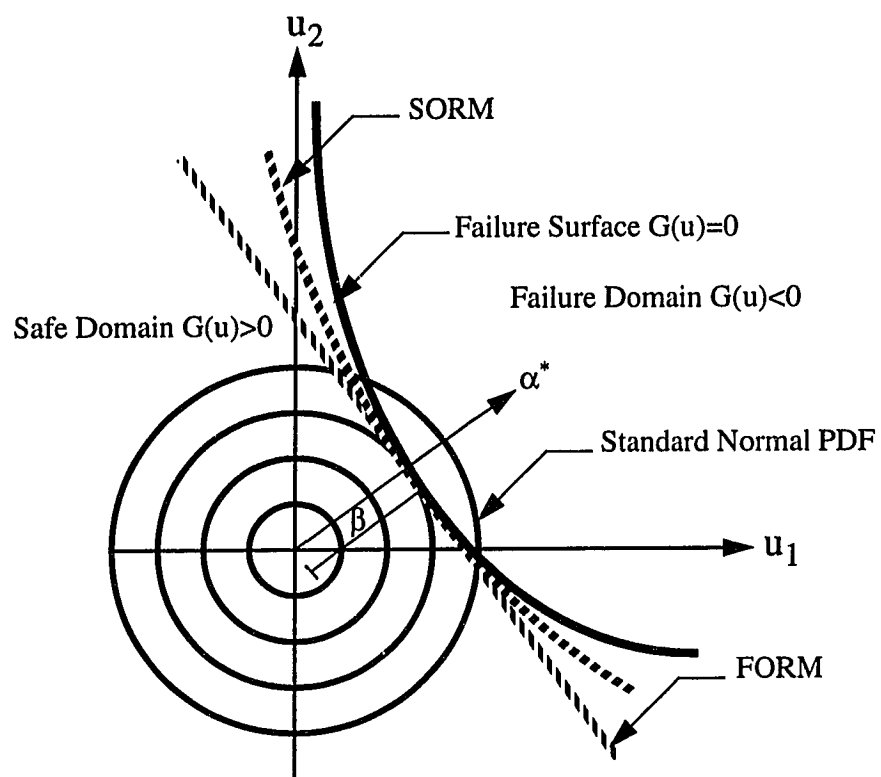


Figure 2.2 FORM and SORM approximations to the failure surface in the standard normal space

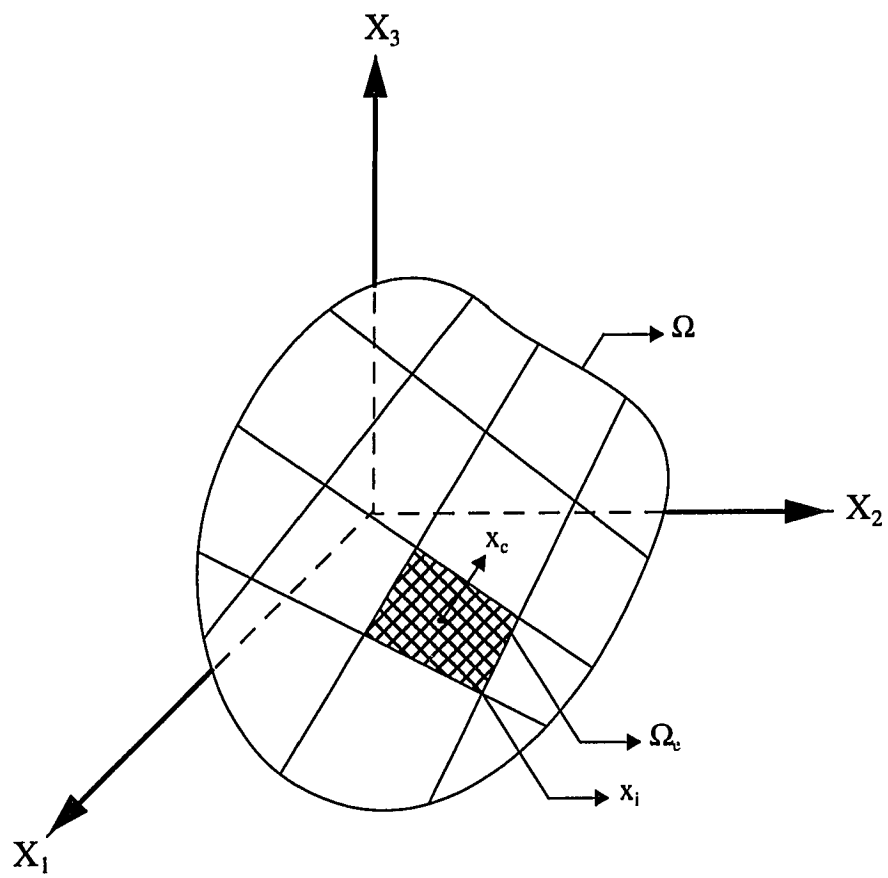


Figure 2.3 Random field mesh

Chapter 3

Stability of Shallow Arches

3.1 Introduction

The buckling resistance of shallow arch-type structures subjected to a random transverse load is investigated. A probabilistic analysis of the randomness in the geometric imperfections along with the uncertainty in the loading and the material properties is presented. The study investigates the effect of spatial variability of different random parameters in the problem on the buckling load and the associated displacements.

In the present study, we first review the deterministic analysis methods for the instability of shallow arches. The plane buckling loads for different modes of instability of the arch under various loads and boundary conditions are obtained by nonlinear energy analysis. The mode of instability depends on a dimensionless shallowness parameter. For large values of this parameter, the perfect arch bifurcates into an unsymmetric mode shape. For small values of the shallowness parameter, the perfect arch reaches a limit load in a symmetric mode shape. Imperfections lead to a limit load instability in both cases with stronger imperfection sensitivity in the unsymmetric case.

Next, considering initial imperfections to be random fields with known autocorrelation coefficient functions over the arch, characterization of the random buckling load is treated

as a problem in structural reliability theory. Various types of autocorrelation coefficient functions are used to better characterize the structure and the imperfections. The random field for the imperfection is discretized by the following methods: a) Midpoint (MP) method; b) Local averaging (LA) method; c) Karhunen-Loeve (KL) theorem; d) Series expansion (SE) method. In the first three of these methods, special calculations are taken to account for inhomogeneity of the autocorrelation function due to end conditions.

Both first- and second-order reliability methods (FORM/SORM) along with Monte Carlo simulation with the aid of the deterministic energy method are used to evaluate different modes of failure based on the buckling load or the associated displacements. Numerical results are presented to compare the convergence of the four discretization methods and evaluate the effect of the non-stationarity. The probability density and the cumulative distribution functions of the buckling load are presented for different distribution inputs. The imperfection sensitivity of the arch is evaluated from consideration of the distribution of the buckling load for various values of the shallowness parameter. An extensive parametric study is performed to establish a better understanding of the effects of the spatially variable imperfections on the buckling arch-structure.

3.2 Deterministic Stability Analysis

Let us consider a shallow circular arch of rectangular cross section, which generalizes readily to other cross sections. Both ends of the arch are either pinned or clamped and the arch is subjected to a radial or a concentrated loading as shown in Fig. 3.1. In view of the shallowness assumption, the elastic axial membrane strain, ϵ , is given by

$$\varepsilon = \frac{1}{R}(u_{,\theta} - w) + \frac{1}{2R^2}(w_{,\theta})^2 \quad (3.1)$$

and the change in curvature, κ , by

$$\kappa = \frac{1}{R^2} w_{,\theta\theta} \quad (3.2)$$

in which θ is the polar angle measured from the center of the arch, R is the radius of the arch, u is the tangential displacement and w is the radial displacement.

The initial geometric imperfections are specified as deviations from the perfect circular shape by the function $\bar{w}(\theta)$. The axial strain can then be written as

$$\varepsilon = \frac{1}{R}(u_{,\theta} - w) + \frac{1}{2R^2}(w_{,\theta} + 2w_{,\theta}\bar{w}_{,\theta})^2 \quad (3.3)$$

in which w and u now are the elastic displacements measured from the imperfect arch, and the change in curvature is still given by Eq. 3.2.

The total potential energy H of the system can be written in the dimensionless form

$$H = \frac{1}{2} \int_{-\beta}^{\beta} \varepsilon^2 d\theta + \frac{t^2}{24R^2} \int_{-\beta}^{\beta} \kappa^2 d\theta - \frac{1}{EtbR} \Omega(P, w) \quad (3.4)$$

where t is the thickness and b is the width of the arch, E is Young's modulus, β is one-half the included angle of the arch, P is the radial load, and the work term $\Omega(P, w)$ depends on the manner of loading.

Two methods of solution can be applied at this point, an exact solution based on the governing differential equations obtained from Eq. 3.4, which will be used for an introductory case involving only a one-variable imperfection. The second method is based on a series solution obtained directly from minimization of H and allows a better

representation of the complete spatial geometric imperfection.

3.3 Exact Stability Solution

For tangential equilibrium, the variation of the energy H , given by Eq. 3.4, with respect to the displacement u must be zero, thus

$$\begin{aligned}\epsilon_{,\theta} &= 0 \\ \epsilon &= C\end{aligned}\tag{3.5}$$

in which C is a constant proportional to the compressive membrane force in the arch.

Schreyer and Masur (1966) suggested a convenient form for C as

$$C = -\frac{t^2}{12R^2}\rho^2\tag{3.6}$$

where ρ is a constant independent of θ .

For radial equilibrium, the variation of the total energy H , given by Eq. 3.4, with respect to the displacement w must be zero. Substituting for ϵ from Eq. 3.5 and Eq. 3.6, with the use of Eq. 3.1, into Eq. 3.4, and differentiating, yields

$$\frac{d^4 w}{d\theta^4} + \rho^2 \frac{d^2 w}{d\theta^2} = \bar{\Theta}(P, \rho)\tag{3.7}$$

where the function $\bar{\Theta}(P, \rho)$ is dependent on the loading case under consideration. The previous differential equation can be reduced to a simpler form by introducing $\eta = \rho\theta$.

Thus Eq. 3.7 can be written as

$$\frac{d^4 w}{d\eta^4} + \frac{d^2 w}{d\eta^2} = \Theta(P)\tag{3.8}$$

in which the function $\Theta(P)$ depends on the loading case considered.

In the general case, the behavior pattern of the arch with a defined initial imperfection at its apex, and linearly varying on both sides till it vanishes at the supports, is similar to that of an arch under an antisymmetric loading component (Masur and Lo 1972). Based on this criterion, it is instructive and convenient to separate any load P into its symmetric and antisymmetric components by setting

$$\begin{aligned} P(\theta) &= P_s(\theta) + P_a(\theta) \\ P_s(\theta) &= P_s(-\theta) \quad P_a(\theta) = -P_a(-\theta) \end{aligned} \quad (3.9)$$

Thus, a general solution of Eq. 3.8 may be expressed in the form

$$\begin{aligned} w &= w_s(\eta) + w_a(\eta) \\ \frac{d^4 w_s}{d\eta^4} + \frac{d^2 w_s}{d\eta^2} &= \Theta_s(P_s) \quad w_s(\theta) = w_s(-\theta) \\ \frac{d^4 w_a}{d\eta^4} + \frac{d^2 w_a}{d\eta^2} &= \Theta_a(P_a) \quad w_a(\theta) = -w_a(-\theta) \end{aligned} \quad (3.10)$$

where the functions $\Theta_s(P_s)$ and $\Theta_a(P_a)$ are loading functions in the same way as the function $\Theta(P)$ based on the use of the symmetric and antisymmetric components, respectively, of the applied load. Although the governing equation is nonlinear, a linear superposition of the displacements is feasible at this stage since the nonlinearity of the problem will be taken care of later in the analysis.

As earlier described, linear initial geometric imperfection or load position imperfection will result in analyzing a stability problem with a combination of both symmetric and antisymmetric loading components, even if the original applied load was symmetric.

3.3.1 Uniform Radial Loading

The loading function $\Omega(P, w)$ in this case will be

$$\Omega(P, w) = \int_{-\beta}^{\beta} p w d\theta \quad (3.11)$$

where $p = P/2\beta$ is the intensity of the pressure per unit length acting on the arch. The governing equation will be in the form

$$\frac{d^4 w}{d\eta^4} + \frac{d^2 w}{d\eta^2} = \frac{q}{\gamma^2} \quad (3.12)$$

where $\gamma = \rho\beta$ and

$$q = \frac{24R^3\beta^3P}{Et^3b\gamma^2} - 4R\beta^2 \quad (3.13)$$

The general solution of Eq. 3.12 is

$$w = \frac{q(\eta^2 - 2)}{2\gamma^2} + C_1 \cos \eta + C_2 \sin \eta + C_3 \eta + C_4 \quad (3.14)$$

and by substituting the following boundary conditions in the solution

$$\begin{aligned} w = \frac{dw}{d\eta} = 0 \quad \text{at } \eta = \pm\gamma \quad & \text{for clamped ends} \\ w = \frac{d^2 w}{d\eta^2} = 0 \quad \text{at } \eta = \pm\gamma \quad & \text{for hinged ends} \end{aligned} \quad (3.15)$$

a set of four simultaneous equations in terms of C_1, C_2, C_3, C_4 and q (in terms of γ) are obtained. The fifth equation may be obtained by applying the boundary condition $u = 0$ at $\eta = \pm\gamma$ and using Eq. 3.5 and Eq. 3.1 as

$$\frac{1}{2\mu} \int_{-\gamma}^{\gamma} \epsilon d\eta = -\frac{t^2 \rho^2}{12R^2} \quad (3.16)$$

thus

$$\int_{-\gamma}^{\gamma} w d\eta - \frac{\gamma^2}{2R\beta^2} \int_{-\gamma}^{\gamma} \left(\frac{dw}{d\eta}\right)^2 d\eta - \frac{t^2 \gamma^3}{6R\beta^2} = 0. \quad (3.17)$$

Using the value of w from Eq. 3.14 in the previous relation gives a quadratic in terms of q .

In order to get the load-deflection relation, we start by setting a value for γ , solve for q from the previous quadratic, then obtain w and P from Eq. 3.14 and Eq. 3.13 respectively.

This gives two points on the load-deflection curve (starting from both ends).

3.3.2 Center Point Normal Loading

The loading function $\Omega(P, w)$ in this case will be

$$\Omega(P, w) = Pw_o \quad (3.18)$$

where w_o is the deflection at the center point of the arch and P is the magnitude of the concentrated load. The governing equation will be in the form

$$\frac{d^4 w}{d\eta^4} + \frac{d^2 w}{d\eta^2} = \frac{1}{\gamma^2} \left[\frac{12PR^3\beta^3}{Et^3b\gamma} \delta(\eta) - R\beta^3 \right] \quad (3.19)$$

The general solution of Eq. 3.19 is

$$w = \frac{1}{\gamma^2} \{ C_1(1 - \cos\eta) + C_2(\eta - \cos\eta) + C_3\eta + C_4 \} \\ - \frac{12PR^3\beta^3}{Et^2b\gamma^3} \left[\sin\left(\eta - \frac{\gamma}{2}\right) - \left(\eta - \frac{\gamma}{2}\right) \right] U(\eta) - \frac{R\beta^2}{\gamma^2} \left(\frac{\eta^2}{2} - 1 + \cos\eta \right) \quad (3.20)$$

in which

$$U(\eta) = \begin{cases} 0 & \eta < 0 \\ 1 & \eta > 0 \end{cases} \quad (3.21)$$

The aforementioned boundary conditions and the additional relation given by Eq. 3.17 still applies.

3.3.3 Linearly Varying Radial Loading

The loading function $\Omega(P, w)$ in this case will be

$$\Omega(P, w) = \frac{P}{8\beta^2} \int_{-\beta}^{\beta} \theta w d\theta \quad (3.22)$$

where P is the total radial load acting on the arch. The governing equation will be in the form

$$\frac{d^4 w}{d\eta^4} + \frac{d^2 w}{d\eta^2} = \frac{1}{\gamma^2} \left[\frac{\eta(q + R\beta^2)}{2\gamma} - R\beta^2 \right] \quad (3.23)$$

The general solution of Eq. 3.23 is

$$\begin{aligned} w = & C_1 \cos \eta + C_2 \sin \eta + C_3 \eta + C_4 \\ & + (q + R\beta^2) \left[\frac{\eta^3}{12\gamma^2} - \frac{\eta}{2\gamma^3} \right] + \frac{R\beta^2}{\gamma^2} \left[1 - \frac{\eta^2}{2} \right] \end{aligned} \quad (3.24)$$

The aforementioned boundary conditions and the additional relation given by Eq. 3.17 still applies.

3.3.4 Limit-load vs. Bifurcation Buckling

For a general shallow arch with unsymmetrical conditions either in the boundaries or in the loading, the previous solutions yield only one equilibrium path and the

corresponding buckling load.

The limit buckling load is the maximum load P associated with a symmetrical deformation, whereas the bifurcation load is the load at which the deformation bifurcates into an unsymmetrical form from a previous symmetric shape. For initially symmetric arches, with symmetric boundary conditions and loads, both the limit buckling load, P_l , and the bifurcation buckling load, P_b , can be determined numerically. Example load versus center deflection curves are shown in Fig. 3.2 for a typical case in which bifurcation buckling occurs first.

Depending on the value of λ , the perfect arch would buckle either symmetrically or unsymmetrically. In order to determine which type of buckling actually takes place, the corresponding deflections, w_l and w_b , must be examined. Although P_b is always less than P_l . If $w_b < w_l$, then the arch deformation will bifurcate unsymmetrically. Otherwise, the bifurcation occurs in the unstable region ($w_b > w_l$), and symmetric limit buckling occurs first. In the last case, the arch passes into a transitional asymmetric equilibrium path after it has already buckled along a symmetrical equilibrium path, and the governing buckling load is P_l .

Schreyer and Masur (1971) showed that for arches with clamped ends, under uniform radial loading, the buckling mode depends on the value of μ and λ as follows:

1. For $\lambda < 2.85$, i.e. $\gamma_{max} < \pi$, no buckling occurs.
2. For $2.85 \leq \lambda < 5.02$, i.e. $\pi \leq \gamma_{max} < 1.43\pi$, only symmetric buckling occurs.
3. For $5.02 \leq \lambda < 5.74$, i.e. $\gamma_{max} \geq 1.43\pi$, antisymmetric bifurcation occurs but the arch is still governed by the symmetric buckling criterion.

4. For $\lambda > 5.74$, i.e. $\gamma_{max} > 1.43\pi$, only antisymmetric buckling occurs.

Where λ is a geometric parameter given by

$$\lambda = \frac{\beta^2 R}{t} \equiv 2 \frac{h}{t} \quad (3.25)$$

in which h is the height of the arch.

The previous relations are valid for a perfect arch with no imperfections. Depending on the amount of the initial imperfection and its standard deviation, the arch can buckle in either mode for each single realization of the random numbers in the same problem.

3.3.5 Numerical Results

The buckling behavior of three shallow arches with the properties defined in Table 3.1 are studied. Numerical values are considered for the geometrical parameters and for the

Table 3.1: Arch properties

Arch Number	β degree	Young's Modulus, E lb/in. ²	λ	R inch	b inch	t inch
1	30	29E6	2.69	3.65	1.00	0.37
2	30	29 E6	5.48	3.65	1.00	0.18
3	30	29 E6	7.31	3.65	1.00	0.14

modulus of elasticity rather than using dimensionless solutions, as considered later in the chapter, in order to facilitate studying the effects of both uncertainties in material and geometric quantities on the buckling load without any normalizations. Load-deflection curves were obtained for each case. Various combinations of loadings and boundary

conditions are considered. An example loading case is considered for the three arches under a combination of a uniformly distributed radial loading combined with a linearly varying load. Both the modulus of elasticity and the magnitude of the linear loading are considered as random variables with statistical properties as shown in Table 3.2. The

Table 3.2: Random variables

Random Variable	Mean μ	Variance σ^2
E	29E6	0.25
P_a	1.0	0.50

consideration of a random variable representing the amount of the varying load allows for considering uncertainty in the loading amount and position and can also be integrated in order to allow for consideration of an initial geometric imperfection.

A basic analysis is first done using the mean values of the random variables. Load-deflection curves are shown in Fig. 3.3 for the case of clamped ends arch. The relation is plotted between the center deflection \bar{w}_o and the load $P^* = P_s R / \beta b E t^2$ while the relation between the axial force γ in the arches and the load applied is shown in Fig. 3.4. Different values for the mean of the linear varying load $\mu(P_a)$ are considered and the resulting response are plotted in Fig. 3.5 and Fig. 3.6. The mean values considered are 0, 0.2, ..., 1.0. The highest mean value correspond to the most inner curves.

The reliability code CALREL is used to evaluate the probability of failure of the arch using the form given by Eq. 2.3. Two failure criteria are considered based on exceeding a defined threshold for the load applied or for the resulting deflection. Both symmetric and

antisymmetric modes of failure are considered. This gives a total of four limit-state functions where any of them can be considered individually as the failure criteria or a combination of two or more formulating a series system reliability problem.

Results will be shown for the failure probability of an arch with clamped ends and having the geometric configuration number 2 given in Table 3.1 where a small change in the value of λ would change the buckling mode of the arch. The complete statistical distribution of the buckling load or the resulting deflection can be obtained by varying the value of the threshold C_l as defined by Eq. 2.3 over a range of values and evaluating the failure probability for each value. Then the CDF can be evaluated as

$$F_{P_f}(C_l) = 1 - P_f(C_l) \quad (3.26)$$

where $F_{P_f}(C_l)$ is the value of the CDF based on a given value of the threshold C_l .

The CDF is shown in Fig. 3.7 for the aforementioned case giving the distribution of the buckling load for the unsymmetric mode only. The PDF can be obtained by computing the gradients of the CDF, Fig. 3.8, or better by using the values of the sensitivity with respect to limit state parameter which is readily available during FORM analysis as shown in Fig. 3.9. The effect of considering the randomness in the modulus of elasticity as well does not have a large effect on the results as shown in Fig. 3.10. The effect of changing the mean of the linear loading component is shown in Fig. 3.11, while the effect of changing the variance is shown in Fig. 3.12.

The previous graphs were plotted for an arch with clamped ends. In order to compare the effect of the boundary conditions, we will consider an arch with hinged supports and having same values for all other parameters as the clamped arch. The loads are normalized

by dividing by the value of the buckling load of the perfect arch, P_{perf}^* , in each case. The CDFs are obtained for both of them as shown in Fig. 3.13.

Considering both symmetric and antisymmetric modes for the buckling of the same arch and using bimodal bounds for the failure probabilities, the CDFs can be obtained as shown in Fig. 3.14. The distribution is shown for the case of considering the symmetric buckling load alone and for the considering the average of the bounds on the probability of failure for the two modes. The figure clearly shows the increase in the failure probability when considering the two modes especially in the lower range of the curve as the bifurcation load is lower than the limit-buckling load.

3.4 Series Stability Solution

The solution technique given in the previous paragraphs has the advantage of working with a closed form formula for obtaining the buckling load and the deflections. This makes it easier and less time consuming for the reliability analysis. However, the exact method can not be applied easily for a general type of imperfections defined at every single point along the arch. Hence the need for a series solution appears in order to be able to expand the initial shape of the arch in terms of Fourier coefficients up to a sufficient accuracy.

The axial membrane strain and the change in curvature are given by Eq. 3.4 and Eq. 3.2 respectively. For tangential equilibrium, the variation of the total energy with respect to the displacement u must be zero. Therefore, the axial strain is found to have a constant value given by

$$\varepsilon = -\frac{1}{2R\beta} \int_{-\beta}^{\beta} \left[w - \frac{1}{2R} (w^2_{,\theta} + 2w_{,\theta} \bar{w}_{,\theta}) \right] d\theta \quad (3.27)$$

Substitution of this value for ε into the energy expression given by Eq. 3.4 yields the total energy H as a function of w in the form

$$H = \frac{1}{4R^2\beta} \left\{ \int_{-\beta}^{\beta} \left[w - \frac{1}{2R} (w^2_{,\theta} + 2w_{,\theta} \bar{w}_{,\theta}) \right] d\theta \right\}^2 + \frac{t^2}{24R^2} \int_{-\beta}^{\beta} w^2_{,\theta\theta} d\theta - \frac{1}{EtbR} \Omega(P, w) \quad (3.28)$$

We expand both w and \bar{w} in generalized Fourier series as

$$w = \sum_{n=1}^{\infty} A_n w_n(\zeta) \quad (3.29)$$

and

$$\bar{w} = \sum_{n=1}^{\infty} C_n w_n(\zeta) \quad (3.30)$$

where

$$\zeta = \theta/\beta \quad (3.31)$$

in which A_n and C_n are the amplitudes of the appropriate basis function $w_n(\zeta)$. Then Eq. 3.28 becomes

$$\begin{aligned} H^* = & \frac{\lambda}{2} \left\{ \int_{-1}^1 \left[\sum_{n=1}^{\infty} a_n w_n \right] d\zeta - \frac{1}{2} \int_{-1}^1 \left[\sum_{n=1}^{\infty} a_n w_{n,\zeta} \right]^2 d\zeta - \int_{-1}^1 \left[\sum_{n=1}^{\infty} a_n w_{n,\zeta} \right] \left[\sum_{n=1}^{\infty} c_n w_{n,\zeta} \right] d\zeta \right\}^2 \\ & + \frac{1}{24\lambda} \int_{-1}^1 \left[\sum_{n=1}^{\infty} a_n w_{n,\zeta\zeta} \right]^2 d\zeta - \Omega(P^*, w) \end{aligned} \quad (3.32)$$

where

$$H^* = \frac{H\lambda}{\beta^5}, \quad \lambda = \frac{\beta^2 R}{t}, \quad P^* = \frac{PR}{\beta b E t^2} \quad (3.33)$$

and

$$a_n = \frac{A_n}{R\beta^2}, \quad c_n = \frac{C_n}{R\beta^2}. \quad (3.34)$$

For any position of equilibrium, the potential energy is stationary, i.e.,

$$\frac{\partial H^*}{\partial a_n} = 0 \quad (3.35)$$

The basis functions $w_n(\zeta)$ in the series defined by Eq. 3.29 and Eq. 3.30 depend upon the end conditions of the arch. Preferably $w_n(\zeta)$ should satisfy all geometric and natural boundary conditions in order to minimize the number of terms required. The following basis functions are used:

Both ends pinned:

$$w_n(\zeta) = \sin\left[\frac{n\pi}{2}(1 + \zeta)\right] \quad (3.36)$$

Both ends clamped:

$$w_n(\zeta) = \frac{1}{2} [(-1)^{n+1} + \cos(n\pi\zeta)] \quad (3.37)$$

The loading function $\Omega(P, w)$ is substituted in Eq. 3.32 depending on the typical loading case as discussed before.

Upon substituting the relevant orthogonal series expression, Eq. 3.36 or Eq. 3.37, and the appropriate loading function into Eq. 3.32, the equilibrium condition Eq. 3.35 yields a set of n simultaneous nonlinear algebraic equations for a_1, \dots, a_n for a given P^* . Solution of this set of equations is carried out numerically using the iterated Newton-Raphson

method. Alternatively one may fix w_o and solve for P^* , thus obtaining the complete load-deflection curve.

The same technique used for the case of the exact stability solution for considering whether symmetrical or antisymmetrical buckling criterion will occur still applies for this method of analysis. A complete agreement in the results is obtained between both methods of analysis for the case of a simple geometric imperfection at the midpoint of the arch.

3.5 Random Field Discretization

The application of the reliability theory to the stability of arches involving continuous random fields for modeling geometrical or material imperfection requires the use of any of the discretization techniques mentioned in the previous chapter. The objective is to put the problem in a form that can be analyzed using the component or system reliability theory. The proposed approach is based on the use of mean, variance and autocorrelation coefficient functions of an assumed known random field to characterize the initial imperfection distribution. Thus, the geometric configuration and the material properties of the arch are defined using a one-dimensional random field for each, which are then discretized using a grid of random-field elements and nodes or as a series.

Four examples of autocorrelation functions are considered. Exact eigenfunctions and eigenvalues are available for the first two of them while a numeric algorithm is used for the other two.

3.5.1 First Degree Exponential Autocorrelation Coefficient Function

Consider the kernel defined by the kernel equation

$$\rho(z, z') = e^{-c|z-z'|} \quad (3.38)$$

where c is a parameter setting the correlation length and z, z' are any two points on the arch. The correlation length, δ , is defined as the length at which the correlation value is e^{-1} , i.e., $\rho(\delta) = e^{-1}$ and is given for this kernel as $\delta = 1/c$. This kernel is related to a first order Markovian process and is used extensively in earthquake engineering. Realizations of this process are considered on the interval $[-a, +a]$. A closed form solution for the eigenvalues and eigenfunctions for this kernel is given by Van Trees (1968) as

for n odd

$$\lambda_n = \frac{2c}{\omega_n^2 + c^2}, \quad (3.39)$$

$$f_n(z) = \frac{\cos(\omega_n z)}{\sqrt{a + \frac{\sin(2\omega_n a)}{2\omega_n}}} \quad (3.40)$$

and for n even

$$\lambda_n^* = \frac{2c}{\omega_n^{*2} + c^2}, \quad (3.41)$$

$$f_n^*(z) = \frac{\sin(\omega_n^* z)}{\sqrt{a - \frac{\sin(2\omega_n^* a)}{2\omega_n^*}}} \quad (3.42)$$

where ω_n and ω_n^* are the solutions to the transcendental equations

$$c - \omega \tan(\omega a) = 0 \quad (3.43)$$

and

$$\omega^* - c \tan(\omega^* a) = 0 \quad (3.44)$$

3.5.2 Triangular Autocorrelation Coefficient Function

Consider the function defined as

$$\rho(z, z') = 1 - d|z - z'| \quad (3.45)$$

where d is a parameter which can be used to adjust the distance $|z - z'|$ of null correlation between z and z' . The correlation length is given for this kernel as $\delta = (1/d)(1 - e^{-1})$. This kernel represents a linear decrease in correlation with separation, which may be useful for certain quality control considerations arising from this study. The formulas for the eigenvalues and eigenfunctions for this kernel are given by Spanos and Ghanem (1989) as

for n odd

$$\lambda_n = \frac{2d}{\omega_n^2 \sigma^2} \quad (3.46)$$

$$f_n(z) = \frac{\cos(\omega_n z) + \tan\left(\frac{\omega_n a}{2}\right) \sin(\omega_n z)}{\sqrt{a + \left[\tan^2\left(\frac{\omega_n a}{2}\right) - 1\right] \left(\frac{a}{2} - \frac{\sin(2\omega_n a)}{4\omega_n}\right) + \frac{1}{\omega_n} \sin^2(\omega_n a) \tan\left(\frac{\omega_n a}{2}\right)}} \quad (3.47)$$

and for n even

$$\lambda_n = \frac{2d}{\omega_n^2 \sigma^2} \quad (3.48)$$

$$f_n(z) = \frac{\cos(\omega_n^* z)}{\sqrt{\frac{a}{2} + \frac{\sin(2\omega_n^* a)}{2\omega_n^*}}} \quad (3.49)$$

where ω_n and ω_n^* are the solutions to the transcendental equations

$$\tan\left(\frac{\omega_n a}{2}\right) = \frac{2}{\omega_n \left(\frac{2}{d} - a\right)} \quad (3.50)$$

and

$$\omega_n^* = (n-1)\frac{\pi}{a}, \quad n=2, 4, 6, \dots \quad (3.51)$$

3.5.3 Second Degree Exponential Autocorrelation Coefficient Function

Consider the function defined as

$$\rho(z, z') = e^{-[c(z-z')]^2} \quad (3.52)$$

where c is a parameter used to adjust the correlation length and z, z' are any two points on the arch. The correlation length, δ , is given for this kernel as $\delta = 1/c$.

3.5.4 Sinusoidal Autocorrelation Coefficient Function

Consider the function defined as

$$\rho(z, z') = \frac{\sin[c(z-z')]}{c(z-z')} \quad (3.53)$$

where the parameter c is used to adjust correlation length. For the last two kernels there is no closed-form solution for the eigenvalues and eigenfunctions of the KL expansion.

3.6 Numerical Results

Results are presented for the stability of shallow arches with various combinations of loadings and boundary conditions. The geometrical imperfection in the arch is assumed to be a one-dimensional Gaussian random field defined in terms of its autocorrelation coefficient function, mean function, and variance function. The four forms of autocorrelation coefficient function defined earlier are used in the computations. We will consider only the random field representing the geometrical imperfection, i.e., the modulus of elasticity is considered to have a deterministic constant value throughout the arch

The random fields are discretized into sets of random vectors using the aforementioned four discretization techniques. Based on each discretization, a set of random variables is introduced into the reliability code CALREL, which calculates estimates for the reliability index, the failure probability and sensitivity measures based on either FORM, SORM or MCS. For each realization of the random variables required by CALREL, a complete deterministic analysis of stability of the arch is performed in order to compute the buckling load and the associated displacements, i.e., in each realization, the imperfections are expanded in terms of Fourier series and a deterministic solution is obtained based on the arch configuration in this realization of the random variables.

Two failure criteria are considered based on exceeding a defined threshold for either the applied load or for the resulting deflection. The limit state functions are given by Eq. 2.3. Both symmetric (limit load) and antisymmetric (bifurcation) modes of failure are possible. This again gives a total of four possible limit-state functions, any of which may

be considered individually or in various combinations of two or more. In the later case we have a series system reliability problem.

Based on a deterministic analysis of an arch with clamped ends under radial loading, a value of $\lambda = 5.74$ in Eq. 3.32 is the defining limit between buckling in either symmetric or asymmetric modes. For $\lambda > 5.74$, antisymmetric (bifurcation) buckling occurs first, whereas for $\lambda < 5.74$ the arch will buckle symmetrically first. Therefore, we choose the values $\lambda = 7.31, 5.74, 5.19$ to illustrate the influence of the geometric configuration on the buckling modes. Deterministic dimensionless load-deflection curves for a perfect clamped arch are shown in Fig. 3.15 for the relation between P^* and the center deflection $W_o = w/2h$ where h is the rise of a perfect arch.

The mean function of the imperfection random field is considered to be the given function $\bar{w}(\theta)$. The imperfections are specified as a ratio of imperfection to arch thickness as $\bar{W} = \bar{w}/t$. Two forms of mean imperfection functions are considered in the analysis. The first is a symmetric higher harmonic mean function while the second field is a second order antisymmetric function. Three different amplitudes are considered for the mean function in each case. For the symmetric imperfection field, values of $\bar{W}_o = 0.5, 1.0$ and 1.50 are considered as shown in Fig. 3.16.

The deterministic load-deflection curves are plotted for the perfect arch and for the arch under the mean values of the three symmetric geometric imperfection random fields as shown in Fig. 3.17, Fig. 3.18, and Fig. 3.19 for values of $\lambda = 7.31, 5.74, 5.19$ respectively, $\sigma^2 = 0.5$ and $\delta/L = 0.25$ for the triangular autocorrelation function. The corresponding CDFs are plotted in Fig. 3.20, Fig. 3.21, and Fig. 3.22.

The CDFs are shown in Fig. 3.23 for the distribution of the buckling load for the imperfection fields with the variance values of $\sigma^2 = 0.05, 0.25, 0.5, 0.75$ and 1.0 . The PDFs shown in Fig. 3.24 can be obtained by computing the gradients of the CDFs or (better) by using the values of the sensitivity with respect to the parameter of the limit-state function which is readily available from the FORM analysis.

The second type of random fields representing the imperfection has a sinusoidal antisymmetric mean function as shown in Fig. 3.25 for the values of the dimensionless maximum imperfection $\bar{W}_1 = 0.5, 1.0$ and 1.50 (at $\zeta = \pm 0.5$). The deterministic load-deflection curves are plotted for the perfect arch and for the arch under the mean values of the three antisymmetric geometric imperfection random fields as shown in Fig. 3.26, Fig. 3.27, and Fig. 3.28 for values of $\lambda = 7.31, 5.74, 5.19$ respectively. For the random imperfections, the corresponding CDFs for the buckling load are plotted in Fig. 3.29, Fig. 3.30, and Fig. 3.31. Values of $\sigma^2 = 0.5$ and $\delta/L = 0.25$ for the triangular autocorrelation function are used in these computations. From these graphs, it can be seen that the mode shapes of the mean functions affect the response greatly in the case of bifurcation buckling. An antisymmetric imperfection lowers the buckling load much more than a comparable symmetric imperfection. However, the limit buckling load remains almost unchanged for different types of imperfection fields with the same amplitude. Further, a narrower distribution is obtained for the buckling load under antisymmetric imperfection showing less sensitivity towards uncertainties in the shape in this case. The corresponding PDFs for the buckling load are plotted in Fig. 3.32

A sufficient number of random variables must be employed in the discretization of the

random field in order to obtain an accurate value of the reliability index for the buckling load. Here, we compare the computational times for convergence of the various discretization methods. Computational effort depends strongly on the number of random variables. Computational time also depends on the efficiency of the computational algorithm. For the sake of comparison, let us consider an arch with clamped ends with $\lambda = 5.74$, $\sigma^2 = 0.5$, $\delta/L = 0.25$ and $\bar{W}_o = 0.5$ throughout the following calculations. For analysis based on the triangular autocorrelation coefficient functions, where exact forms of the eigenvalues and eigenfunctions are available, the KL method requires the least number of random variables to obtain a convergent reliability index as shown in Fig. 3.33. Slightly more random variables are needed for the SE method. Since there is no need to evaluate the eigenfunctions in the KL method, the SE and KL methods take a nearly equal computational time. Both MP and LA methods require a much higher number of random variables and three to four times the computational time to obtain the converged value of the reliability index. The average size of the mesh used to discretize the random field in both MP and LA methods is one half the correlation length. Less finer meshes were sufficient in some cases of study. As expected, the four methods converge to nearly the same value for the reliability index.

For the case of the sinusoidal autocorrelation function given by Eq. 3.53, there is no available exact formulation for the eigenvalues and eigenfunctions in the KL method. An IMSL FORTARN 77 library subroutine is used to evaluate them numerically. This strongly affects the efficiency of the KL discretization method in that discretization of the random field requires a fine mesh for numerical accuracy. This takes away the advantage

of the KL method. A comparison between convergence of the various discretization methods, shown in Fig. 3.34, indicates that the SE method is the most efficient technique for the sinusoidal autocorrelation function.

A comparison is made between the values of the probability of failure obtained using FORM, SORM and MCS. For MCS, 10,000 simulations were required to obtain a reliable estimate of the failure probability while less than 15 iterations were needed for convergence to the design point when using FORM and SORM. As shown in Fig. 3.35, SORM and MCS results appear to be in a very good agreement. As expected, SORM requires only a small fraction of the processor time required for MCS. On the other hand, the increase in the processor time for using SORM instead of FORM is in the range of 5-15%. Thus, FORM could be used to provide an initial estimate of the failure probability, while for a small additional effort, a better estimate may be obtained using SORM.

The effect of the correlation length on the failure probability was studied. Three values of the correlation length $\delta/L = 0.25, 0.5$ and 0.75 are considered in the autocorrelation functions for the cases where $0 \leq |z - z'| \leq L$. For the clamped arch, considering the triangular autocorrelation coefficient function and using the KL method, a comparison is shown in Table 3.3 for different values of the mean and variance of the imperfection. A similar comparison is shown in Fig. 3.36 for the same case. The failure probability is relatively insensitive to the correlation length in this case.

The table also illustrates the effect of the non-stationarity in the autocorrelation function due to the boundary conditions on the failure probability. The effect of the non-stationarity in the autocorrelation function due to the boundary conditions on the failure

probability, which is mentioned in paragraph 2.10, is checked for the same previous arch dimensions. For the case of an arch with clamped ends, the difference between applying

Table 3.3: Values of P_f for the buckling load of the clamped arch under uniformly distributed loading for different correlation lengths ($C_t = 6.35$)

Mean	Variance	P_f			
		$\delta/L = 0.25$		$\delta/L = 0.75$	
		Stationary	Non Stationary	Stationary	Non Stationary
$\bar{W} = 0.5$	0.25	0.956	0.954	0.933	0.928
	1.0	0.912	0.919	0.892	0.902
$\bar{W} = 1.0$	0.25	0.561	0.560	0.542	0.544
	1.0	0.549	0.552	0.531	0.534
$\bar{W} = 1.5$	0.25	0.023	0.030	0.002	0.002
	1.0	0.112	0.118	0.072	0.077

Eq. 2.48 to compensate for the non-stationarity of the function near the supports, and between neglecting this effect is shown in Fig. 3.37. The same comparison is shown in Fig. 3.38 for the case of an arch with pinned supports. As seen from these figures and from Table 3.3, the effect non-stationarity of the autocorrelation function is very small in most of the cases considered. The application of the same Eq. 2.48 to the solution using the SE method gave perfect agreement between the results obtained for either stationary or non-stationary effects. This again proves that the SE method requires no additional considerations.

The previous graphs were plotted for an arch with clamped ends. In order to compare the effect of the boundary conditions, we consider an arch with hinged ends and having

same values for all other parameters as the clamped arch. The loads are normalized by dividing by the value of the buckling load of the perfect arch, P_{perf}^* in each case. The CDFs for both arches are plotted in Fig. 3.39 where the buckling load of the hinged arch is seen to be more sensitive to the uncertainties in the geometrical imperfections.

Results presented in all previous figures are for pressure loading. A similar probabilistic behavior and the same types of sensitivities were obtained for other types of loading.

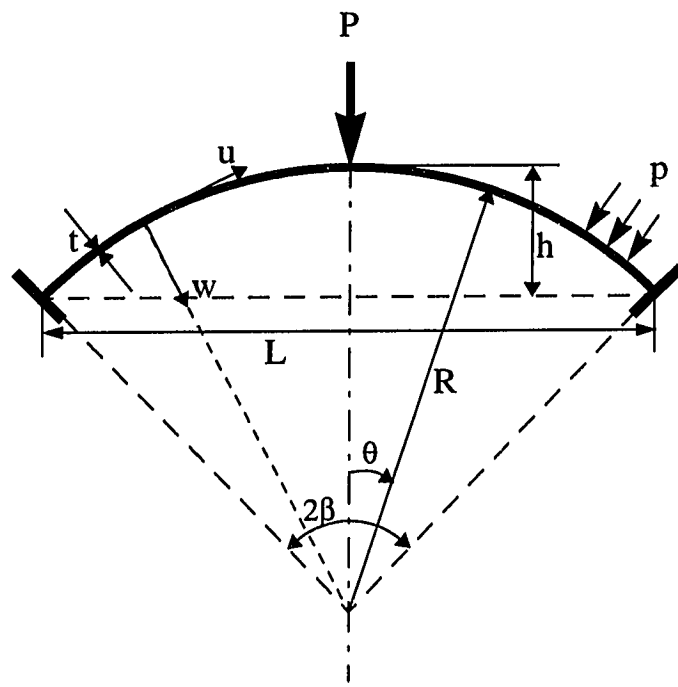


Figure 3.1 Coordinate system

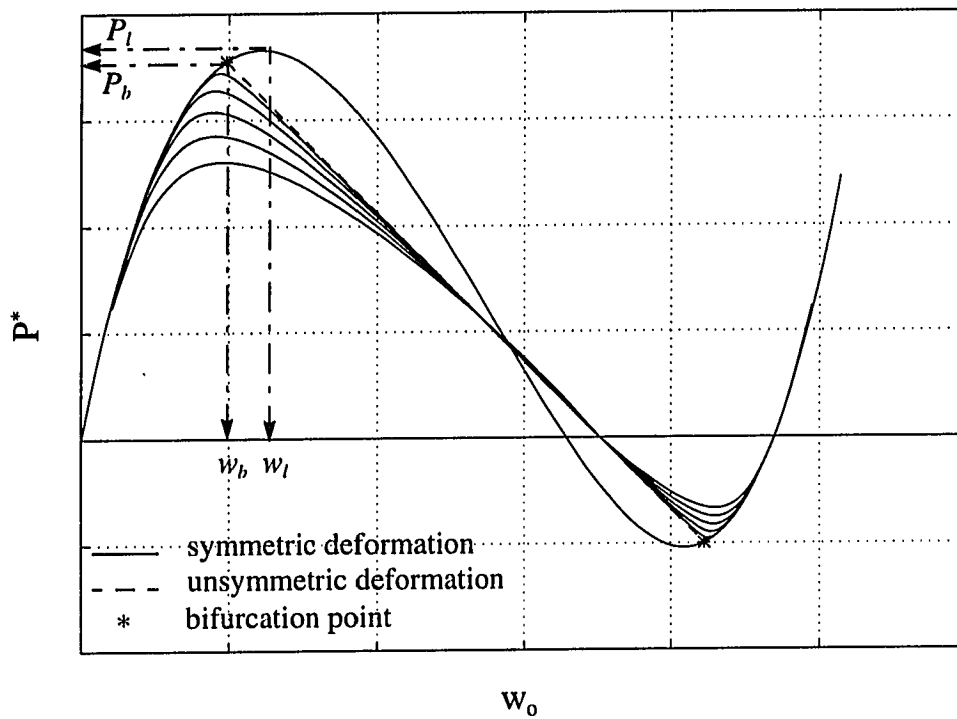


Figure 3.2 Example load-deflection curves illustrating buckling loads for different magnitudes of imperfection in the case $w_b < w_l$

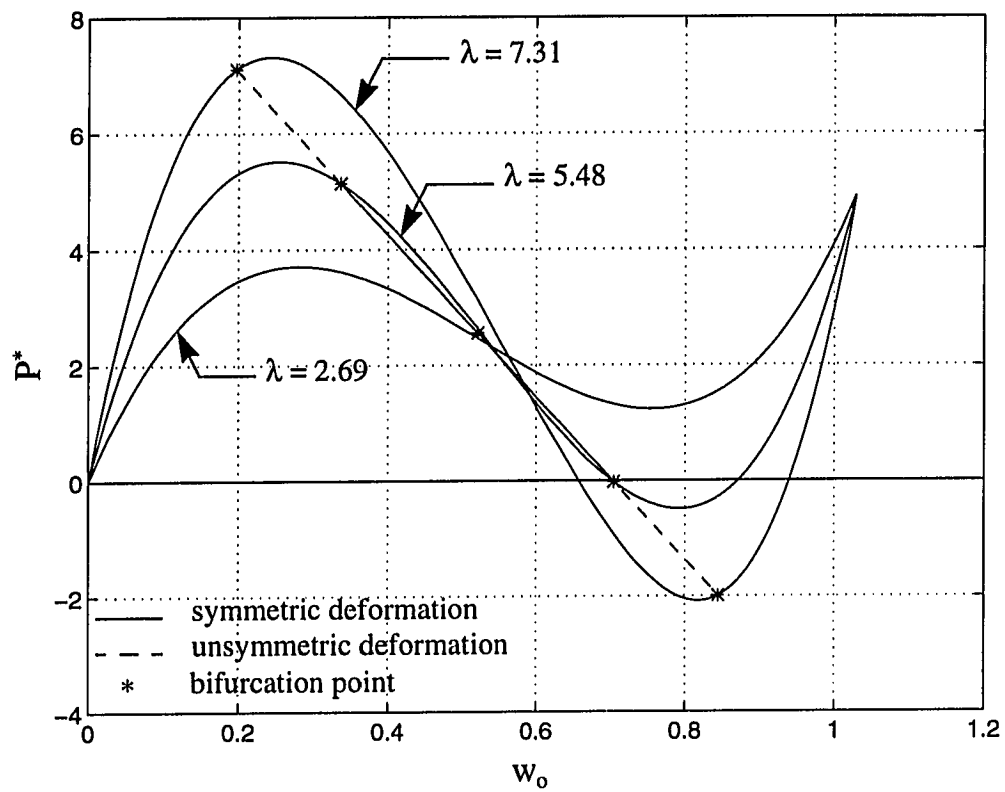


Figure 3.3 Relation between the uniform pressure and the deflection at the middle of a shallow circular arch for different degrees of shallowness

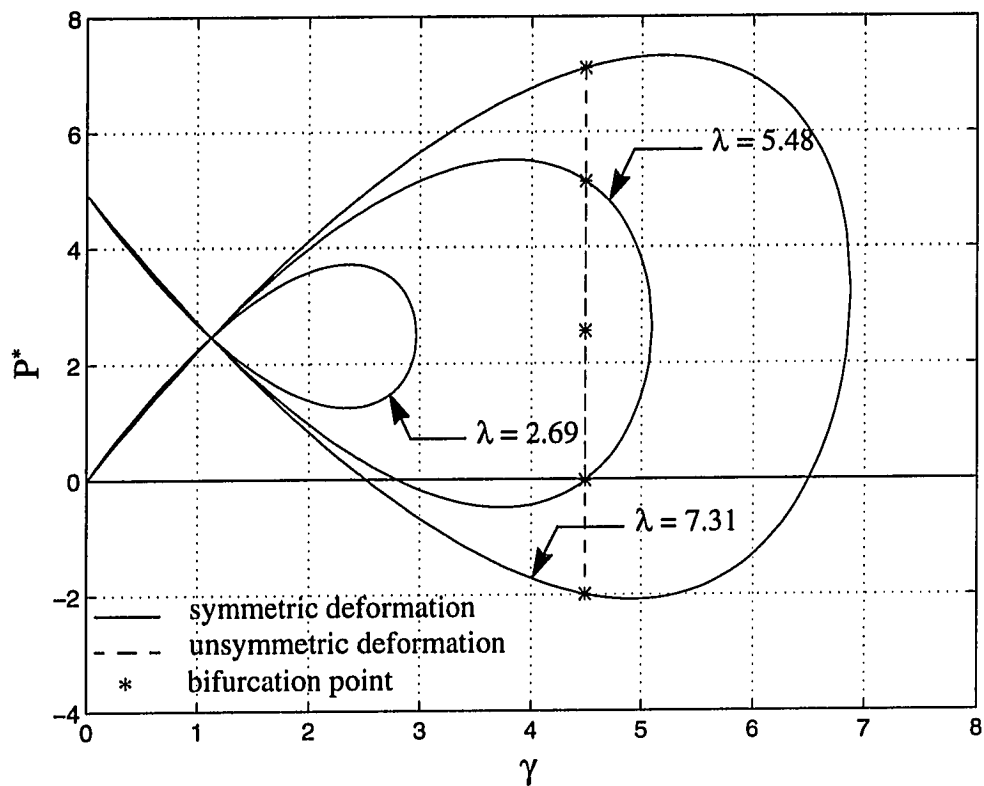


Figure 3.4 Relation between the uniform pressure and the axial membrane force in a shallow circular arch for different degrees of shallowness.

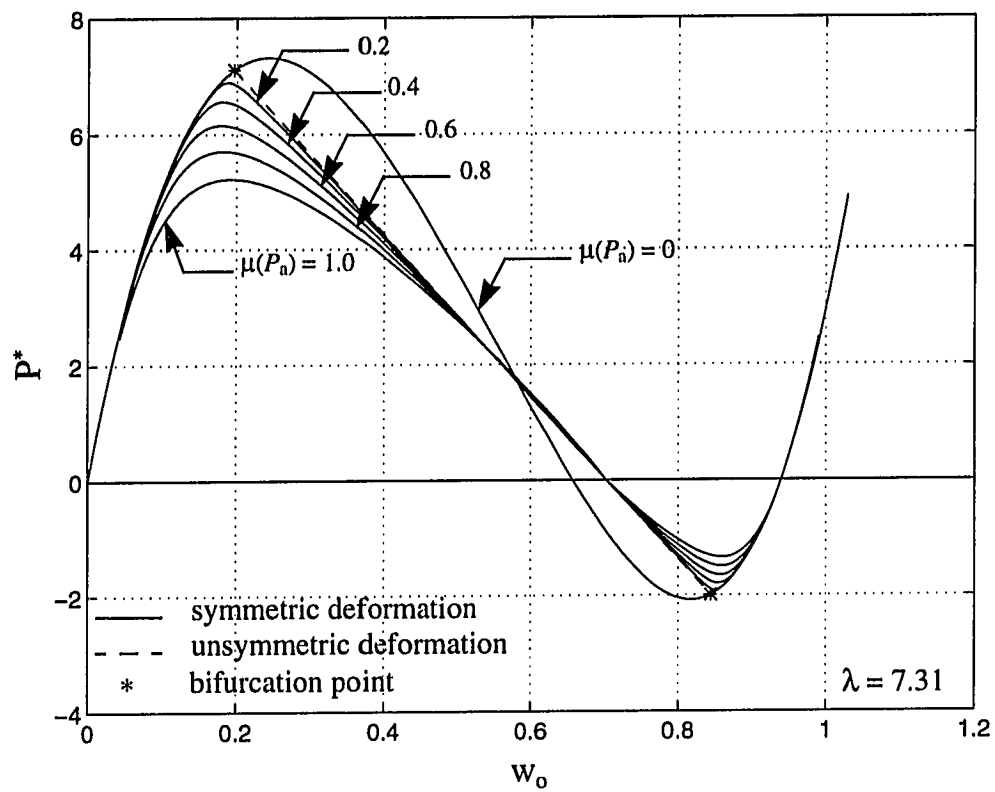


Figure 3.5 Relation between the uniform pressure and the deflection at the middle of a shallow circular arch for different degrees of loading imperfection.

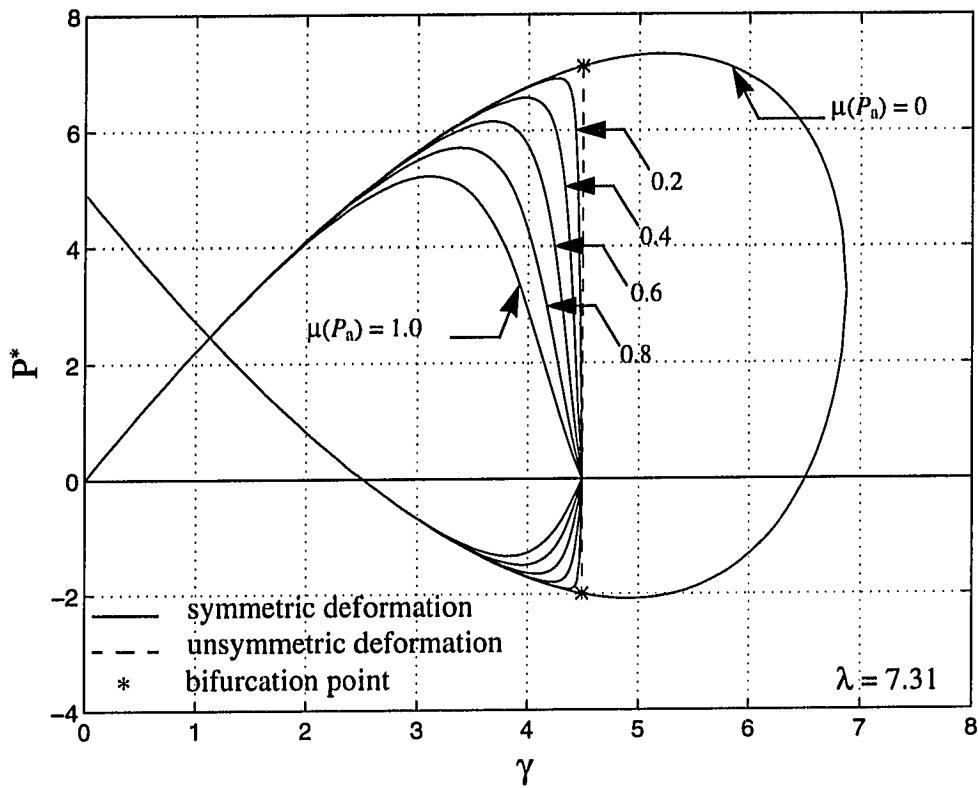


Figure 3.6 Relation between the uniform pressure and the axial membrane force in a shallow circular arch for different degrees of loading imperfection.

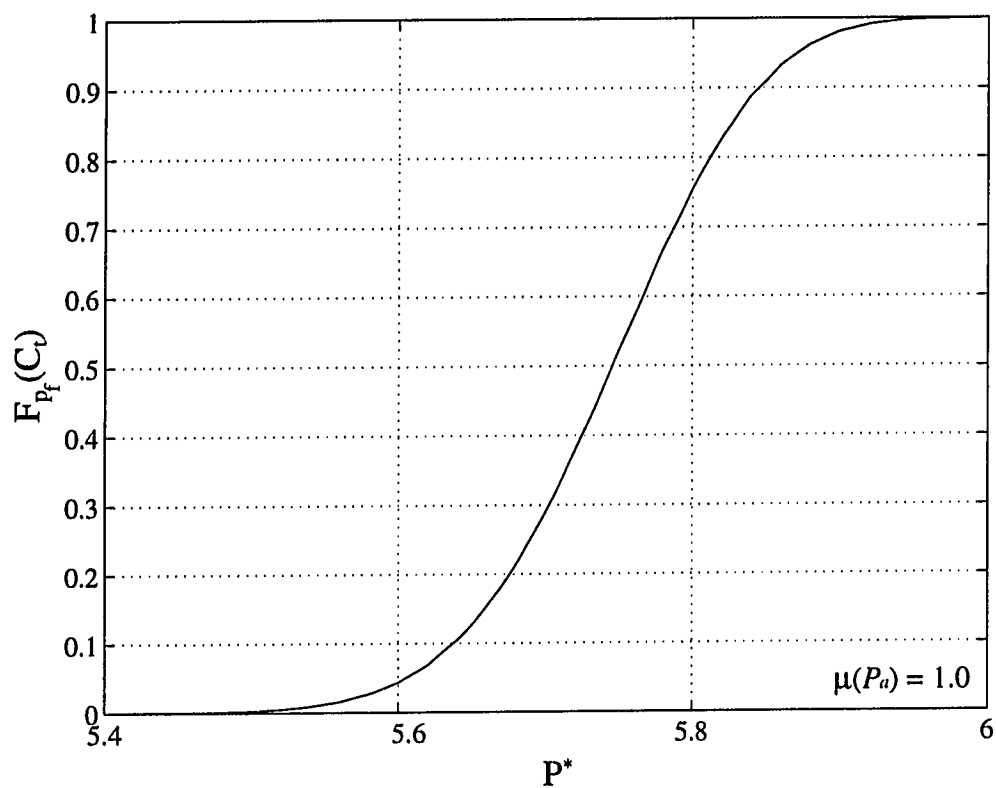


Figure 3.7 Cumulative distribution function for the unsymmetric buckling load of the arch under imperfect uniformly distributed loading.

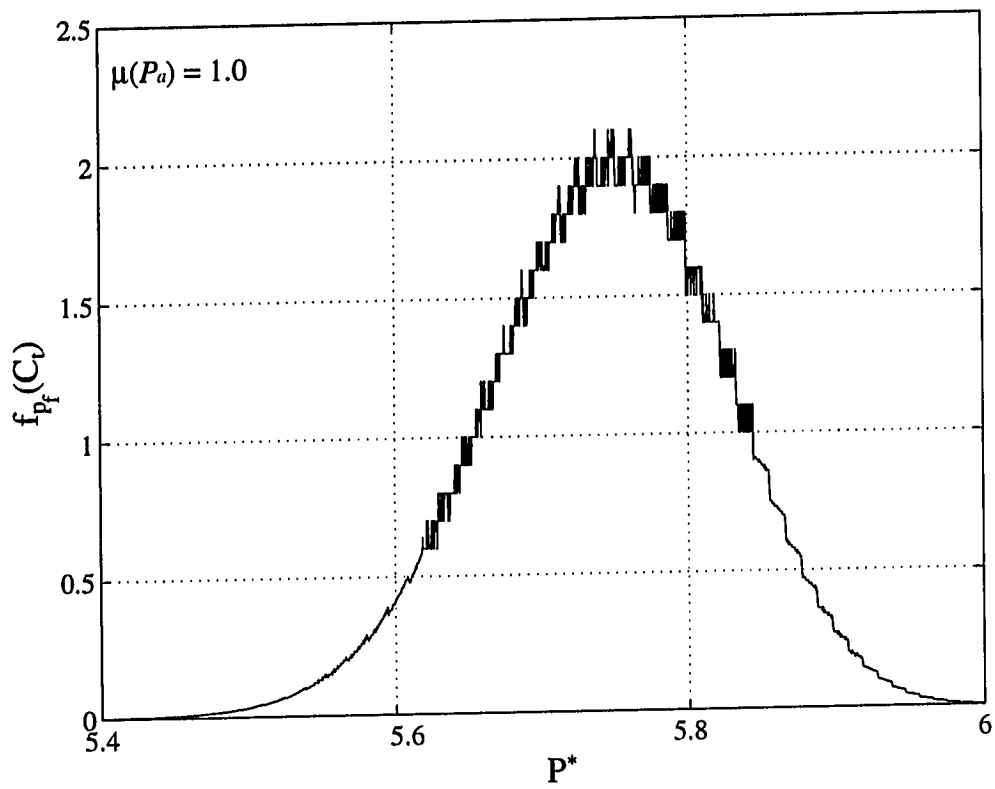


Figure 3.8 Probability density function for the symmetric buckling load of the arch under imperfect uniformly distributed loading using the gradient of the CDF.

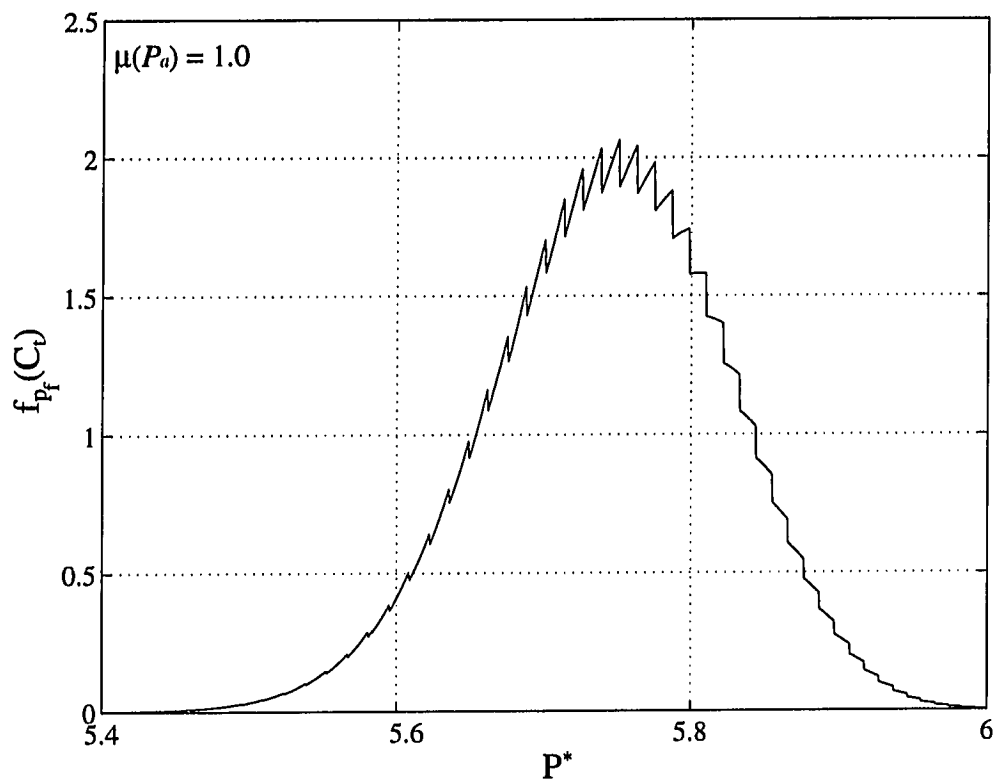


Figure 3.9 Probability density function for the symmetric buckling load of the arch under imperfect uniformly distributed loading using the FORM sensitivity.

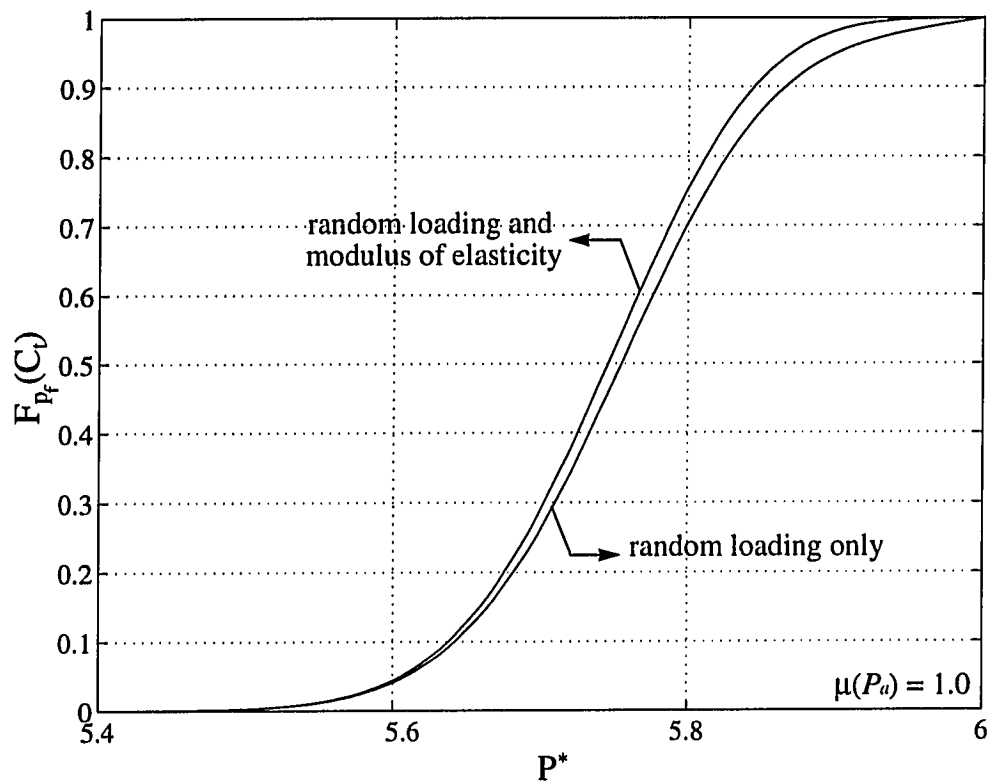


Figure 3.10 Cumulative distribution function for the symmetric buckling load of the arch under uniformly distributed loading with random E and loading.

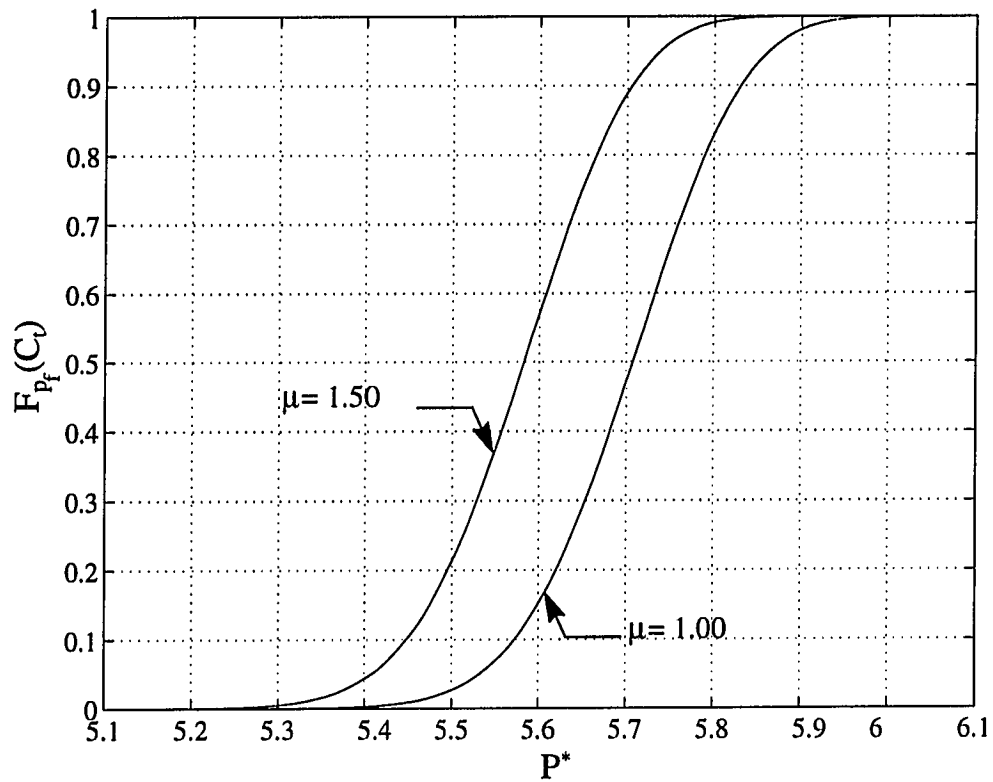


Figure 3.11 Cumulative distribution function for the symmetric buckling load of the arch under uniformly distributed loading for different mean values of the load imperfection.

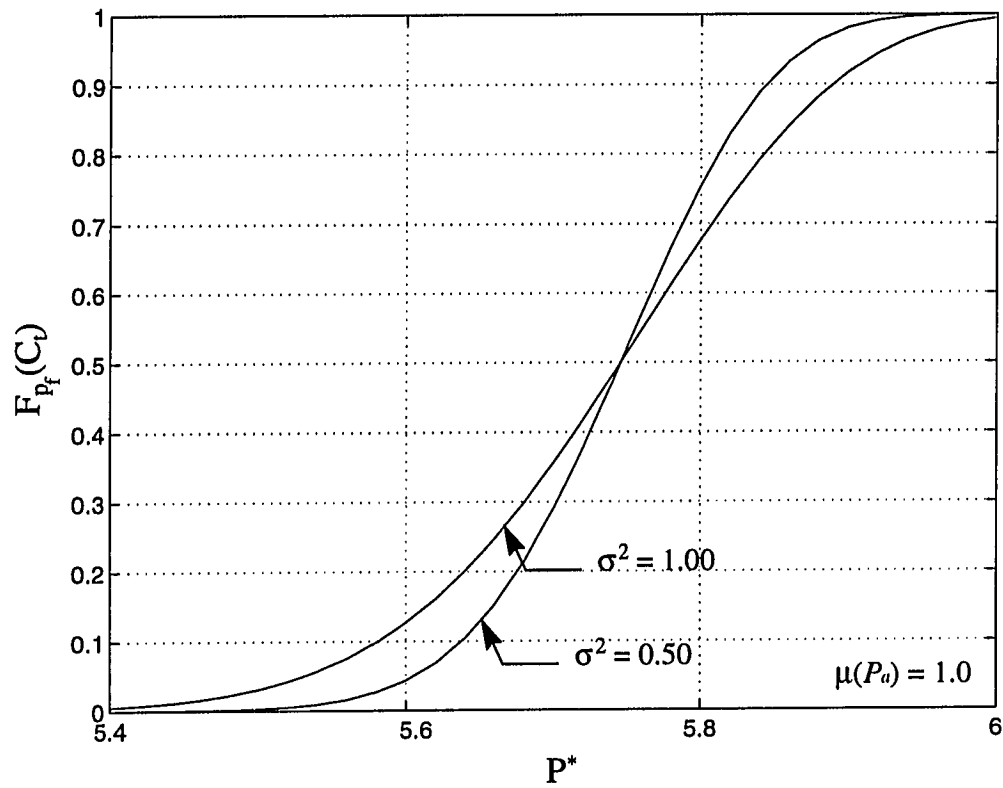


Figure 3.12 Cumulative distribution function for the symmetric buckling load of the arch under uniformly distributed loading for different variances of the load imperfection

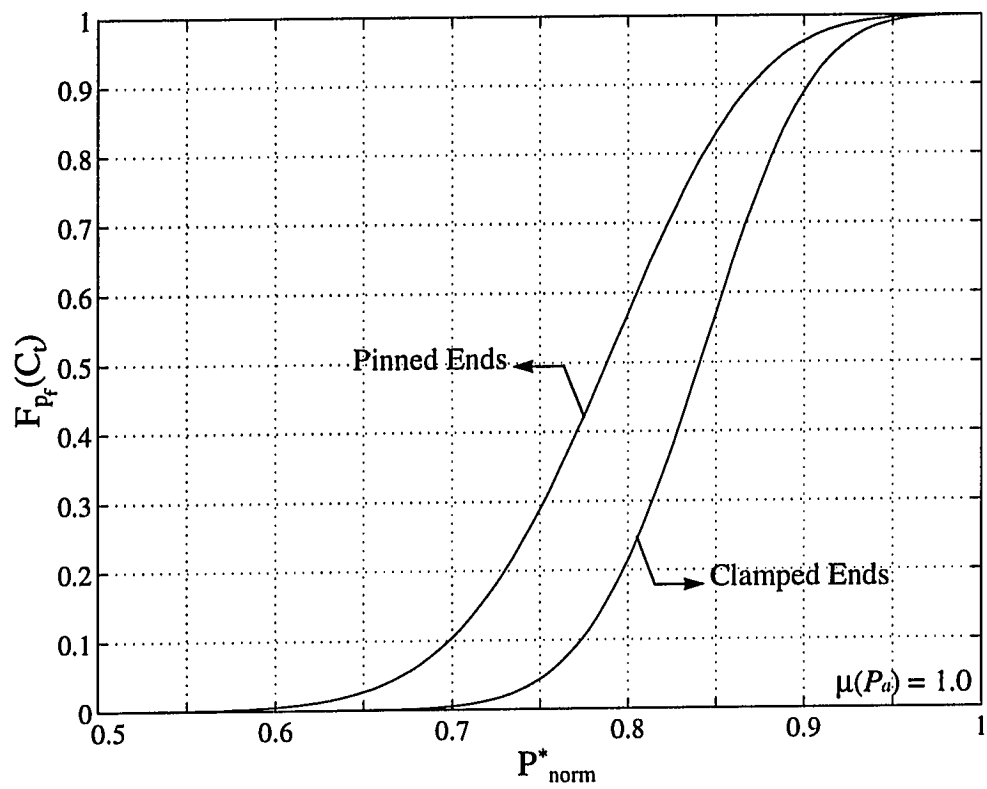


Figure 3.13 Cumulative distribution functions for the symmetric buckling load for both pinned and clamped ends arches under uniformly distributed loading

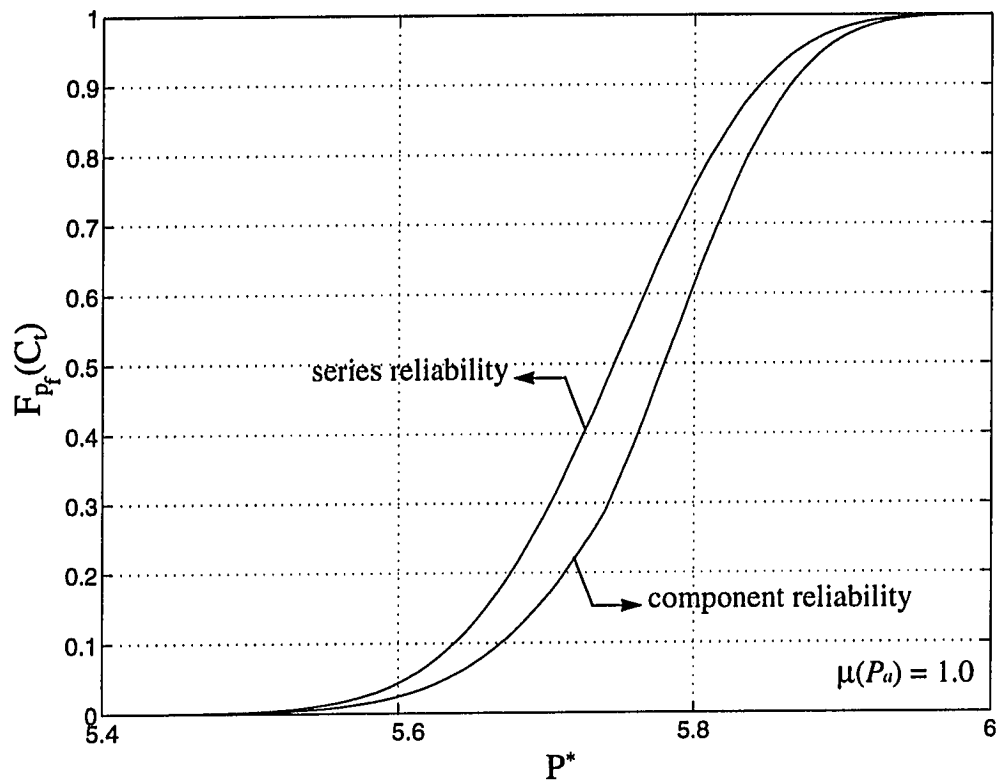


Figure 3.14 Cumulative distribution function for the symmetric buckling load and for both symmetric and antisymmetric modes of the arch under uniformly distributed loading

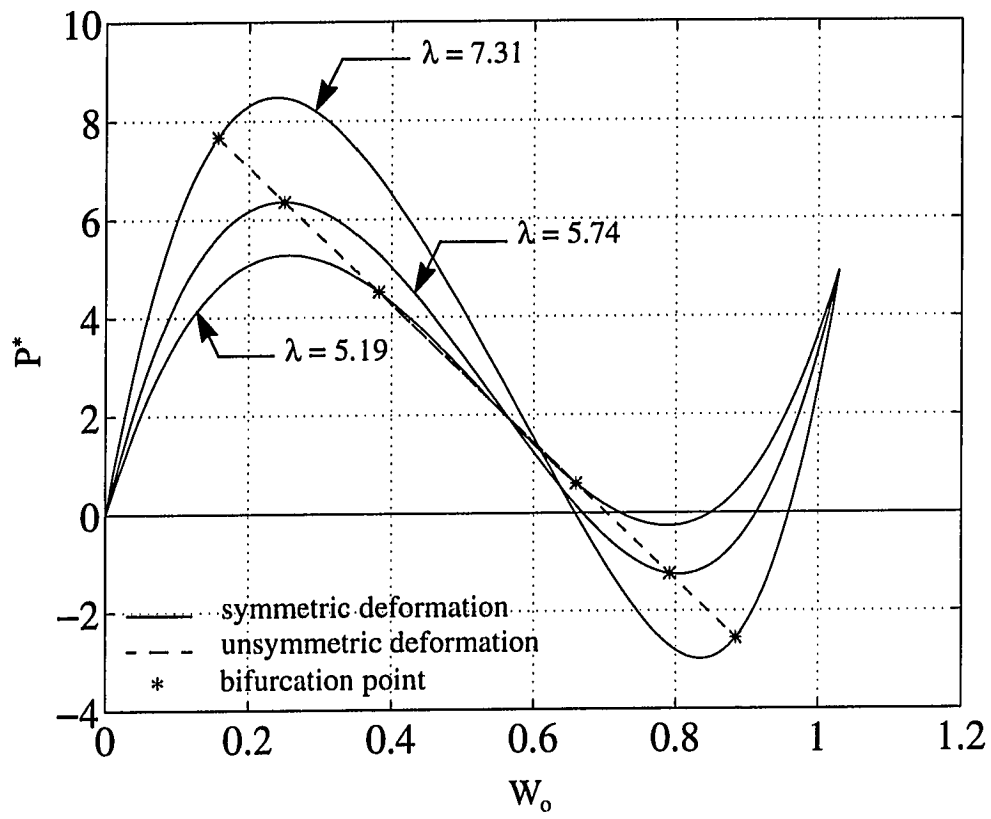


Figure 3.15 Relation between the uniform pressure and the deflection at the middle of a shallow perfect circular arch with clamped ends for different degrees of shallowness.

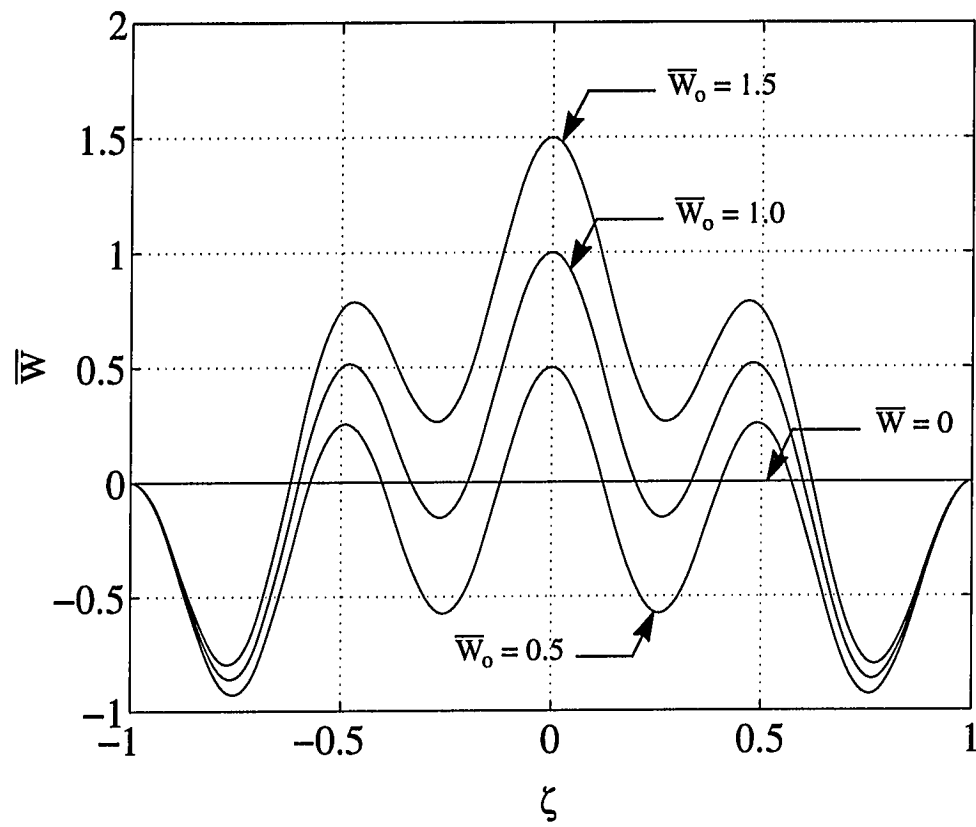


Figure 3.16 Values of the mean functions for three different fields of symmetric geometric imperfection along the arch with clamped ends.

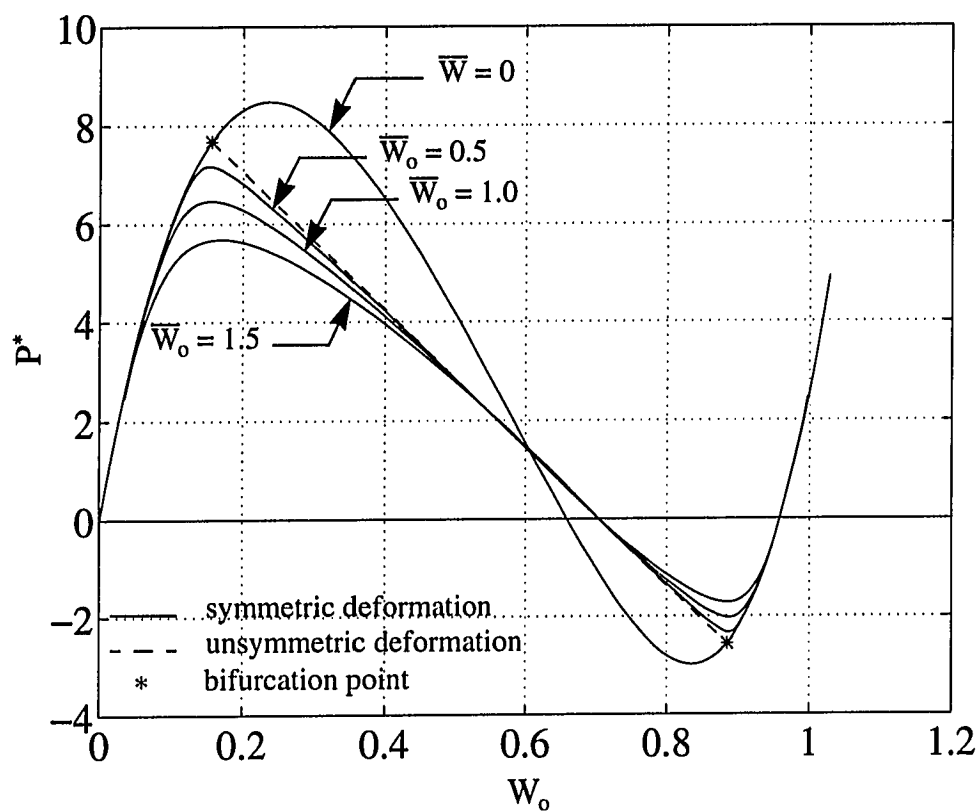


Figure 3.17 Relation between the uniform pressure and the deflection at the middle of a clamped shallow circular arch with $\lambda = 7.31$ for different degrees of symmetric imperfection \bar{W} .

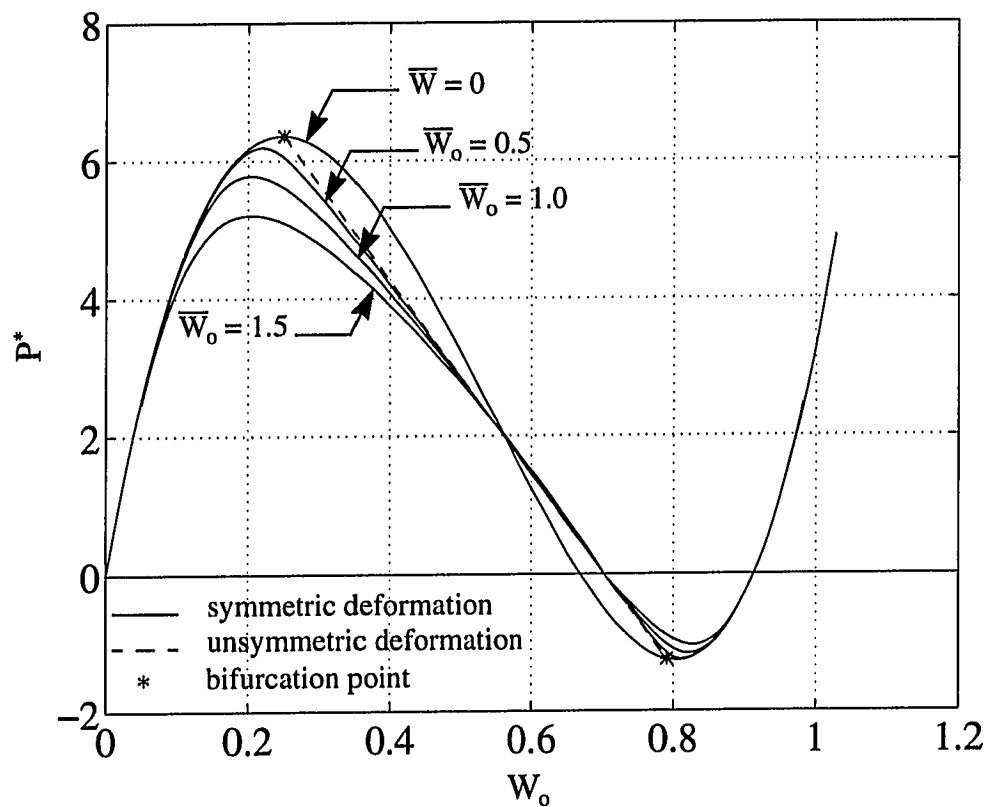


Figure 3.18 Relation between the uniform pressure and the deflection at the middle of a clamped shallow circular arch with $\lambda = 5.74$ for different degrees of symmetric imperfection \bar{W} .

Figure 3.19 Relation between the uniform pressure and the deflection at the middle of a clamped shallow circular arch with $\lambda = 5.19$ for different degrees of symmetric imperfection \overline{W} .

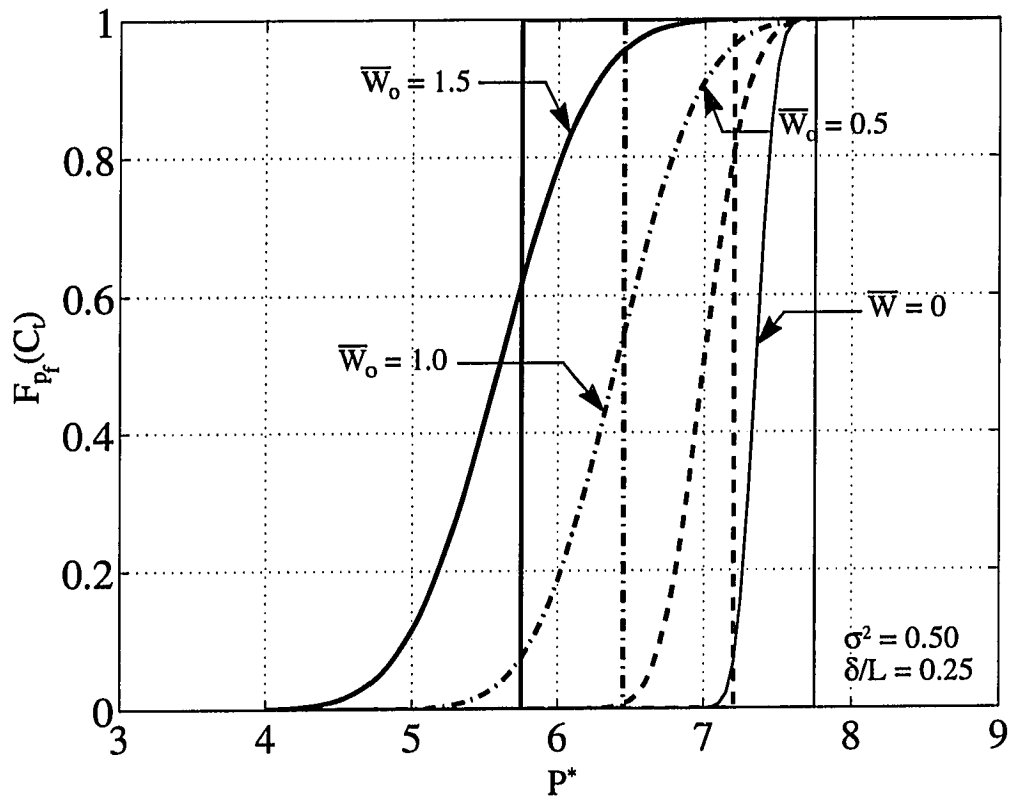


Figure 3.20 Cumulative distribution function for the buckling pressure of a clamped arch with $\lambda = 7.31$, for different symmetric geometric imperfection configurations (Straight lines represent the deterministic cases with imperfection functions equal to the mean imperfections).

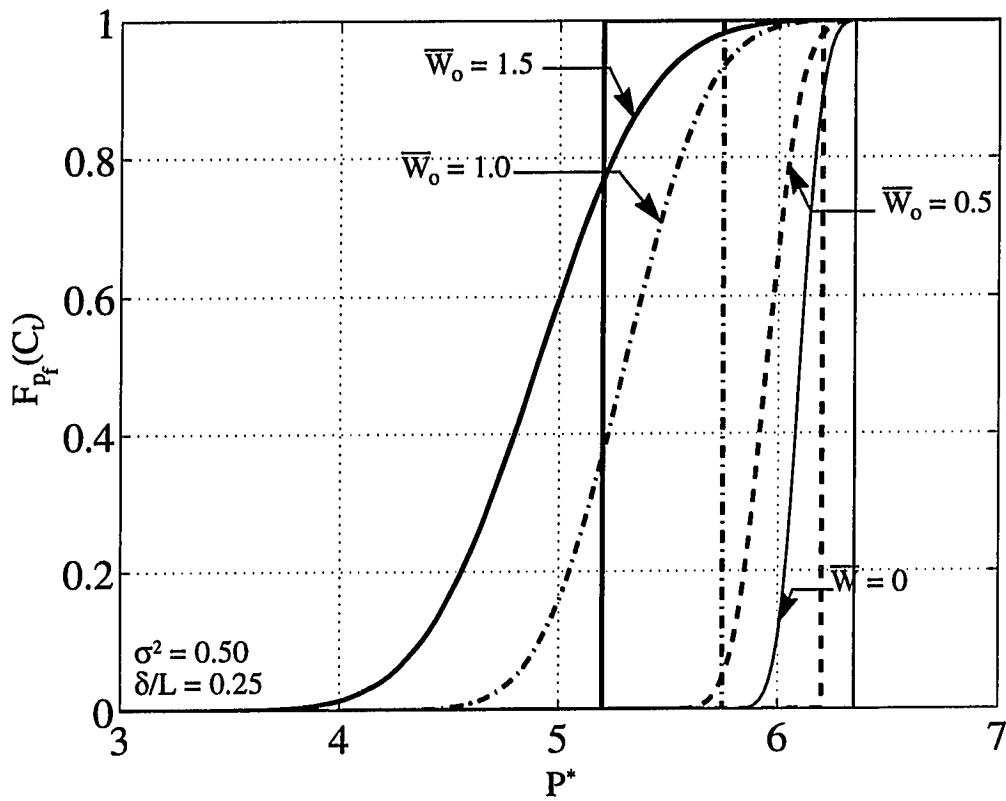


Figure 3.21 Cumulative distribution function for the buckling pressure of a clamped arch with $\lambda = 5.74$ for different symmetric geometric imperfection configurations (Straight lines represent the deterministic cases with imperfections equal to the mean of imperfection functions).

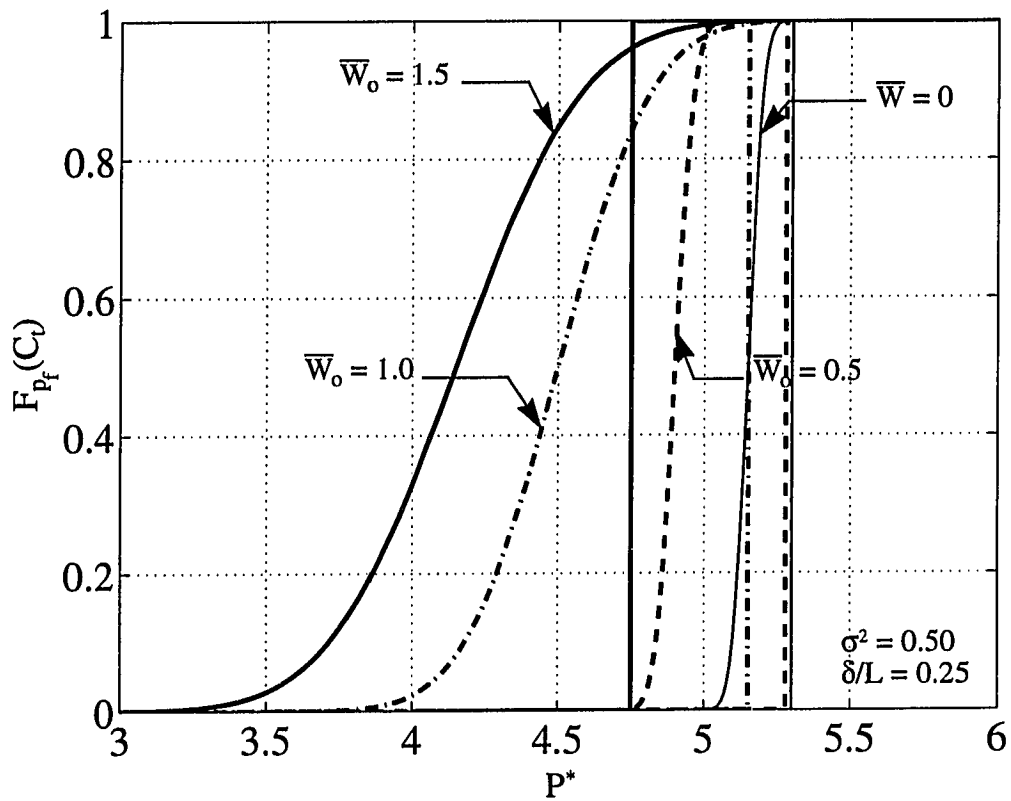


Figure 3.22 Cumulative distribution function for the buckling pressure of a clamped arch with $\lambda = 5.19$ for different symmetric geometric imperfection configurations (Straight lines represent the deterministic cases with imperfections equal to the mean of imperfection functions).

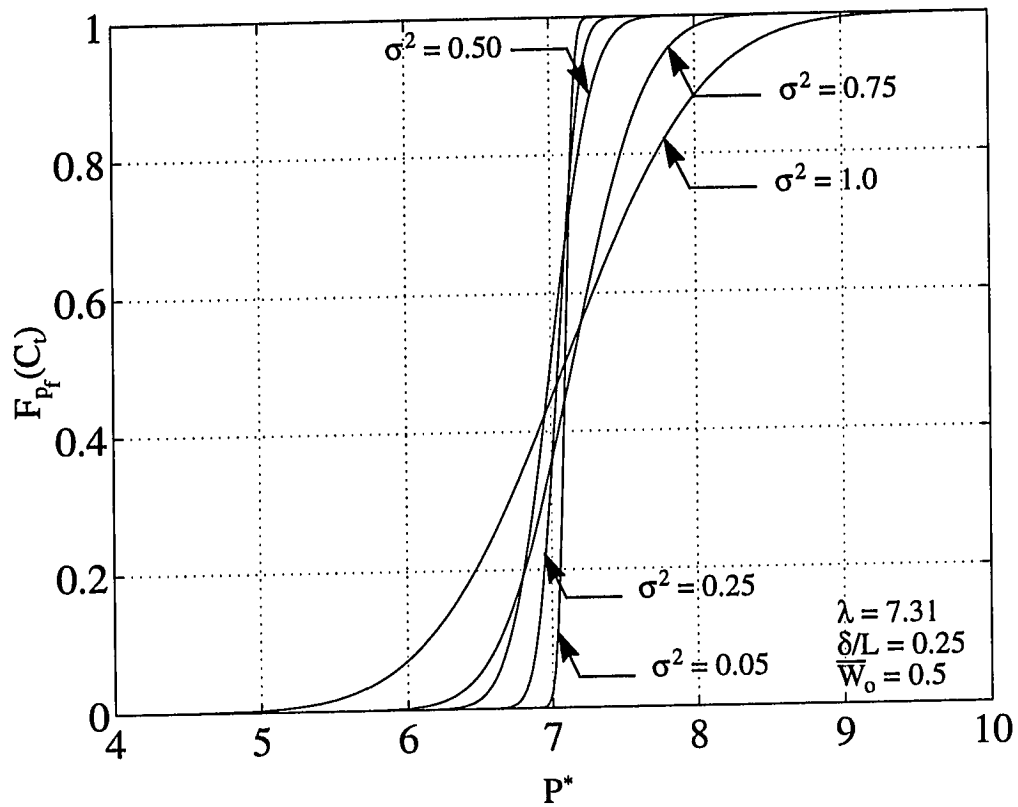


Figure 3.23 Cumulative distribution function for the symmetric buckling load of the clamped arch under uniformly distributed loading for different variances of the

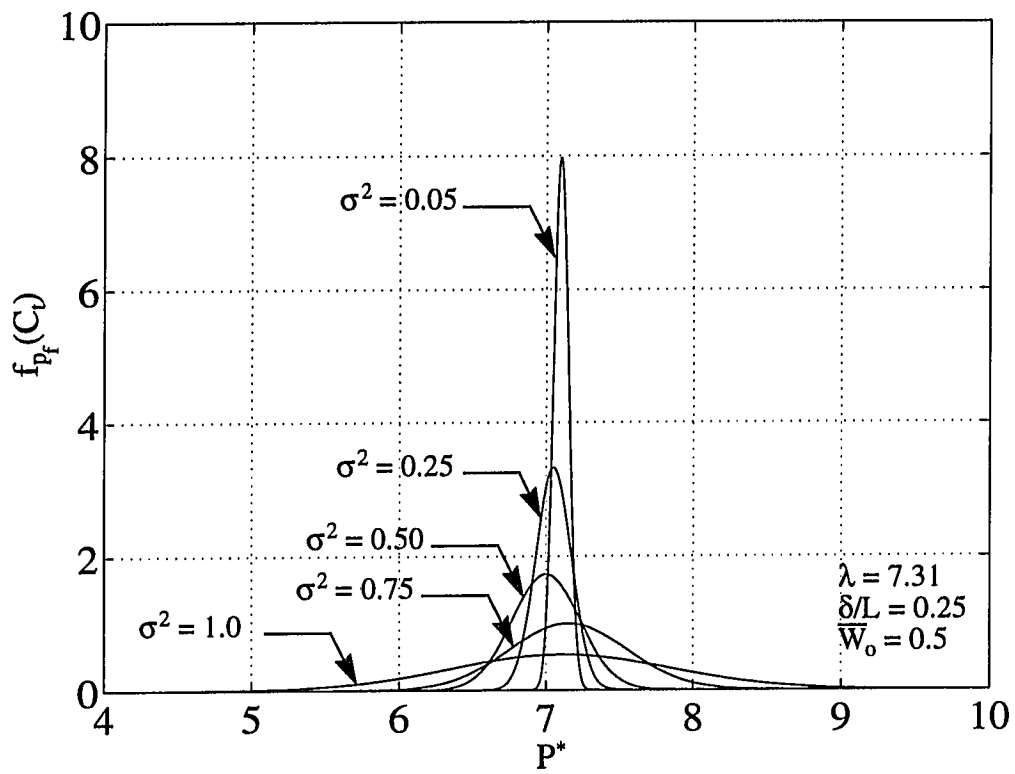


Figure 3.24 Probability density function for the unsymmetric buckling load of the clamped arch under uniformly distributed loading for different variances of the symmetric shape

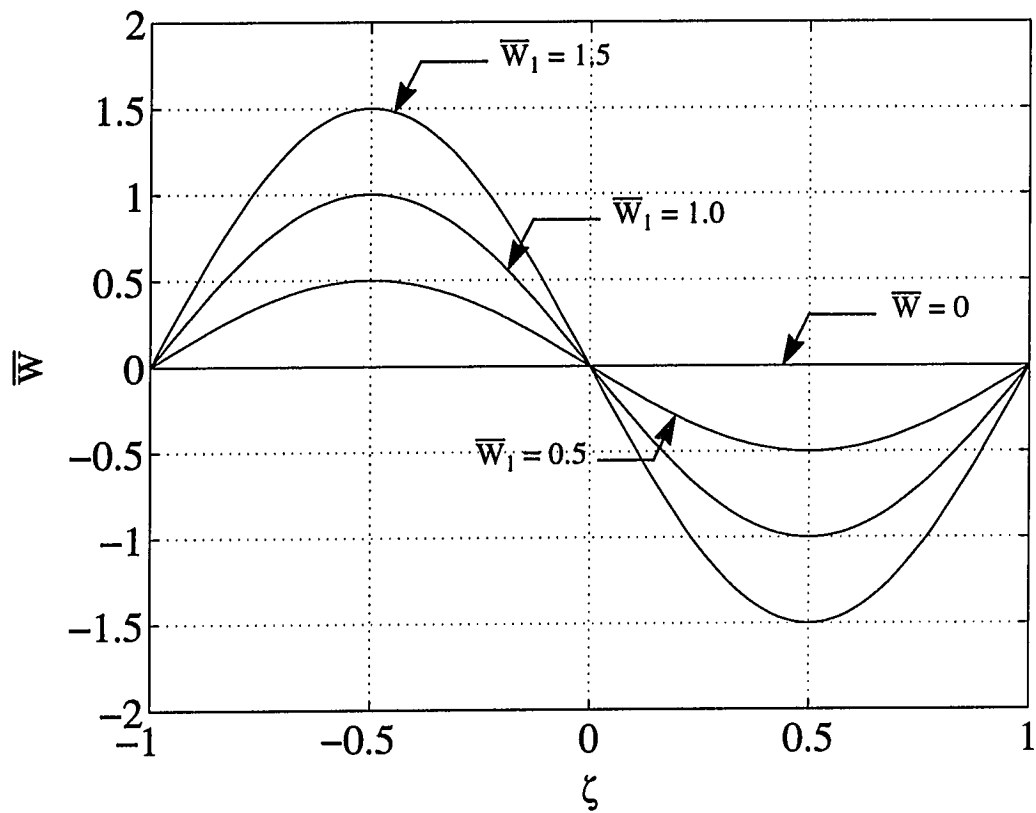


Figure 3.25 Values of the mean functions for three different fields of antisymmetric geometric imperfection along the arch with clamped ends.

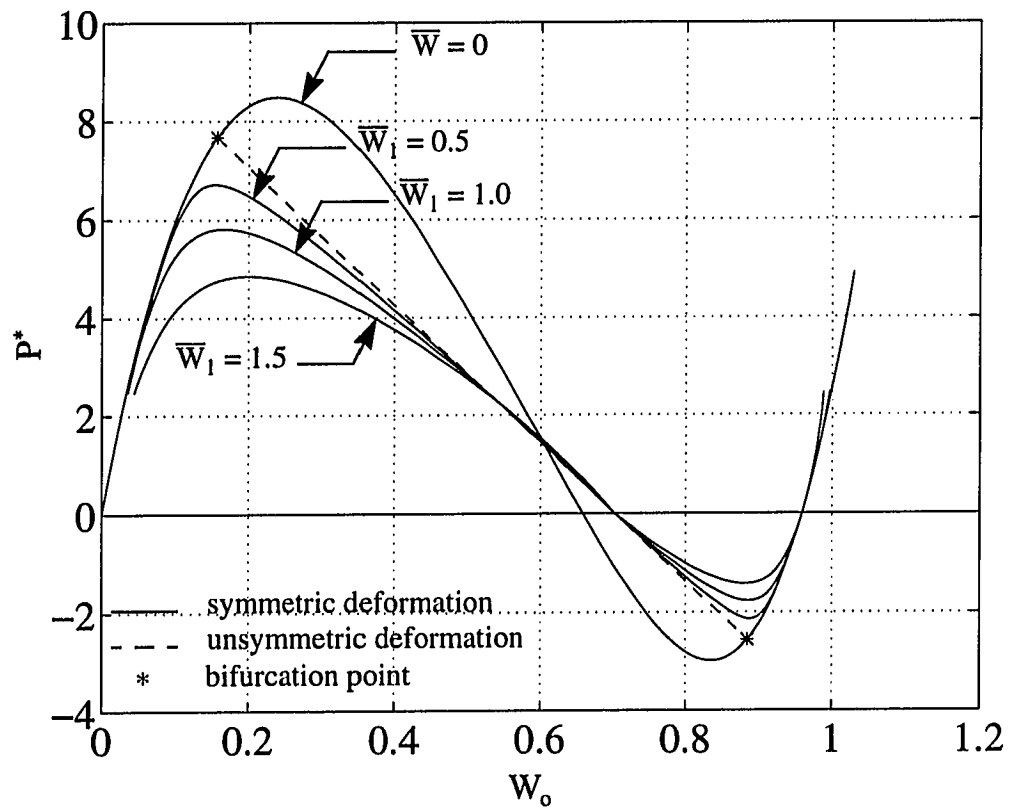


Figure 3.26 Relation between the uniform pressure and the deflection at the middle of a clamped shallow circular arch with $\lambda = 7.31$ for different degrees of antisymmetric imperfection \bar{W} .

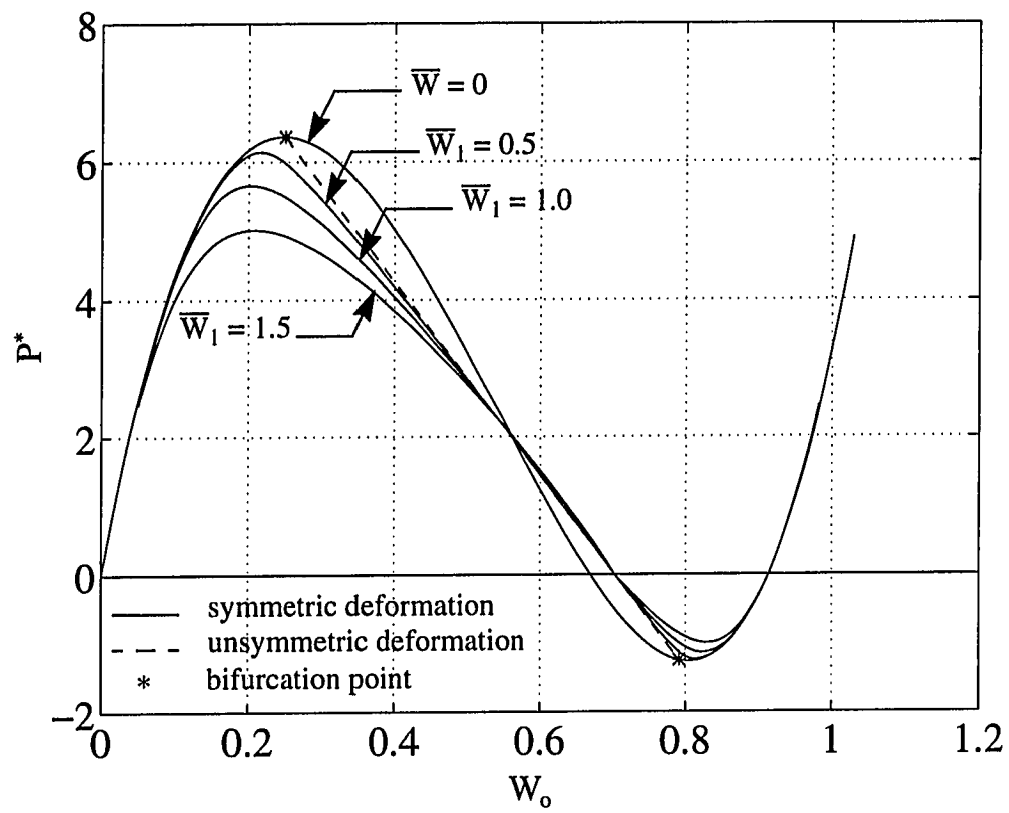


Figure 3.27 Relation between the uniform pressure and the deflection at the middle of a clamped shallow circular arch with $\lambda = 5.74$ for different degrees of antisymmetric imperfection \bar{W} .

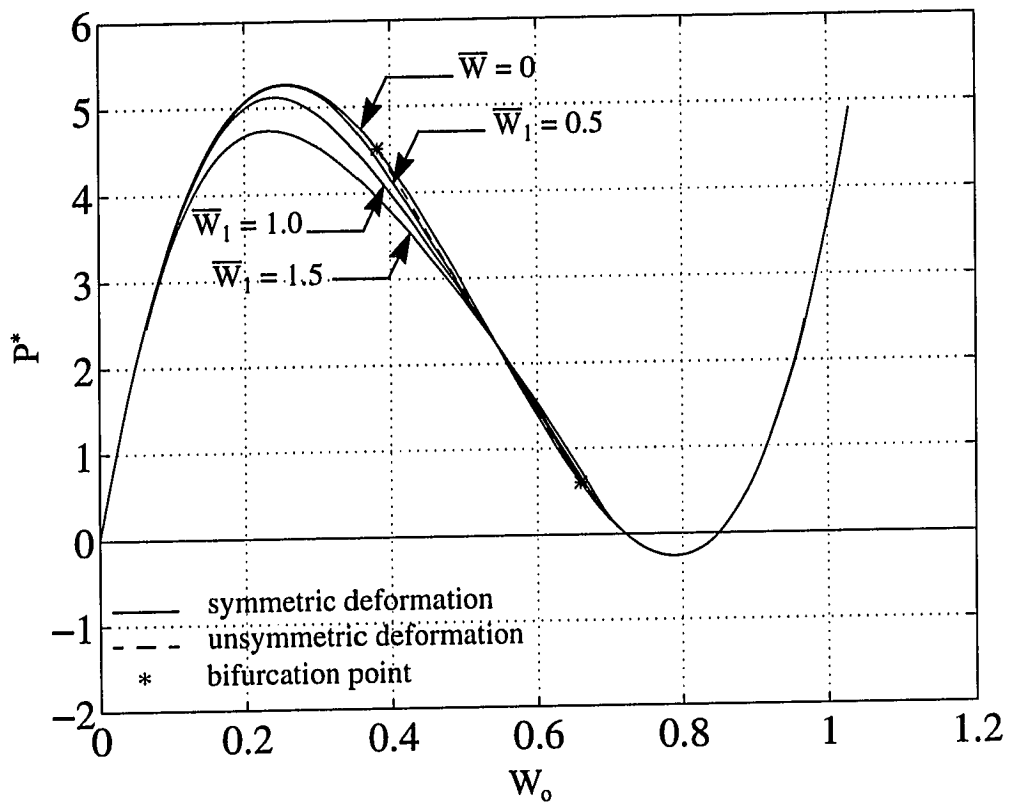


Figure 3.28 Relation between the uniform pressure and the deflection at the middle of a clamped shallow circular arch with $\lambda = 5.19$ for different degrees of symmetric imperfection \bar{W} .

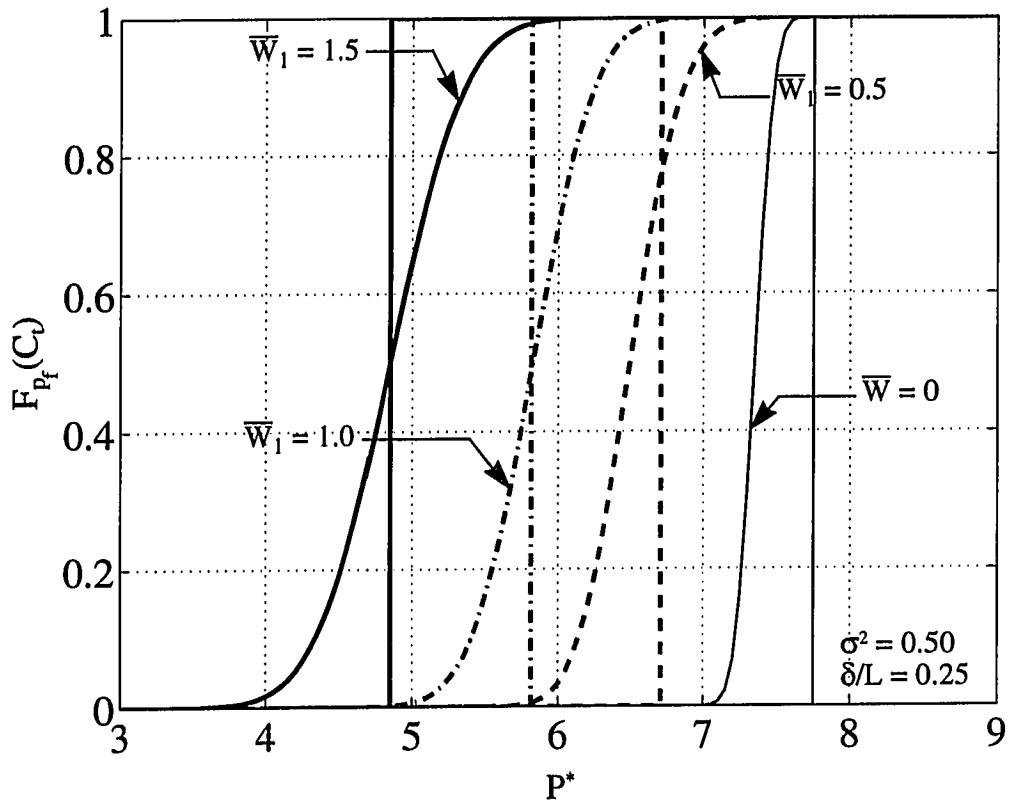


Figure 3.29 Cumulative distribution function for the buckling pressure of a clamped arch with $\lambda = 7.31$, for different antisymmetric geometric imperfection configurations (Straight lines represent the deterministic cases with imperfections equal to the mean of imperfection functions).

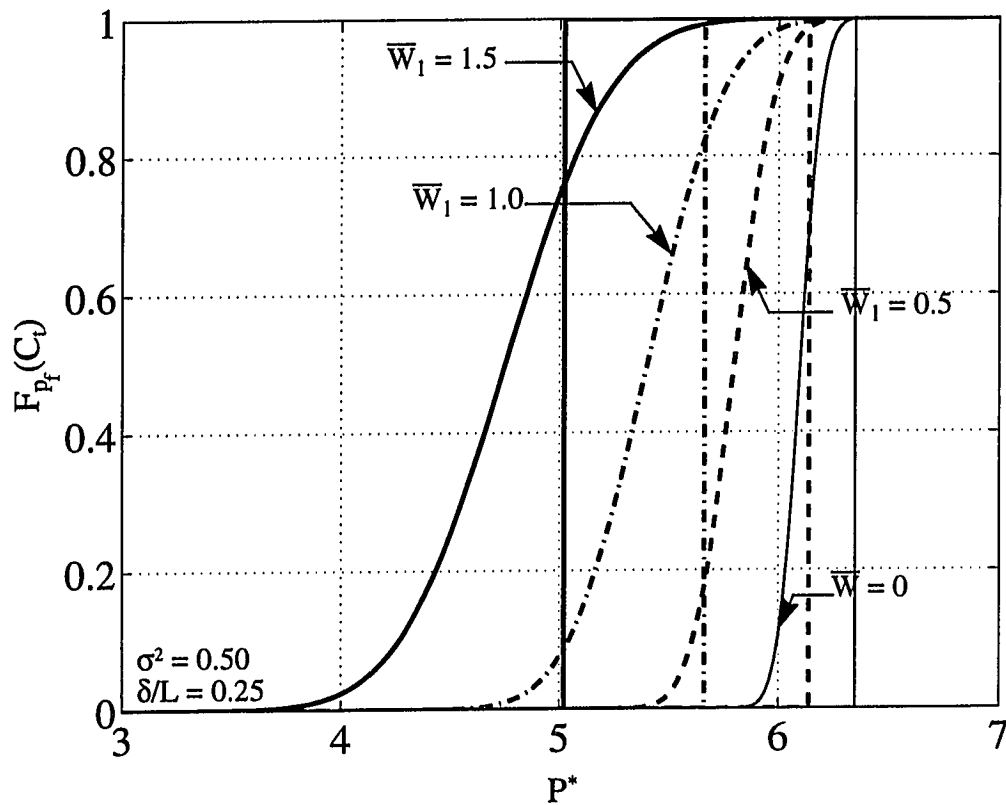


Figure 3.30 Cumulative distribution function for the buckling pressure of a clamped arch with $\lambda = 5.74$ for different antisymmetric geometric imperfection configurations (Straight lines represent the deterministic cases with imperfections equal to the mean of imperfection functions).

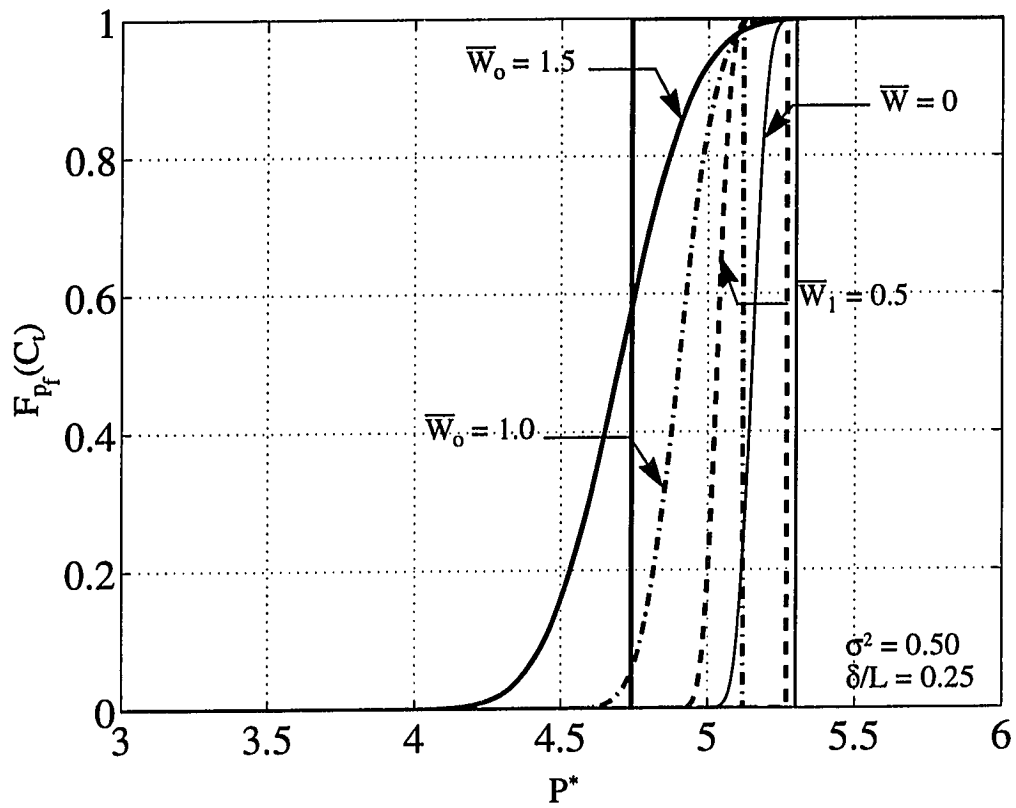


Figure 3.31 Cumulative distribution function for the buckling pressure of a clamped arch with $\lambda = 5.19$ for different antisymmetric geometric imperfection configurations (Straight lines represent the deterministic cases with imperfections equal to the mean of imperfection functions).

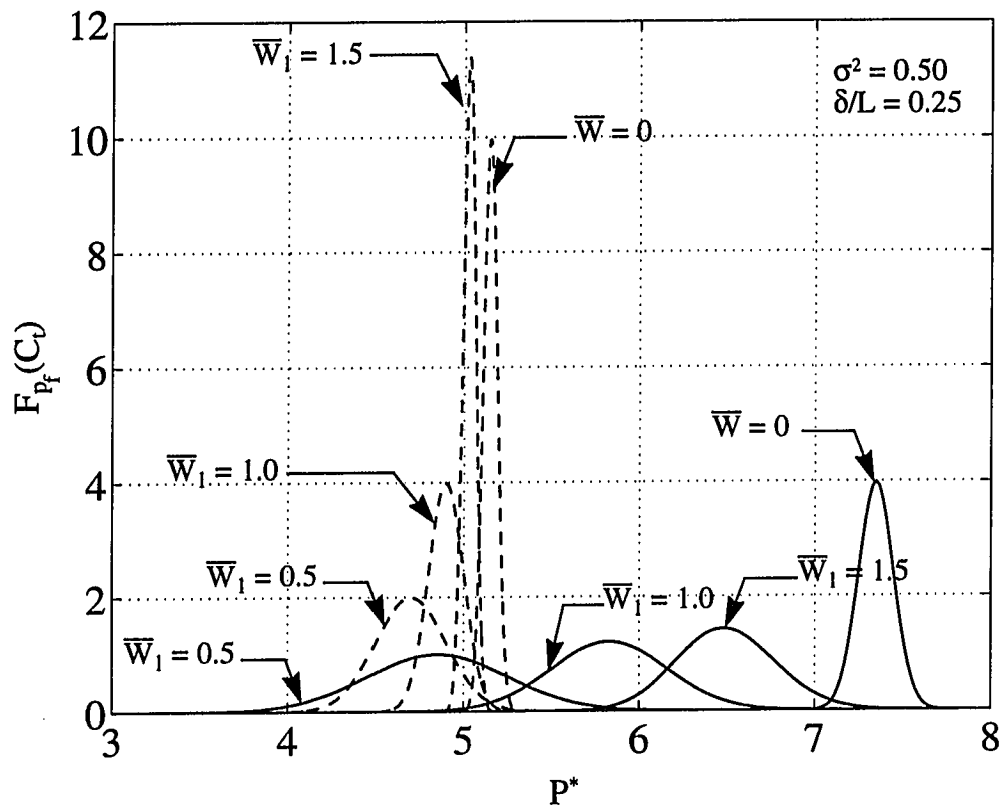


Figure 3.32 Cumulative distribution function for the buckling pressure of a clamped arch with $\lambda = 7.31$ (solid lines) and $\lambda = 5.19$ (dashed lines), for different antisymmetric geometric imperfection configurations.

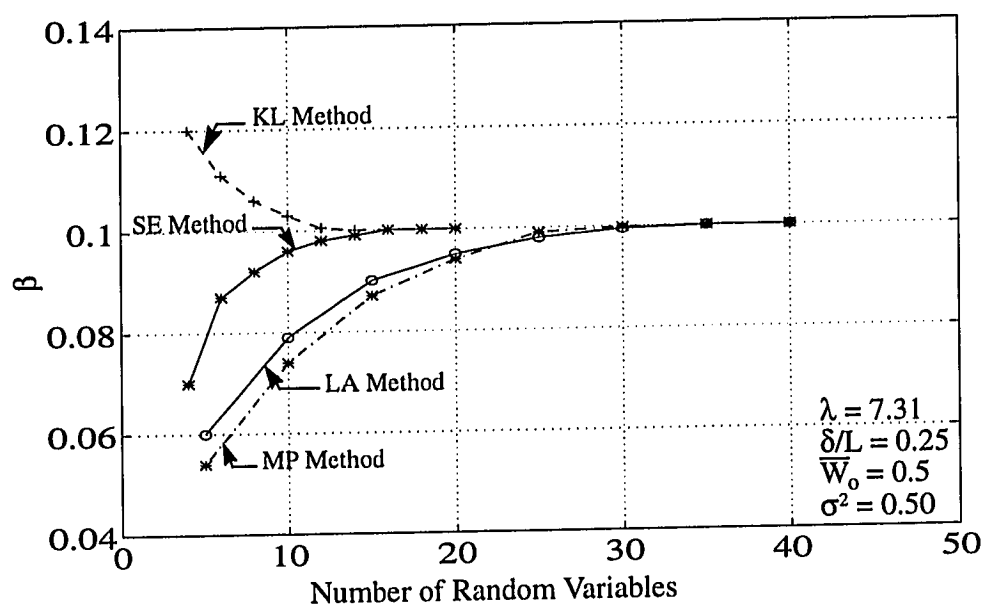


Figure 3.33 Rate of convergence of the reliability index for different discretizations methods for clamped ends arch under pressure loading

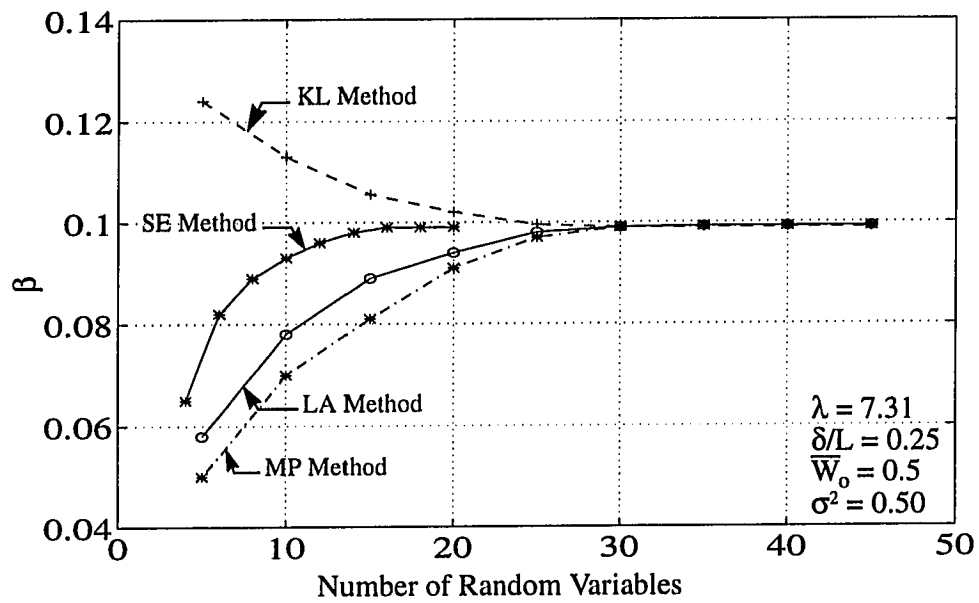


Figure 3.34 Rate of convergence of the reliability index for different discretizations methods for clamped ends arch under pressure loading using a sinusoidal autocorrelation coefficient function

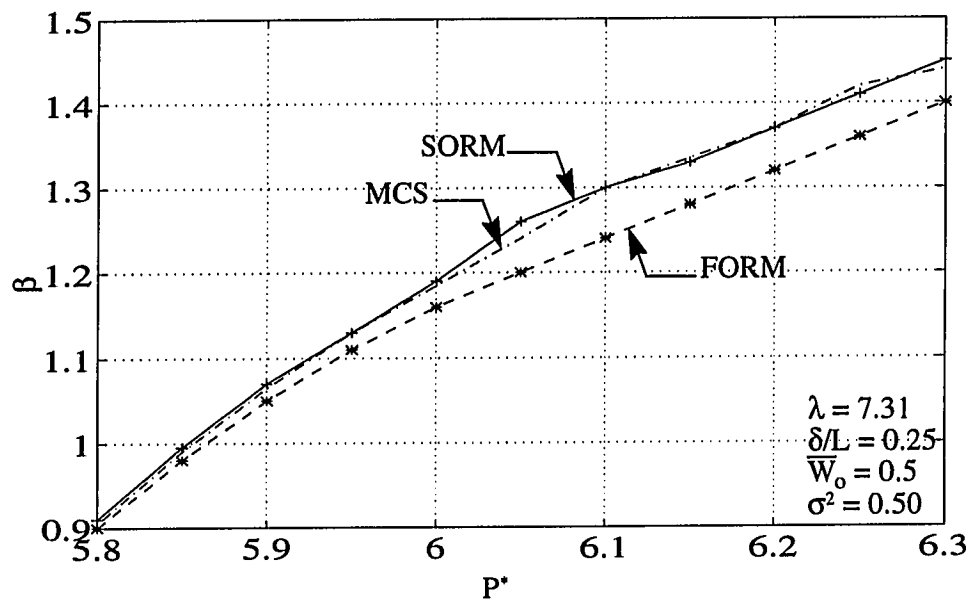


Figure 3.35 Effect of the reliability method used on the reliability index for a clamped ends arch under pressure loading using SE method.

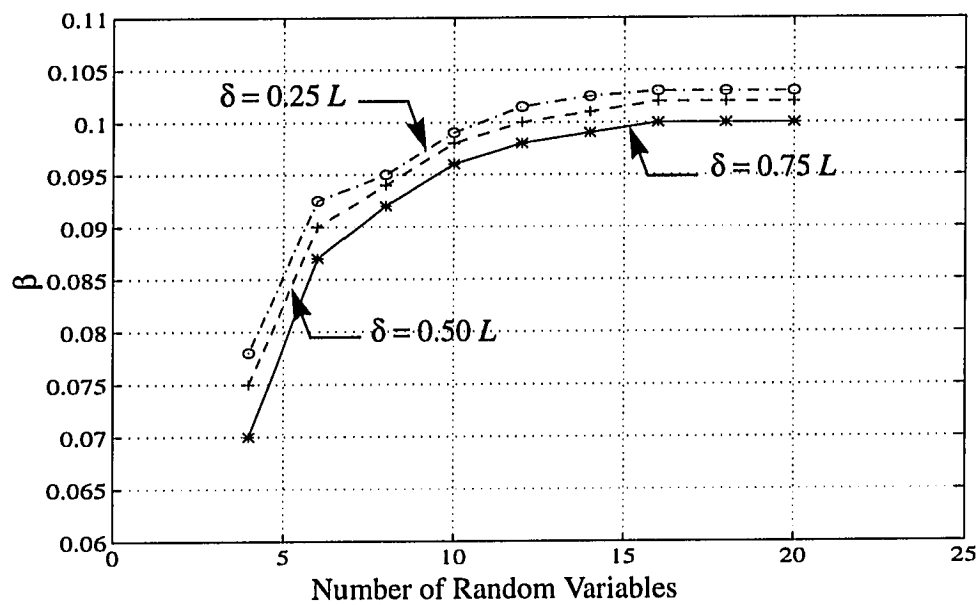


Figure 3.36 Rate of convergence of the reliability index for different correlation lengths for a clamped ends arch under pressure loading using a triangular autocorrelation coefficient function

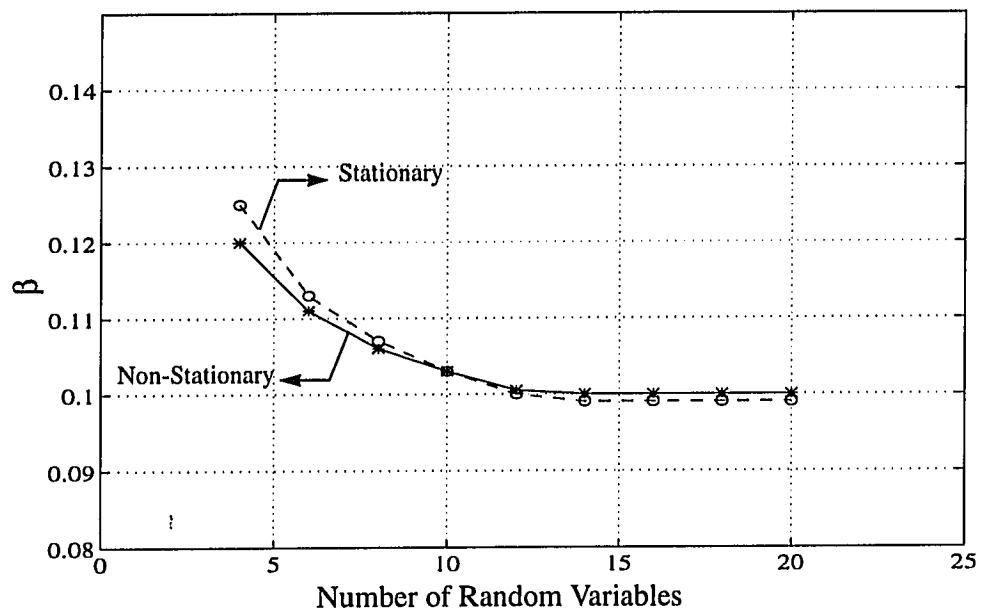


Figure 3.37 The effect of the non-stationarity of the autocorrelation coefficient function on the reliability index for a clamped ends arch under pressure loading using KL method

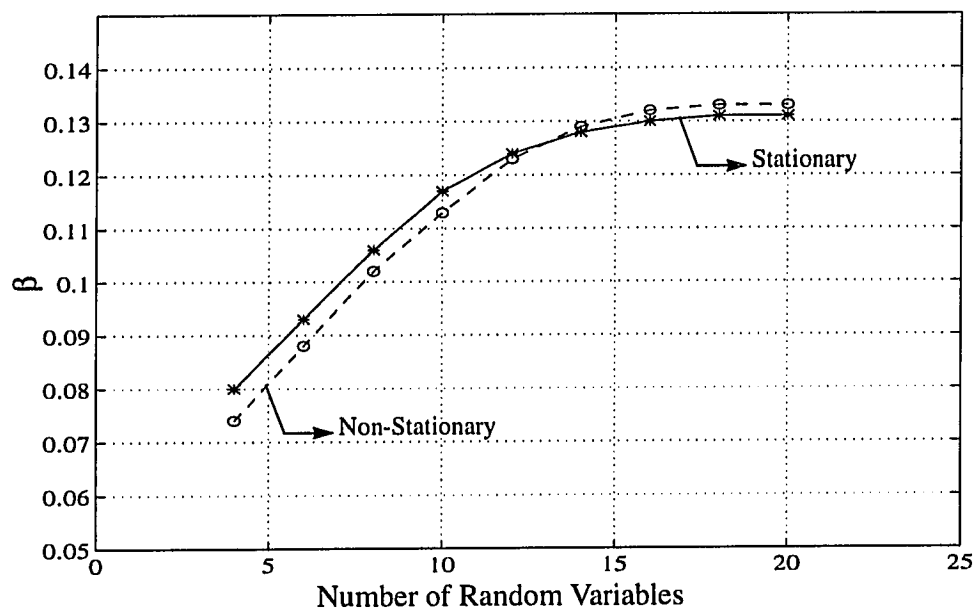


Figure 3.38 The effect of the non-stationarity of the autocorrelation coefficient function on the reliability index for a pinned ends arch under pressure loading using KL method

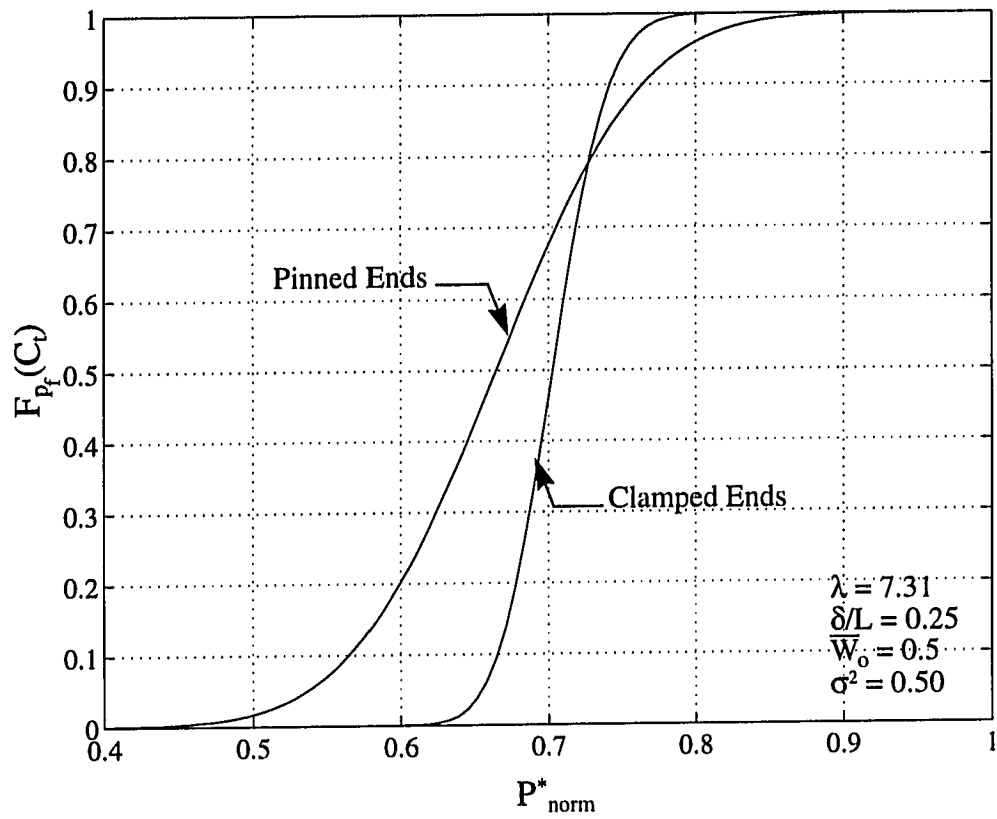


Figure 3.39 Cumulative distribution functions for the unsymmetric buckling load for both pinned and clamped ends arches under uniformly distributed loading.

Chapter 4

Stability of Cylindrical Shells

4.1 Introduction

The analysis of the stability of circular cylindrical shells represents one of the best known examples of the very complicated stability behavior that can occur in thin-walled structures. The presence of initial geometric imperfections in cylindrical shells is recognized as a dominant factor in reducing the buckling load significantly below the classical value obtained from linear theory. Due to the importance of cylindrical shells in different types of civil, marine and aerospace structures, their behavior under various loading conditions has received an enormous amount of research in the past.

For analysis of stability of cylindrical shells, the displacements, rotations and strains are not small enough in comparison with unity to allow the use of linear theories. For the considered cases, where deformations are accompanied by small strains and large rotations, the linear stress-strain relations remain valid, but the nonlinear effect of the rotations need to be considered in the displacement-strain relations. Further, the equilibrium conditions have to be examined in the deformed state. The fundamental deterministic analysis is based on two nonlinear theories given by Flugge (1932) and Donnell (1933).

In the present analysis, nonlinear geometric behavior in the buckling of cylindrical shells is considered. The deterministic buckling loads for different modes of instability are obtained using various energy minimization techniques. The shells are analyzed for different shapes and amounts of geometric imperfections. Both axial compression and/or uniform pressure loadings are considered with different boundary conditions. The postbuckling behavior is studied for all possible responses depending on the chosen initial imperfections of the shell.

A probabilistic analysis of the randomness in the geometric imperfections and the uncertainties of the material properties is presented. The study investigates the effect of the random spatial variability of these parameters on the buckling load and the associated displacements.

Two-dimensional random fields are introduced with different types of autocorrelation coefficient functions to characterize the material properties and the geometrical imperfections. These random fields are discretized using two forms of the series expansion method with a sufficient number of terms. The first technique employs the Karhunen-Loeve theorem to express the field in terms of its eigenfunctions while in the other technique the field is expanded in terms of its spectral decomposition using a set of trigonometric functions. These techniques are compared with both the midpoint and the local averaging methods and prove to be more computationally efficient within a given level of accuracy.

Both first- and second-order reliability methods (FORM/SORM) are used to evaluate different modes of failure based on the buckling load or the associated displacements. The

probability density and the cumulative distribution functions of the buckling loads are presented for different distribution inputs. The sensitivity of the buckling load and the postbuckling displacements to different parameters is also presented. An extensive parametric study is performed to establish a better understanding of the effects of the spatially variable imperfections on the buckling of cylindrical shells.

4.2 Deterministic Stability Analysis

We shall consider moderately large deformations of a circular cylindrical shell with radius R , length L , and thickness t . The shell is made of a homogenous, isotropic and elastic material with a modulus of elasticity E , and Poisson's ratio ν . The coordinate system is taken along the middle surface of the shell as shown in Fig. 4.1, and the displacement components are denoted by U , V and W respectively.

4.3 Analysis Based on Flugge's Equations

The basic nonlinear equations derived by Flugge (1932) are applicable to problems with any buckling configuration, including the Euler buckling of long shells under axial compression.

Flugge's theory is based on the following set of assumptions:

General shell theory assumptions:

1. The shell is sufficiently thin, i.e., $t/R \ll 1$ and $t/L \ll 1$, so that $O\left(\frac{t^3}{R^3}\right)$ terms can be neglected in the derivation of the governing equations.
2. Hooke's law holds as the stress-strain relationship.
3. The strains ϵ are sufficiently small, i.e., $\epsilon \ll 1$, so that the shell remains elastic.

Kirchhoff-Love hypothesis assumptions:

4. Straight lines normal to the middle surface before deformation remain straight and normal to the middle surface with their length unchanged after deformation.
5. In-plane displacements are infinitesimal, i.e., $|U| \ll t$ and $|V| \ll t$.
6. The shell is in a state of plane stress.

Flugge's assumptions:

7. The rotations are moderately small, but the effect of their products and squares on the mid-surface strains are retained.
8. The curvature changes are small enough to allow linearized expressions for the strain-displacement relations for bending strains.
9. In stress resultants expressions, terms with orders higher than $(t/R)^2$ are neglected compared to the unity.
10. Equations of equilibrium are referred to the deformed geometry.

The governing nonlinear differential equations for a perfect shell were developed by Flugge based on a variational principle. Introducing the initial geometrical imperfection component \bar{W} into the equations, we have the equilibrium equations

$$[N_x(1 + U_{,x})]_{,x} + [N_{yx}(1 + U_{,x})]_{,y} + (N_y U_{,y})_{,y} + (N_{xy} U_{,y})_{,x} + p_x - p(W_{,x} + \bar{W}_{,x}) = 0 \quad (4.1)$$

$$[N_{xy}\{1 + V_{,y} - R^{-1}(W + \bar{W})\}]_{,x} + [N_y\{1 + V_{,y} - R^{-1}(W + \bar{W})\}]_{,y} - R^{-1}(M_{y,y} + M_{xy,x}) + (N_x V_{,x})_{,x} + (N_{yx} V_{,x})_{,y} + R^{-1}N_{yx}(W_{,x} + \bar{W}_{,x}) + p_y - (p + R^{-1}N_y)[(W_{,y} + \bar{W}_{,y}) + R^{-1}V] = 0 \quad (4.2)$$

$$\begin{aligned}
M_{x,xx} + (M_{xy} + M_{yx})_{,xy} + M_{y,yy} + R^{-1}N_y\{1 + V_{,y} - R^{-1}(W + \bar{W})\} \\
+ \{N_x(W_{,x} + \bar{W}_{,x}) + N_{xy}[(W_{,y} + \bar{W}_{,y}) - R^{-1}V]\}_{,x} \\
+ \{N_{yx}(W_{,x} + \bar{W}_{,x}) + N_y[(W_{,y} + \bar{W}_{,y}) - R^{-1}V]\}_{,y} \\
+ R^{-1}N_{yx}V_{,x} + p\{1 + U_{,x} + V_{,y} + R^{-1}(W + \bar{W})\} = 0
\end{aligned} \tag{4.3}$$

with the boundary conditions

$$N_x = p_x^* \quad \text{or} \quad U = U^* \tag{4.4}$$

$$N_{xy} - R^{-1}M_{xy} = p_y^* \quad \text{or} \quad V = V^* \tag{4.5}$$

$$M_{x,x} + (M_{xy} + M_{yx})_{,y} = p_z^* \quad \text{or} \quad W = W^* \tag{4.6}$$

$$M_x = M_x^* \quad \text{or} \quad W_{,x} = W_x^* \tag{4.7}$$

where p_x , p_y and p are the x, y and z components, respectively of the distributed forces per unit area of the shell, and the stress resultants per unit length, acting along the $x = \text{const.}$ and $y = \text{const.}$ are defined as

$$N_x, N_{xy} = \int_{-t/2}^{t/2} (\sigma_x, \tau_{xy}) \left(1 - \frac{z}{R}\right) dz, \tag{4.8}$$

$$N_{yx}, N_y = \int_{-t/2}^{t/2} (\tau_{yx}, \sigma_y) dz, \tag{4.9}$$

$$M_x, M_{xy} = \int_{-t/2}^{t/2} (\sigma_x, \tau_{xy}) \left(1 - \frac{z}{R}\right) z dz, \tag{4.10}$$

$$M_{yx}, M_y = \int_{-t/2}^{t/2} (\tau_{yx}, \sigma_y) z dz. \tag{4.11}$$

The stress components σ_x , σ_y and τ_{xy} are related to the strain components ϵ_x , ϵ_y and γ_{xy}

using Hooke's law for the state of plane stress, namely

$$\sigma_x = \frac{E}{1-\nu^2}(\epsilon_x + \nu\epsilon_y), \quad (4.12)$$

$$\sigma_y = \frac{E}{1-\nu^2}(\epsilon_y + \nu\epsilon_x), \quad (4.13)$$

$$\tau_{xy} = \frac{E}{2(1+\nu)}\Upsilon_{xy}. \quad (4.14)$$

The nonlinear strain-displacement relations are given by Flugge (1932) and Yamaki (1984) for the perfect shell. The corresponding relations for the imperfect shell are given by

$$\epsilon_x = U_{,x} - zW_{,xx} + \epsilon_{xo}, \quad (4.15)$$

$$\epsilon_y = V_{,y} - \frac{R}{R-z}zW_{,yy} - \frac{1}{R-z}W + \epsilon_{yo}, \quad (4.16)$$

$$\Upsilon_{xy} = \frac{R-z}{R}V_{,x} + \frac{R}{R-z}U_{,y} - \left(1 + \frac{R}{R-z}\right)zW_{,xy} + \Upsilon_{xyo}, \quad (4.17)$$

where

$$\epsilon_{xo} = \frac{1}{2}[U_{,x}^2 + V_{,x}^2 + (W_{,x}^2 + W_{,x}\bar{W}_{,x})], \quad (4.18)$$

$$\epsilon_{yo} = \frac{1}{2}[U_{,y}^2 + \{V_{,y} - R^{-1}W\}^2 + \{W_{,y} + R^{-1}V\}^2], \quad (4.19)$$

$$\Upsilon_{xyo} = U_{,x}U_{,y} + V_{,x}\{V_{,y} - R^{-1}W\} + W_{,x}\bar{W}_{,y} + W_{,y}\bar{W}_{,x} + W_{,x}W_{,y} + R^{-1}VW_{,x}. \quad (4.20)$$

Thus, using Hooke's law and the previous strain-displacement relations, the stress resultants can be obtained in terms of the displacements after performing the integrations in Eq. 4.8 to Eq. 4.11.

Since the boundary conditions of the shells are usually defined in terms of specified values for the displacements or rotations at the ends, a displacement approach will be considered to obtain the solution. For a typical case of a complete shell hinged in both the tangential and the radial directions at both ends, the displacement components can be introduced as

$$U = \sum_{m=1}^{\infty} \sum_{n=1}^{\infty} A_{mn} \cos\left(\frac{m\pi x}{L}\right) \cos\left(\frac{ny}{R}N\right), \quad (4.21)$$

$$V = \sum_{m=1}^{\infty} \sum_{n=1}^{\infty} B_{mn} \sin\left(\frac{m\pi x}{L}\right) \sin\left(\frac{ny}{R}N\right), \quad (4.22)$$

$$W = \sum_{m=1}^{\infty} \sum_{n=1}^{\infty} C_{mn} \sin\left(\frac{m\pi x}{L}\right) \cos\left(\frac{ny}{R}N\right), \quad (4.23)$$

and the imperfection as

$$\bar{W} = \sum_{m=1}^{\infty} \sum_{n=1}^{\infty} D_{mn} \sin\left(\frac{m\pi x}{L}\right) \cos\left(\frac{ny}{R}N\right). \quad (4.24)$$

where D_{mn} are known parameters based on the chosen imperfection while A_{mn} , B_{mn} and C_{mn} are unknown coefficients.

The next step is to substitute for the values of the deflections and the imperfection in the three governing equations, along with obtaining the values of the stress resultants starting with the expanded displacements and applying Hooke's law. Due to complexity of the equations, a numerical procedure is developed for the analysis based on discretizing the shell and applying Galerkin method to obtain a set of cubic equations in the unknown parameters. An iterated Newton-Raphson method, from an IMSL FORTRAN 77

subroutine, is then used for solving the equations. The terms were usually kept till the tenth term and convergence of the solution was checked in each case. The equations obtained are general for any value of N . In the solution, only one value was considered at a time.

The linearized Flugge's equations, were compared with the nonlinear equations. Typical results for obtaining the linear buckling load are shown in Fig. 4.2 and Fig. 4.3 under either a uniform hydrostatic pressure or an axial loading applied to a perfect clamped cylindrical shell. It should be noted that the mathematical complexity in the linear case is a tiny fraction of the analysis required to evaluate the nonlinear buckling behavior.

4.4 Analysis Based on Donnell's Equations

Donnell's nonlinear theory of circular cylindrical shells was established by Donnell (1933). Owing to its relative simplicity and practical accuracy for many cases, the theory has been widely used for analyzing both buckling and postbuckling problems.

The shell equations given by Donnell have a deficiency that makes them inapplicable to the analysis of the deformations of a cylinder in which the magnitude of the in-plane displacements are of the same order as that of the normal deflection. This deficiency affects the buckling of a long cylindrical shell with a circular circumferential wave number less than four.

Donnell's theory still uses the general shell theory assumptions and the Kirchhoff-Love hypothesis assumptions, given by items number 1-6 in the previous section, in addition to the following set of assumptions:

Donnell's approximations:

1. Out-of-plane displacement is of the same order as the shell thickness, i.e.,

$$W = O(t).$$

2. The derivatives of W are small and can be neglected compared to unity but their squares and products are of the same order as the strains ε considered herein, i.e.,

$$\left\{ \left| \frac{\partial W}{\partial x} \right|, \left| \frac{\partial W}{\partial y} \right| \right\} \ll 1 \quad \left\{ \left(\frac{\partial W}{\partial x} \right)^2, \left| \frac{\partial W}{\partial x} \right| \cdot \left| \frac{\partial W}{\partial y} \right|, \left(\frac{\partial W}{\partial y} \right)^2 \right\} = O(\varepsilon) \quad (4.25)$$

3. Curvature changes are small and the influence of the in-plane displacements on them is negligible.
4. Shear resultants are negligible in the tangential force equilibrium equations.

The governing nonlinear differential equations are given by Donnell, based on a variational principle, as

$$N_{x,x} + N_{xy,y} + p_x = 0 \quad (4.26)$$

$$N_{xy,x} + N_{y,y} + p_y = 0 \quad (4.27)$$

$$D\nabla^4 W - R^{-1}N_y - N_x W_{,xx} - 2N_{xy}W_{,xy} - N_y W_{,yy} - p + p_x W_{,x} + p_y W_{,y} = 0 \quad (4.28)$$

where p_x , p_y and p are the x, y and z components, respectively of the distributed forces per unit area of the shell. The stress resultants per unit length, acting along the $x=\text{const.}$ and $y=\text{const.}$ are defined as

$$N_x, N_{xy}, N_y = \int_{-t/2}^{t/2} (\sigma_x, \sigma_y, \tau_{xy}) dz \quad (4.29)$$

where σ_x and σ_y are the stresses in the shell in the x, y directions and τ_{xy} is the shear stress

in the x - y plane. The flexural rigidity of the shell is defined as

$$D = \frac{Et^3}{12(1-\nu^2)} \quad (4.30)$$

The boundary conditions are given along the boundaries $x = 0$ and $x = L$ in terms of prescribed displacements, rotation or loads as

$$N_x = p_x^* \quad \text{or} \quad U = U^* \quad (4.31)$$

$$N_{xy} = p_y^* \quad \text{or} \quad V = V^* \quad (4.32)$$

$$M_{x,x} + 2M_{xy,y} + N_x W_{,x} + N_{xy} W_{,y} = p_z^* \quad \text{or} \quad W = W^* \quad (4.33)$$

$$M_x = M_x^* \quad \text{or} \quad W_{,x} = W_x^* \quad (4.34)$$

where p_x^* , p_y^* and p_z^* are components of the external loads, per unit length, applied along the edges and U^* , V^* , W^* and W_x^* are the prescribed values of the displacement components and the rotation, respectively, along the edges. Various boundary conditions can be constructed by selecting one condition from each pair of the previous equations.

For all cases under study, $p_x = p_y = 0$, which enables the use of the stress function F defined as

$$N_x = F_{,yy}, \quad N_y = F_{,xx}, \quad N_{xy} = -F_{,xy}. \quad (4.35)$$

Thus, the governing equations can be obtained in a more convenient form in terms of the stress function instead of the stress resultant as a compatibility condition given by

$$\nabla^4 F + Et(R^{-1}W_{,xx} - W_{,xy}^2 + W_{,xx}W_{,yy}) = 0, \quad (4.36)$$

and an equilibrium equation given by

$$D\nabla^4 W - R^{-1}F_{,xx} - F_{,yy}W_{,xx} + 2F_{,xy}W_{,xy} - F_{,xx}W_{,yy} - p = 0. \quad (4.37)$$

The strain-displacement relations for analysis based on Donnell's equations were given by Yamaki (1984).

4.4.1 Imperfection Modeling

Denoting the initial geometric imperfection as \bar{W} and introducing it into the previous derivation, the Donnell type basic equations governing the finite deformation of the shell become

$$\nabla^4 F + Et(R^{-1}W_{,xx} - W^2_{,xy} + W_{,xx}W_{,yy} - 2\bar{W}_{,xy}W_{,xy} + \bar{W}_{,xx}W_{,yy} + \bar{W}_{,yy}W_{,xx}) = 0 \quad (4.38)$$

and

$$D\nabla^4 W - R^{-1}F_{,xx} - F_{,yy}(W + \bar{W})_{,xx} - F_{,xx}(W + \bar{W})_{,yy} + 2F_{,xy}(W + \bar{W})_{,xy} - p = \vartheta(W) = 0 \quad (4.39)$$

Both W and \bar{W} are expanded in generalized Fourier series as

$$W = \sum_{m=1}^{\infty} \sum_{n=1}^{\infty} a_{mn} W_{mn}, \quad (4.40)$$

$$\bar{W} = \sum_{m=1}^{\infty} \sum_{n=1}^{\infty} c_{mn} W_{mn}, \quad (4.41)$$

where c_{mn} are known parameters based on the chosen imperfections while a_{mn} are the unknown coefficients, and W_{mn} is a complete set of basis functions chosen to satisfy the boundary conditions of the shell at $x = \pm \frac{L}{2}$. For built-in ends

$$W_{mn} = \frac{1}{2} \left[(-1)^{m+1} + \cos\left(\frac{2\pi mx}{L}\right) \right] \cos\left(\frac{n y}{R} N\right), \quad (4.42)$$

and for simply supported ends

$$W_{mn} = \sin\left[\pi m\left(\frac{x}{L} + 0.5\right)\right] \cos\left(\frac{ny}{R}N\right), \quad (4.43)$$

where N is the number of waves in which the shell buckles in the circumferential direction.

A general solution for the stress function F is obtained by substituting Eq. 4.40 and Eq. 4.41 into the first of the two governing equations, Eq. 4.38, and integrating analytically, we are able to get F in a series form. The homogenous boundary conditions on the stress function are satisfied during the integration step. These conditions for a cylindrical shell subjected to axial or pressure loading and clamped to stiff end plates along both edges, $x = \pm \frac{L}{2}$, are

$$\begin{aligned} U_{,y} = V_{,y} = 0 \\ \text{i.e. } F_{,xx} - \nu F_{,yy} = F_{,xxx} + (2 + \nu)F_{,xyy} = 0 \end{aligned} \quad (4.44)$$

and

$$\int_0^{2\pi R} N_{xy} dy = 0, \quad \int_0^{2\pi R} N_x dy = \Pi(p) \quad (4.45)$$

$$\text{i.e. } F_{,x}\big|_{y=0}^{2\pi R} = 0, \quad F_{,y}\big|_{y=0}^{2\pi R} = \Pi(p) \quad (4.46)$$

where $\Pi(p)$ depends of the type of loading considered as

$$\begin{aligned} \Pi(p) &= -\pi R^2 p & \text{for pressure loading} \\ \Pi(p) &= -P & \text{for axial loading} \end{aligned} \quad (4.47)$$

where P is the axial load applied on the shell.

Thus, the expressions for W and F are obtained. The final step is applying the Galerkin method to Eq. 4.39, which leads to

$$\int_{-\frac{L}{2}}^{\frac{L}{2}} \int_{-\frac{\pi R}{N}}^{\frac{\pi R}{N}} \vartheta(W) W_{rs} dx dy = 0, \quad r = 1, 2, 3, \dots \quad s = 1, 2, 3, \dots \quad (4.48)$$

where W_{rs} are given from Eq. 4.42 and Eq. 4.43. Performing integration, we finally obtain a set of cubic equations in a_{mn} . Solution of this set is carried out using the iterated Newton-Raphson method and thus determining the unknown deflections.

For a chosen problem with a deterministic field of imperfections, the analysis based on Flugge's equations required 15 minutes of computing time on a Sun SparcStation 5 machine, mostly because of the size of iterations required to solve the resulting set of equations. On the other hand, a solution in a very good agreement based on Donnell's equation was obtained in less than one minute for the same problem. Since application of the reliability theory requires solving the deterministic stability problem for many realizations, only Donnell nonlinear equations are used in the reliability analysis, and the results are applicable to cases where the buckling mode has $N \geq 4$.

4.5 Random Field Discretization

As in the previous chapter, continuous random fields are used for modeling geometrical and material imperfections. The same discretization techniques previously mentioned are used. Thus, the geometric configuration and the material properties of the shell are defined using a two-dimensional random field for each, which are then discretized using a grid of random-field elements and nodes or a series expansion.

Two types of autocorrelation functions are considered. The eigenfunctions and eigenvalues are obtained numerically for both of them.

4.5.1 First Degree Exponential Autocorrelation Coefficient Function

Consider the kernel defined by the equation

$$\rho(x, y, x', y') = e^{-(c_1|x-x'| + c_2|y-y'|)} \quad (4.49)$$

where c_1 and c_2 are parameters used to adjust the correlation length in the axial and circumferential direction respectively, and $(x, y), (x', y')$ are any two points on the shell. Two, loosely named, correlation lengths, δ_x and δ_y , are given for this kernel as $\delta_x = 1/c_1$ and $\delta_y = 1/c_2$.

A more widely used formulation for the first degree exponential autocorrelation function is defined in the form

$$\rho(x, y, x', y') = e^{-c|d|} \quad (4.50)$$

as

$$d = \sqrt{(x-x')^2 + (y-y')^2} \quad (4.51)$$

where the correlation is based on the absolute distance between the points without reference to the directions. The first formulation allows for studying the effect of having two different correlation magnitudes in different direction as will be shown later in the analysis.

4.5.2 Triangular Autocorrelation Coefficient Function

Consider the function defined as

$$\rho(x, y, x', y') = \begin{cases} 1 - (c_1|x-x'| + c_2|y-y'|) & \text{if } > 0 \\ 0 & \text{otherwise} \end{cases} \quad (4.52)$$

where c_1 and c_2 are parameters used to adjust the distances $|x-x'|$ and $|y-y'|$ of null

correlation between any two points on the shell, namely (x, y) and x', y' . The correlation lengths in the axial and circumferential direction are defined as $\delta_x = (1/c_1)(1 - e^{-1})$ and $\delta_y = (1/c_2)(1 - e^{-1})$ respectively. This kernel represents a linear decrease in correlation, which may be useful for some quality control problems which is an application of the results of this study.

The linear autocorrelation function can be given by a more widely used formulation in the form

$$\rho(x, y, x', y') = \begin{cases} 1 - c|d| & \text{if } |d| < \frac{1}{c} \\ 0 & \text{otherwise} \end{cases} \quad (4.53)$$

where d is given by Eq. 4.51 defining the absolute distance between the points without reference to the directions.

4.6 Numerical Examples

Calculations were carried out for three geometric configurations for the cylindrical shells. A geometric parameter, z , representing the relative length of the shell

$$z = \sqrt{1 - \nu^2} \frac{L^2}{Rt} \quad (4.54)$$

where ν is Poisson's ratio ($\nu = 0.3$ here). The values 50, 100, 500 for z were considered during the analysis in order to study different cases of either short or long cylindrical shells. A value of $R/t = 400$ is considered throughout the analysis. This value was considered in order to be able to compare the results obtained herein with similar experiment work given by Yamaki (1984).

The geometrical imperfection in the shells is assumed to be a two-dimensional Gaussian random field defined in terms of its autocorrelation coefficient function, mean function, and variance function. The two types of autocorrelation coefficient functions defined by Eq. 4.49 and Eq. 4.52 are used. The correlation lengths in both of Eq. 4.49 and Eq. 4.52 are chosen as $0.25L$ in the longitudinal directional and $1.5R$ in the circumferential directional which is slightly less than one quarter of the circumferential length of the cylinder. A value of $0.25L$ is considered for the correlation length in Eq. 4.50 and Eq. 4.53. The mean function is considered to be defined in terms of a chosen value of the imperfections all over the shell. Three different fields of imperfections are considered with maximum amplitudes of the initial imperfections having the values $\bar{W}_1 = 0.2t$, $0.4t$ and $0.6t$. The expansions of the mean functions for the fields, with increasing imperfections, in Fourier series, as defined in Eq. 4.41, are shown in Fig. 4.4, Fig. 4.5 and Fig. 4.6, respectively. These expansions are evaluated for the case of a cylindrical shell having clamped ends for which the basis functions are given in Eq. 4.42. The variance function is considered to be constant and having a value of 0.5.

The modulus of elasticity $E(x)$ is assumed to be a homogeneous Gaussian random field with a constant mean function having a value of $29 \times 10^6 \text{ lb/in.}^2$ and a constant variance of 0.25. The two types of autocorrelation coefficient functions defined earlier are also used for this case with correlation lengths of $\delta_x = 0.25L$ and $\delta_y = 1.5R$ in the longitudinal and circumferential directions respectively.

The random fields are discretized into sets of random vectors using the earlier mentioned four methods. Based on each discretization, a set of random variables is

introduced in the reliability code CALREL, which is then used to provide an estimate for the reliability index, failure probability and sensitivity measures based on FORM and SORM. The use of MCS proved to be very time consuming even in combination with Donnell's equation rather than Flugge's.

4.6.1 Pressure Loading

The limit state functions considered in the probabilistic analysis are based on the form given by Eq. 2.3. Two failure criteria are considered based on exceeding a defined threshold for the load applied or for the resulting deflection. This again allows for the possibility of either considering a component or system reliability problem.

Compared with the arch buckling problem considered in the previous chapter, the number of random variables required for the buckling of cylindrical shells is much higher. This makes it extremely important to use the most efficient method for discretizing the random fields. For sake of comparison, we will consider a clamped ends cylindrical shell and we will consider only the random field representing the geometrical imperfection, i.e., the modulus of elasticity is considered to have a deterministic constant value throughout the shell.

The complete statistical distribution of the buckling load or the resulting deflection can be obtained by varying the value of the threshold C_l over a range of values and evaluating the failure probability for each value. Then the CDF can be evaluated as

$$F_{P_f}(C_l) = 1 - P_f(C_l) \quad (4.55)$$

where $F_{P_f}(C_l)$ is the value of the CDF based on a given value of the threshold C_l .

The analysis is carried out using nonlinear Donnell's equations and the relations between the pressure and the deflection, edge shortening, or the volume change are obtained for different wave numbers in the circumferential direction, N . The lowest buckling load for different values of N is considered to be the critical buckling load. Depending on the value of the geometrical parameter, z , and based on a considerable number of problems analyzed, a certain range of N is considered for each problem as shown in Table 4.1. More than one value of N can be considered for the same shell as each

Table 4.1: Values of N for the lowest buckling loads.

z	N			
	Pressure Loading		Axial Loading	
	Min.	Max.	Min.	Max.
50	21	25	16	21
100	17	20	15	19
500	11	14	11	17

value will account for a different buckling mode with a combination of two or more required in order to obtain the lowest possible buckling load at every stage throughout the buckling process. This is another important aspect requiring the use of system reliability methods in order to take into account different modes of failure.

During the reliability analysis, the complete deterministic solution for the stability of the shells is carried out in order to compute the buckling load and the associated displacements for each realization of the random variables, i.e., in each realization, the imperfections are expanded in terms of Fourier series and a deterministic solution is

obtained based on the shell configuration in this realization of the random variables.

Before discussing the probabilistic behavior of the shells, the difference between the three types of imperfection fields considered during the analysis is checked deterministically. The deterministic relations between the pressure $K_p = pRL^2/\pi^2D$, and the relative edge shortening $\bar{\Delta} = \Delta R/Lt$, where Δ is the axial edge shortening, are plotted under the mean values of the three geometric imperfection configurations considered in the analysis as shown in Fig. 4.7, Fig. 4.8 and Fig. 4.9 for values of $z = 500$, 100 and 50, respectively. The relations are plotted for $N = 13$, 19 and 23 respectively which give the lowest buckling loads for these configurations. The effect of increasing the geometric imperfection magnitude is clear in comparison with the perfect shell response.

Using Eq. 4.55, the CDFs for the distribution of the buckling load under the random imperfection fields are obtained. The effect of changing the dimensions of the shell or the length to radius ratio on the response is shown in Fig. 4.10 for clamped shells under the same imperfection distribution. On the other hand, the effect of considering various imperfection distributions on the same shell with $z = 500$ is shown in Fig. 4.11.

To compare the effect of the mode shape of the mean function of the random field representing the imperfections on the behavior of the shells, we will consider a simplified function for the mean based on a single value of N . For the case of $z = 500$, where the critical N value is 13, we shall consider two types of imperfection fields. The first random field has a mean function with $N = 13$ with the maximum amplitudes of $\bar{W}_2 = 0.2t$, $0.4t$ and $0.6t$. The second field has $N = 15$ with the maximum amplitudes of $\bar{W}_3 = 0.2t$, $0.4t$ and $0.6t$. The distributions for both cases are plotted in Fig. 4.12 and Fig. 4.13 respectively. It

can be seen that an imperfection shape similar to that of the critical buckling mode lowers the bulking load considerably. However, the buckling load also becomes less sensitive to the uncertainties in the imperfections since the distributions are narrower in Fig. 4.12 than in Fig. 4.11. For an imperfection shape (\bar{W}_3) with a value of N other than the critical value, the buckling behavior is very similar to that of a shell under a general random field (\bar{W}_1) with the same maximum amplitude.

Due to the fact that no exact forms are available for the eigenvalues and eigenfunctions of the autocorrelation functions for the two-dimensional case, the KL method does not prove to be superior to either the MP or LA methods in terms of efficiency. On the other hand, the SE method shows a better convergence rate for the reliability index within a lower number of random variables as shown in Fig. 4.14. For a number of problems, the number of random variables required using the SE method is usually in the order of 50-75% of that required using the other three methods. As expected, the four methods converge to almost the exact same reliability index.

A comparison is made between the values of the probability of failure obtained using FORM and SORM. As shown in Fig. 4.15 for the shell with clamped ends, FORM results appear to be in an acceptable agreement with SORM. Since FORM solutions were obtained in a very short computing time, as it required less than 15 iterations to converge, it can be used to provide an initial estimate of the failure probability. For the cases under study, SORM required a 4-15% increase in the computational time over FORM. Also, this analysis shows the efficiency of using SORM compared to MCS as almost the same results can be obtained using the former in a small fraction of the processor time required

for the latter.

The values of the probability of failure based MCS were obtained for only three values of the coefficient C_1 in the limit state function. The difference between these values and results based on SORM showed to be less than 0.5% of the probability of failure. This agrees with the good agreement between MCS and SORM previously shown for the arch buckling problem. It should be emphasized here that around 10,000 simulations are required to get a reliable estimate of the failure probability using MCS which requires a tremendous computing time compared with the 15 iterations needed for FORM/SORM.

In order to obtain a complete statistical representation of the buckling load, in the form of a CDF, it is required to obtain the value of the failure probability for a large number, namely 100 in the current analysis, of limit state functions by changing the value of C_1 . Based on the previous comparisons, only SORM results and the use of the SE method were considered in all the examples.

The effect of the non-stationarity in the autocorrelation function which is mentioned in paragraph 2.10 is checked for a shell with clamped ends. The difference between applying Eq. 2.49 to compensate for the non-stationarity of the function near the supports, and between neglecting this effect is shown in Fig. 4.16 for a shell with $z = 500$ under imperfection mode number 1.

The type and properties of the autocorrelation coefficient function used in the analysis play an important role in affecting the failure probability. Considering a clamped ends shell and identical values for the correlation lengths and only changing the type of correlation from exponential to linear has the effect shown in Fig. 4.17 on the results. It

can be concluded that the higher the correlation between the points, shown for the linear function, the lower is the resulting buckling loads.

Another effect of the correlation properties is shown when changing the correlation lengths in both the axial and circumferential directions as shown in Fig. 4.18 and Fig. 4.19 respectively. As before, we can still see that higher correlation between the points results in lower buckling loads. It is worth noting here that, as shown from the figures, the change in the correlation lengths in the circumferential direction affects the buckling behavior much more, up to 50% in some cases, than the same change in the axial direction.

4.6.2 Axial Loading

The same principles considered in the previous analysis for the case of pressure loading will be used herein. Some of the parameters checked for the previous case will be considered again along with various other parameters which seem to have more effect on the case of axial loading compared with pressure loads.

The difference between the three types of imperfection fields considered before is checked deterministically first for the three geometric configurations of the shell. The relations between the axial load and the edge shortening are plotted for the mean values of the geometric imperfection fields considered in the analysis as shown in Fig. 4.20, Fig. 4.21 and Fig. 4.22 for values of $z = 500, 100$ and 50 , respectively. The relations are plotted for $N = 15, 17$ and 18 respectively which give the lowest buckling loads for these configurations. The effect of increasing the geometric imperfection magnitude is again clear in comparison with the perfect shell response. The value of the axial buckling ratio, Σ , considered in all the graphs is a normalized value of the buckling load, P , by dividing it

by the classical value, P_{cl} , for the case of $N = 0$ as

$$\Sigma = \frac{P}{P_{cl}}, \quad P_{cl} = \frac{2\pi Et^2}{\sqrt{3(1-\nu^2)}} \quad (4.56)$$

for the case of a clamped shell.

The CDFs for the three geometric configurations under the same imperfection distribution are shown in Fig. 4.23 illustrating the effect of changing the length to radius ratio on the buckling behavior. On the other hand, the effect of considering various imperfection distributions for the same shell is shown in Fig. 4.24. A behavior similar to that in the case of pressure loading is obtained when considering other types of functions for the mean of the imperfections.

Solutions based on the Donnell's equations are expected to be inaccurate for long shells which buckle in small number of circumferential waves because of the assumptions included in the derivation. Yamaki (1984) showed that the error in the Donnell solutions is only significant when the number of the buckled waves N is equal or less than 4. He showed also that the error is less than 1% for cases where N equals 5 and 6. This confirms the applicability of Donnell solutions for the analysis as they are practically accurate for all the cases considered in the study. A comparison between the buckling behavior for the shell based on the two solutions together with the linear Flugge's equations is shown in Fig. 4.25. This clearly represents the excellent agreement between both nonlinear methods.

The possibility that having more than one value of N corresponding to the lowest buckling load because of the uncertainty in the imperfections is checked for a clamped

cylindrical shell with $z = 100$. The shell is analyzed for both values of $N = 17, 19$. The first of these two values corresponds to the critical buckling load under the mean values of the imperfection while the second value corresponds to the second lowest buckling load under the same imperfections. The CDFs for these two cases are compared with the CDF resulting from considering a series system with two limit state functions based on the lowest buckling load for the two values of N as shown in Fig. 4.26. It can be easily concluded that considering $N = 19$ results in higher buckling loads than for $N = 17$. On the other hand, the values of buckling loads for the series system is lower in general than that of any of the two N 's and is closer to that of the most critical one, that is $N = 17$.

A comparison between the different techniques used for random field discretizations is shown in Fig. 4.27. Also CDFs based on both FORM and SORM are shown in Fig. 4.28. These two comparisons agree with the conclusion made earlier that the SE method proves to be the most efficient discretization technique for the cases under study in this chapter and that SORM displays the ability to give both accurate and efficient results compared with FORM and MCS.

The effect of the non-stationarity in the autocorrelation function is checked for a shell with clamped ends. The difference between applying Eq. 2.49 to compensate for the non-stationarity of the function near the supports, and between neglecting this effect is shown in Fig. 4.29 for a shell with $z = 100$. As in the case of pressure loading, the error in neglecting the non-stationarity of the autocorrelation function is minimal.

The same discussion mentioned in pressure loading case regarding the effects of the type and properties of the autocorrelation coefficient function on the buckling behavior

applies here. Considering a clamped ends shell and changing the correlation function from exponential to linear with the same correlation lengths has the effect shown in Fig. 4.30 on the results.

The effect of the correlation length is checked here in more than one way. First using the autocorrelation function defined in Eq. 4.50, where the direction of the correlation does not come into question, the effect of changing the correlation length is shown in Fig. 4.31.

Alternatively, when using the autocorrelation function defined by Eq. 4.49, we can see in Fig. 4.32 and Fig. 4.33 that the change in the correlation lengths in the circumferential direction affects the buckling behavior more than the same change in the axial direction. This also still agrees with the previous conclusion that higher correlation between the points results in lower buckling load.

The uncertainty in the value of the modulus of elasticity of the shell material has a slight effect on the buckling behavior of the shell compared with uncertainties in shape as shown in Fig. 4.34. This also agrees with the previously illustrated results for the buckling behavior of shallow arches where the geometric imperfections are the dominant factor in lowering the buckling loads.

The effect of the boundary conditions of the shell is shown in Fig. 4.35 where the probabilistic distributions of the buckling load are plotted for both cases of clamped ends and hinged ends cylindrical shell having the same dimensions and under the same imperfection. The same conclusions made till now regarding the buckling behavior of clamped cylindrical shells applies when comparing the same parameters affecting either

hinged-hinged or hinged-clamped shells.

4.6.3 Combined Loading

The same previous methods of analysis, namely Donnell's nonlinear equations, can be used to obtain practically accurate solutions for cases of combined hydrostatic pressure and axial loading. Axial compression can be combined with either external or internal pressure on the shell. The possibility of buckling also exists for the case of a cylinder under both axial tension and external pressure.

As an example of this case, we shall look at the case of a clamped cylindrical shell under an increasing axial loading combined with various ratios, α , of the hydrostatic pressure. The deterministic behavior of a shell with $z = 500$ and with the imperfection configuration number 1 is shown in Fig. 4.36 for $\alpha = -3.0, 0, 0.3$. This accounts for both cases of internal and external pressures. The buckling load, as expected, increases with the application of internal pressure and decreases with external pressure.

The probabilistic distribution for three values of α is shown in Fig. 4.37. It can be seen that the effect of existence of the pressure makes almost parallel shifts for the CDF curve which is equivalent to changing the values of the mean of the distribution of the buckling load.

For the previous case of combined loading and for most of other cases, the stochastic behavior of the buckling load is the same as that for the case of either an axial load or a hydrostatic pressure only. The same criteria and conclusions previously established still apply for these cases.

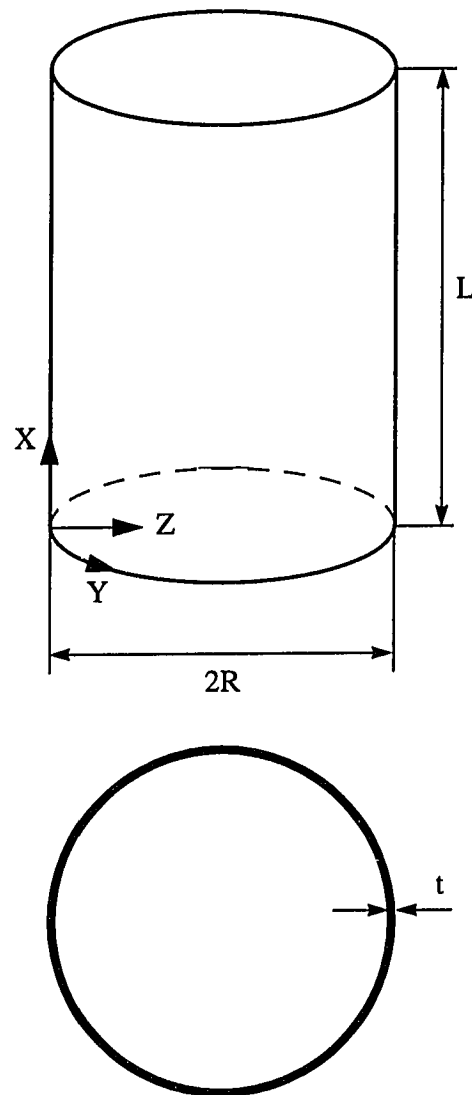


Figure 4.1 Coordinate system

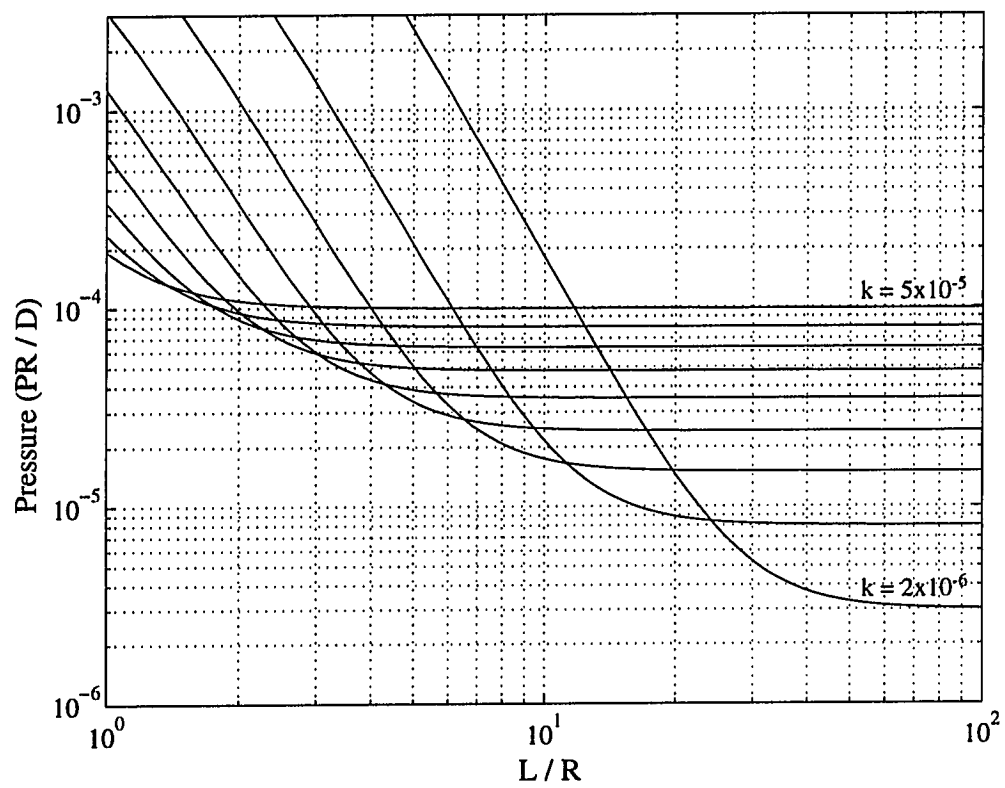


Figure 4.2 An example of the buckling diagram for a clamped perfect cylindrical shell under hydrostatic pressure using linear Flugge's equations for different values of $k = t^2 / 12 R^2$.

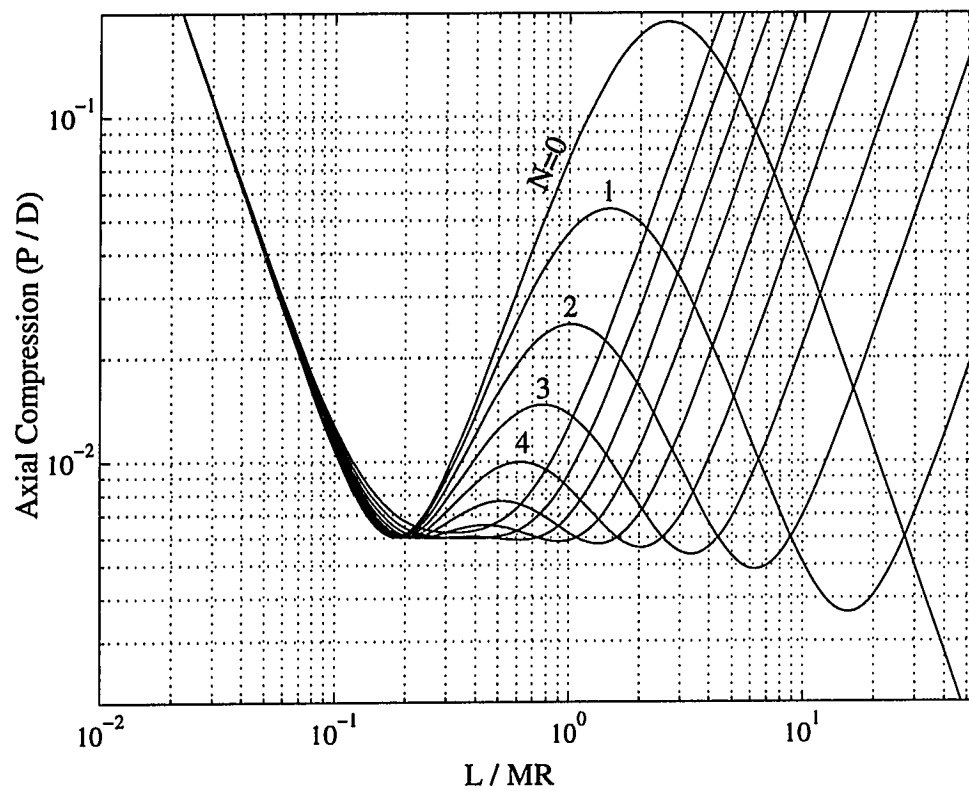


Figure 4.3 An example of the buckling diagram for a clamped perfect cylindrical shell under axial compression using linear Flugge's equations ($k = t^2 / 12 R^2 = 10^{-5}$).

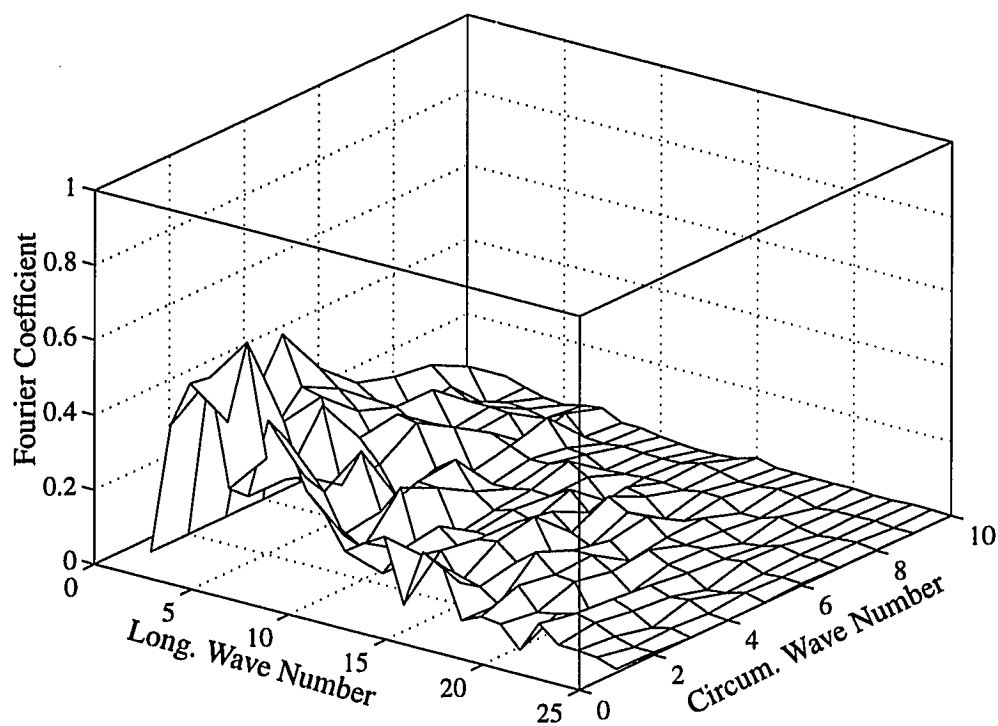


Figure 4.4 Series coefficients of the Fourier expansion of the mean function for the geometric imperfection configuration number 1 ($\bar{W}_1 = 0.2t$) of a clamped cylindrical shell.

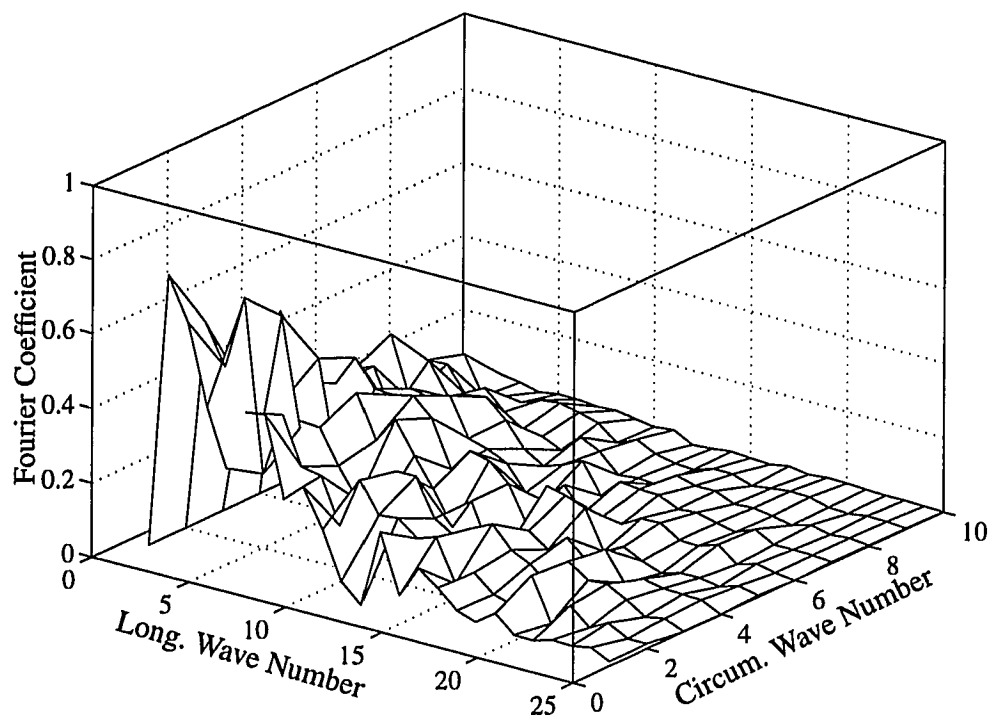


Figure 4.5 Series coefficients of the Fourier expansion of the mean function for the geometric imperfection configuration number 2 ($\bar{W}_1 = 0.4t$) of a clamped cylindrical shell.

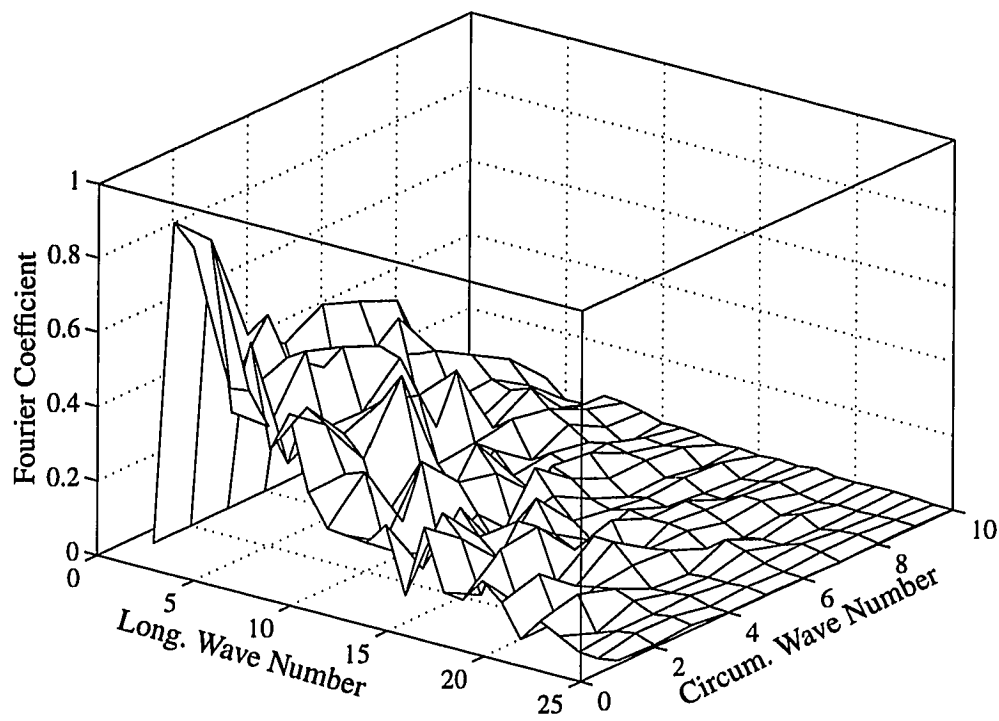


Figure 4.6 Series coefficients of the Fourier expansion of the mean function for the geometric imperfection configuration number 3 ($\bar{W}_1 = 0.6t$) of a clamped cylindrical shell.

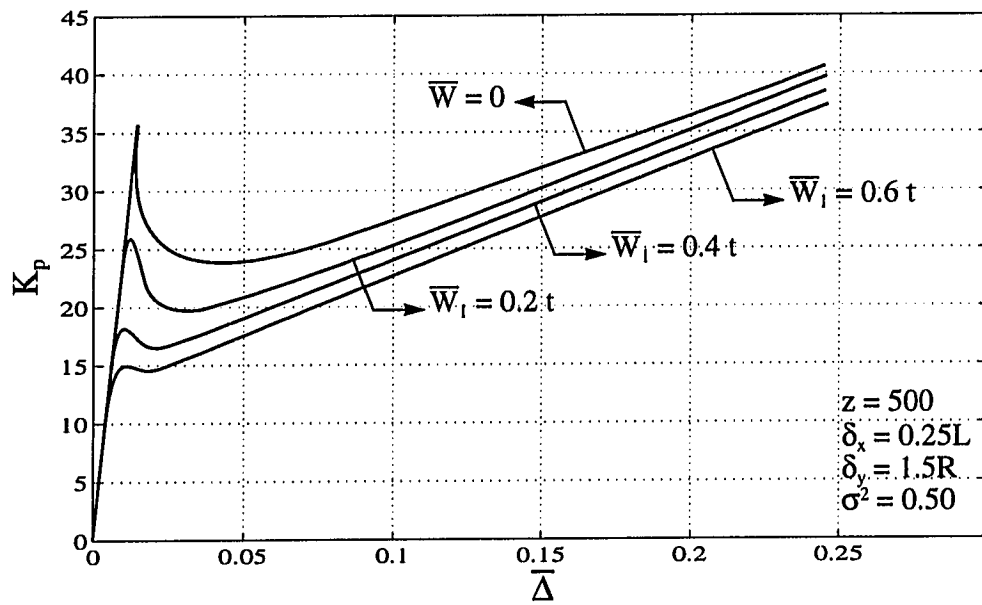


Figure 4.7 Effect of deterministic initial geometric imperfections on the typical postbuckling behavior of a clamped cylindrical shell under pressure loading for $z = 500$.

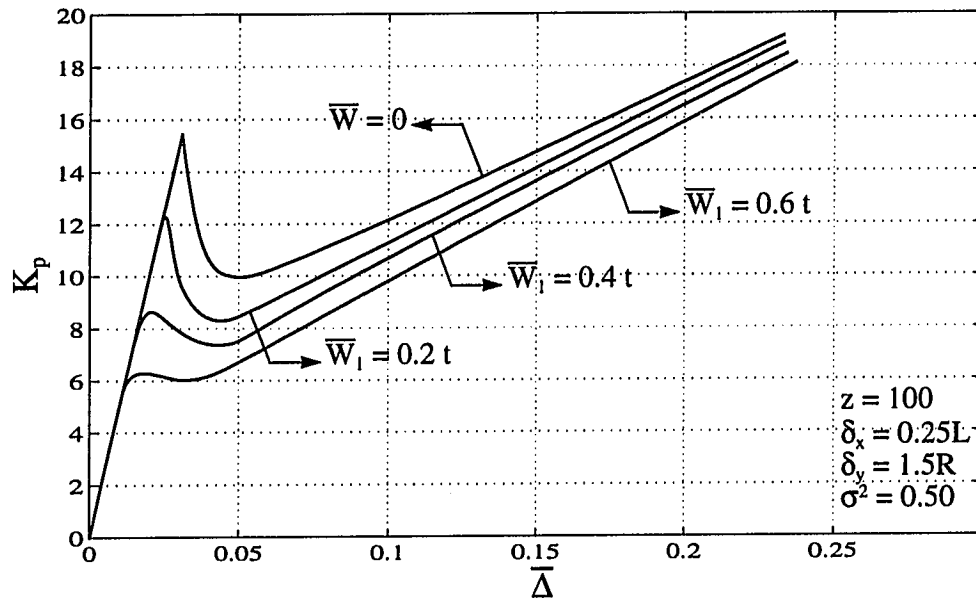


Figure 4.8 Effect of deterministic initial geometric imperfections on the typical postbuckling behavior of a clamped cylindrical shell under pressure loading for $z = 100$.

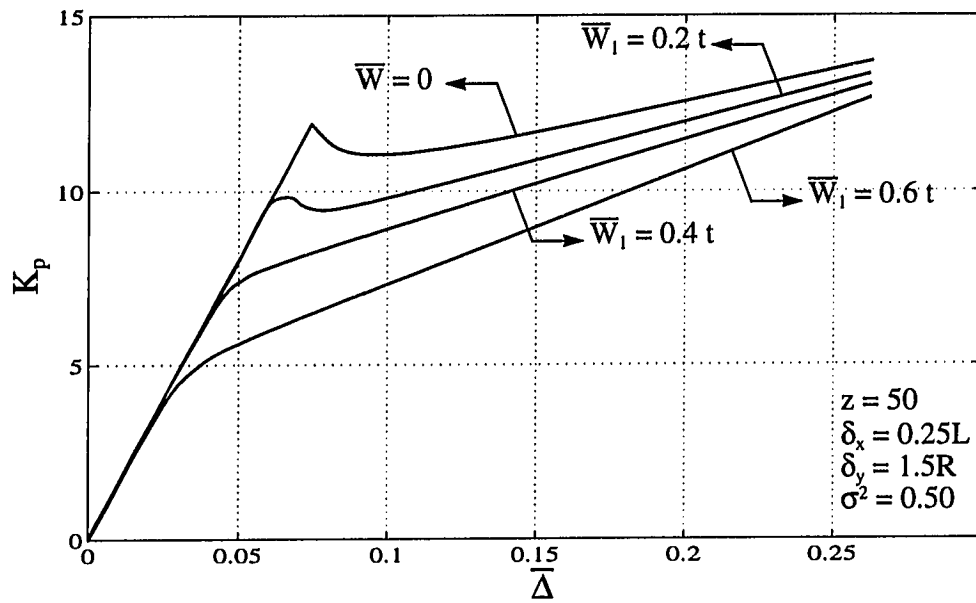


Figure 4.9 Effect of deterministic initial geometric imperfections on the typical postbuckling behavior of a clamped cylindrical shell under pressure loading for $z = 50$.

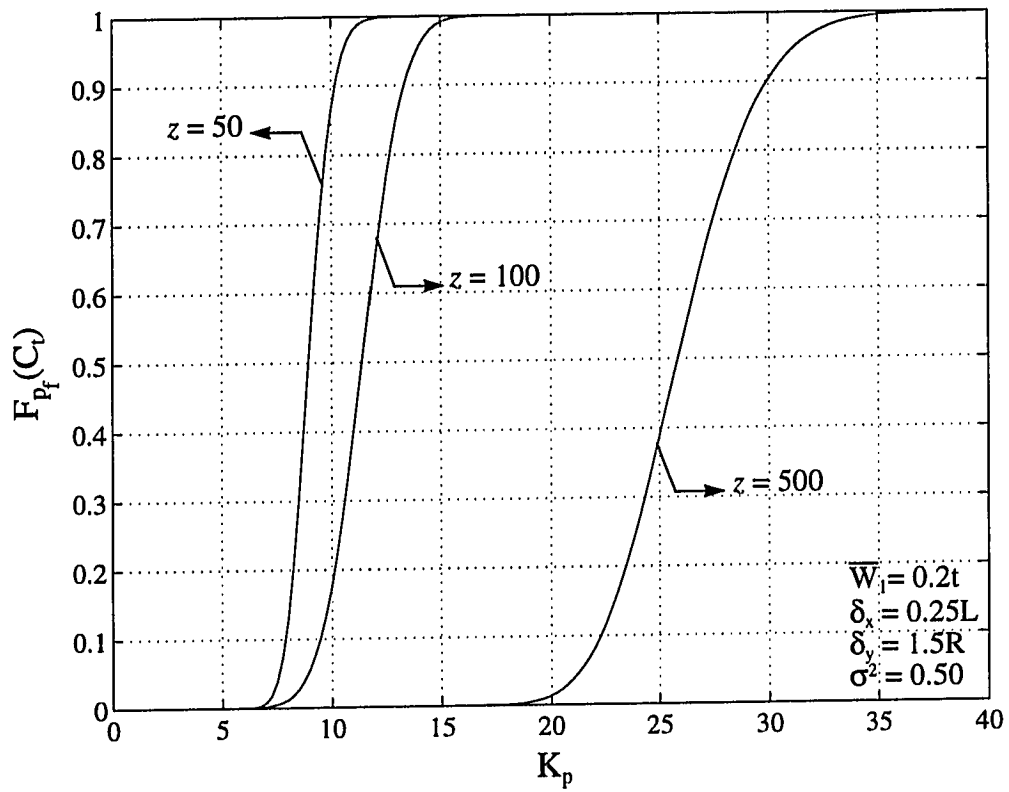


Figure 4.10 Cumulative distribution function for the buckling pressure of a clamped cylindrical shell for different geometric configurations under imperfection field $\bar{W}_1 = 0.2t$.

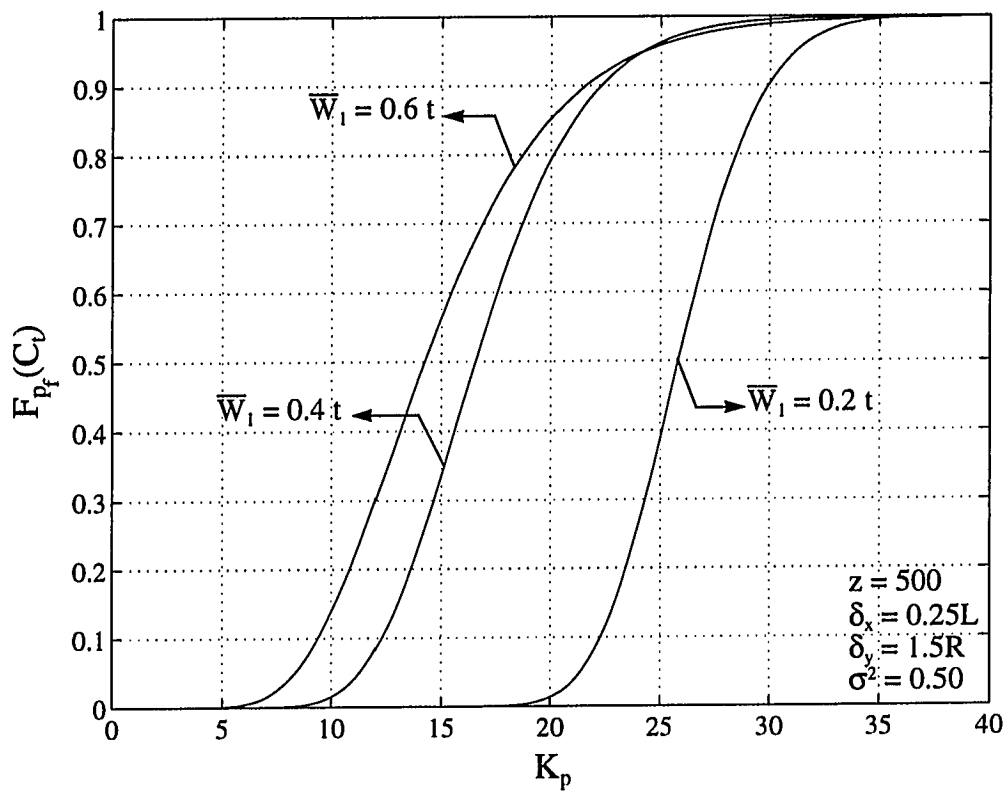


Figure 4.11 Cumulative distribution function for the buckling pressure of a clamped cylindrical shell for different amplitudes of the geometric imperfection configuration \bar{W}_1 .

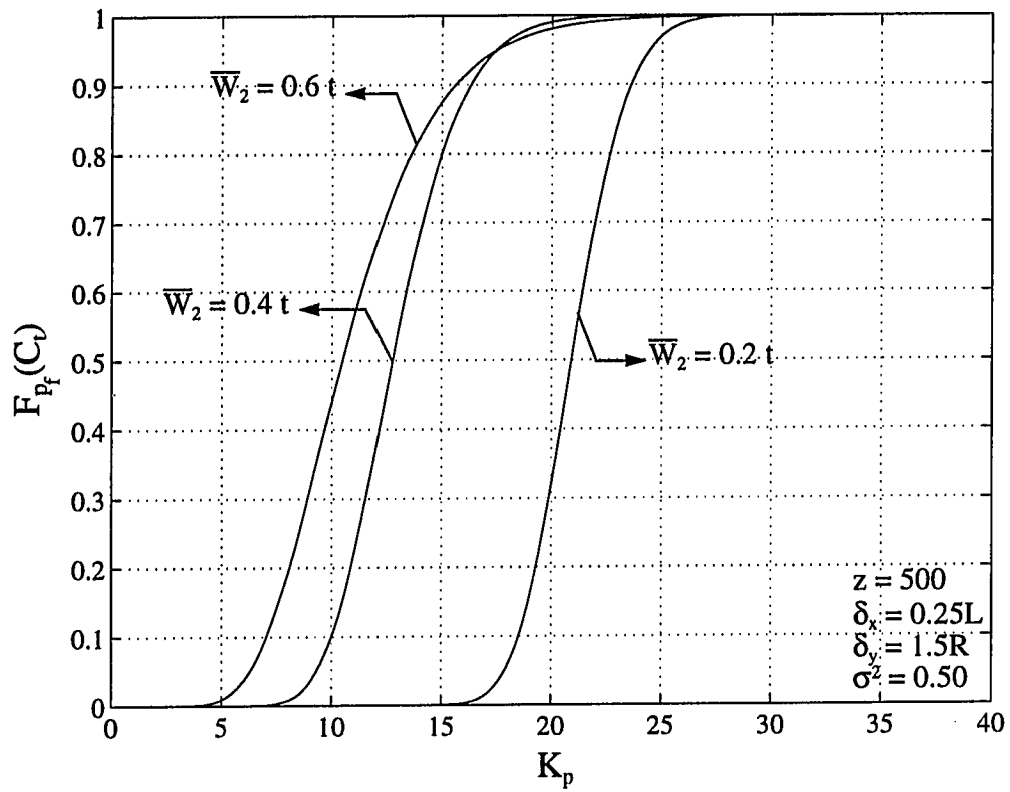


Figure 4.12 Cumulative distribution function for the buckling pressure of a clamped cylindrical shell for different amplitudes of the geometric imperfection configuration \bar{W}_2 ($N = 13$).

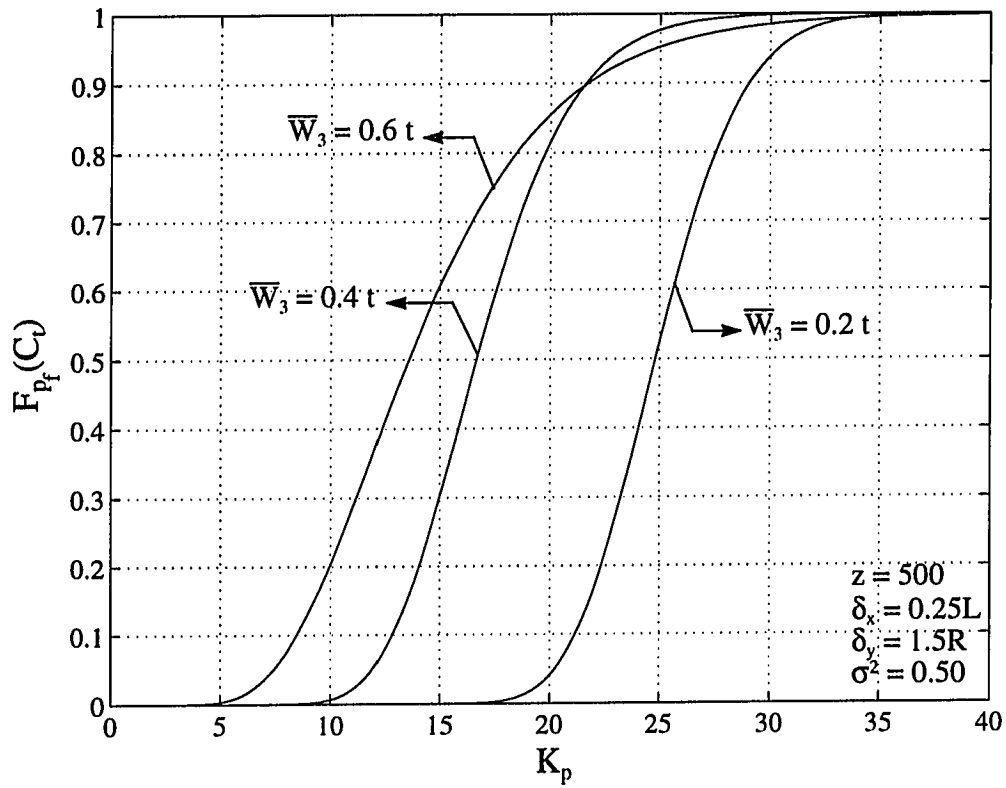


Figure 4.13 Cumulative distribution function for the buckling pressure of a clamped cylindrical shell for different amplitudes of the geometric imperfection configuration \bar{W}_3 ($N = 15$).

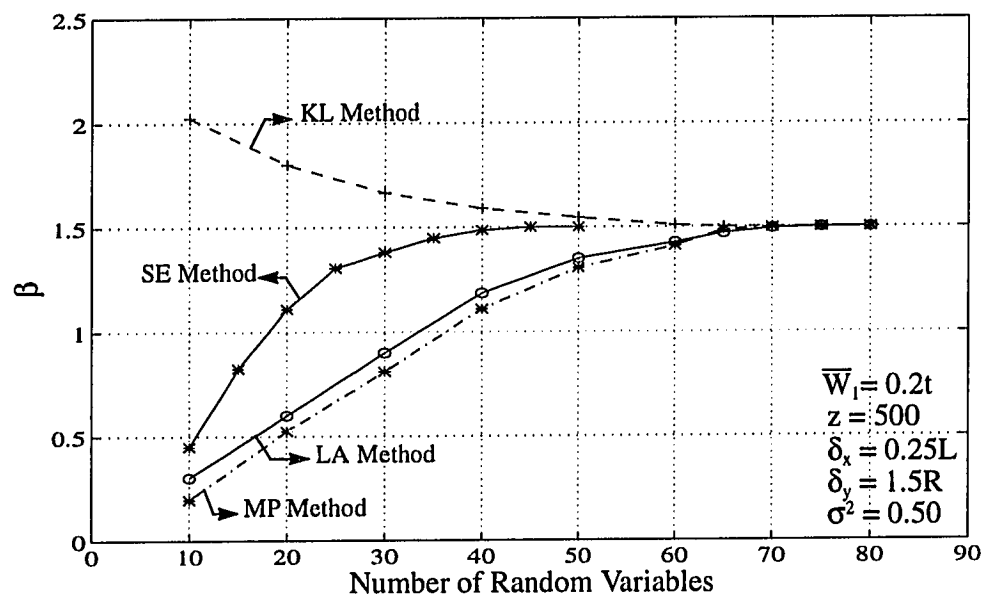


Figure 4.14 Rate of convergence of the reliability index for different discretizations methods for clamped ends cylindrical shell under pressure loading.

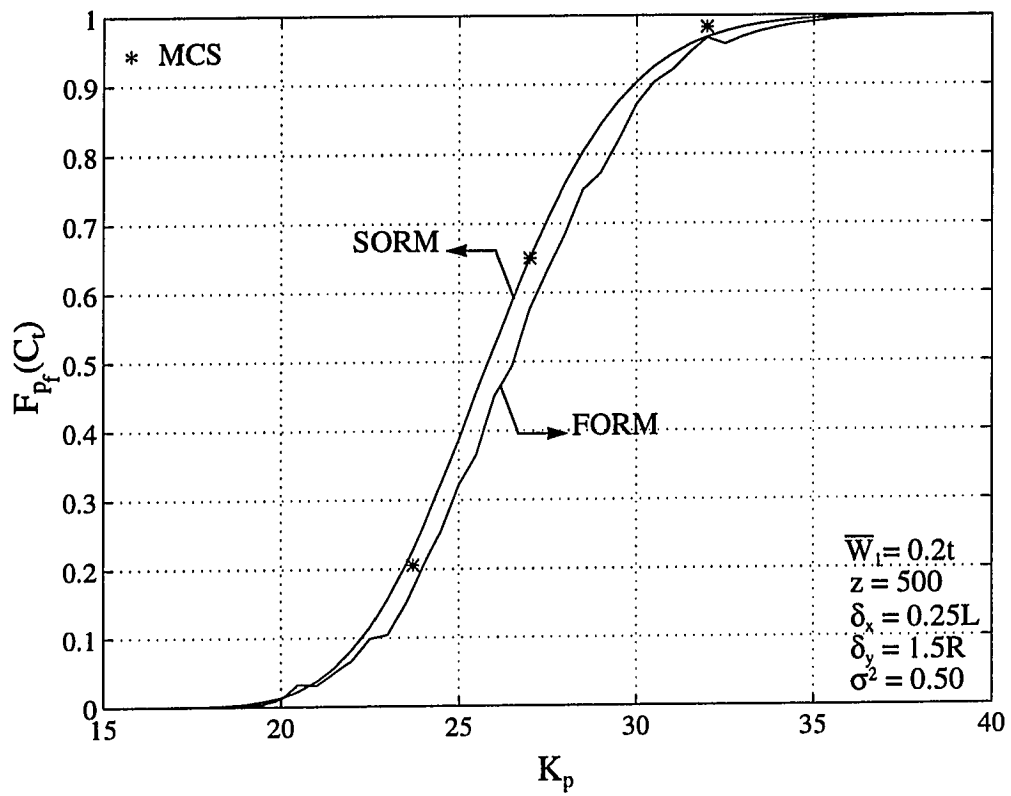


Figure 4.15 Effect of the reliability method used on the CDF for a clamped ends cylindrical shell under pressure using SE method.

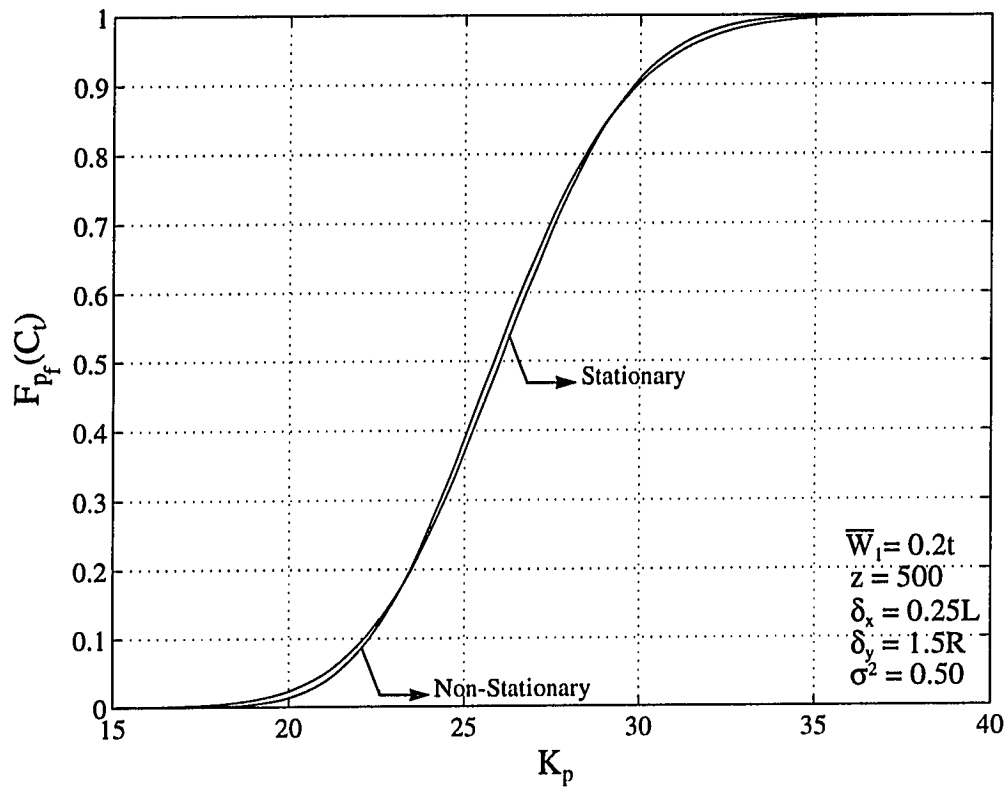


Figure 4.16 The effect of the non-stationarity of the autocorrelation coefficient function on the CDF for a clamped ends cylindrical shell under pressure using KL method.

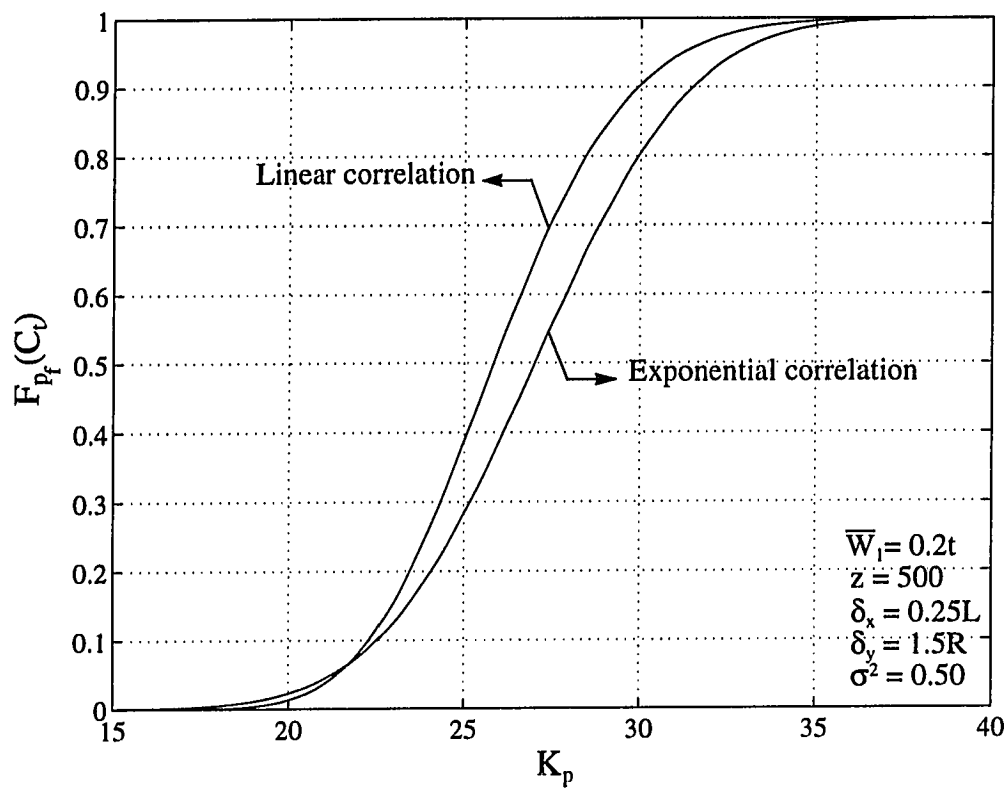


Figure 4.17 Cumulative distribution function for the buckling pressure of a clamped cylindrical shell for different autocorrelation coefficient functions.

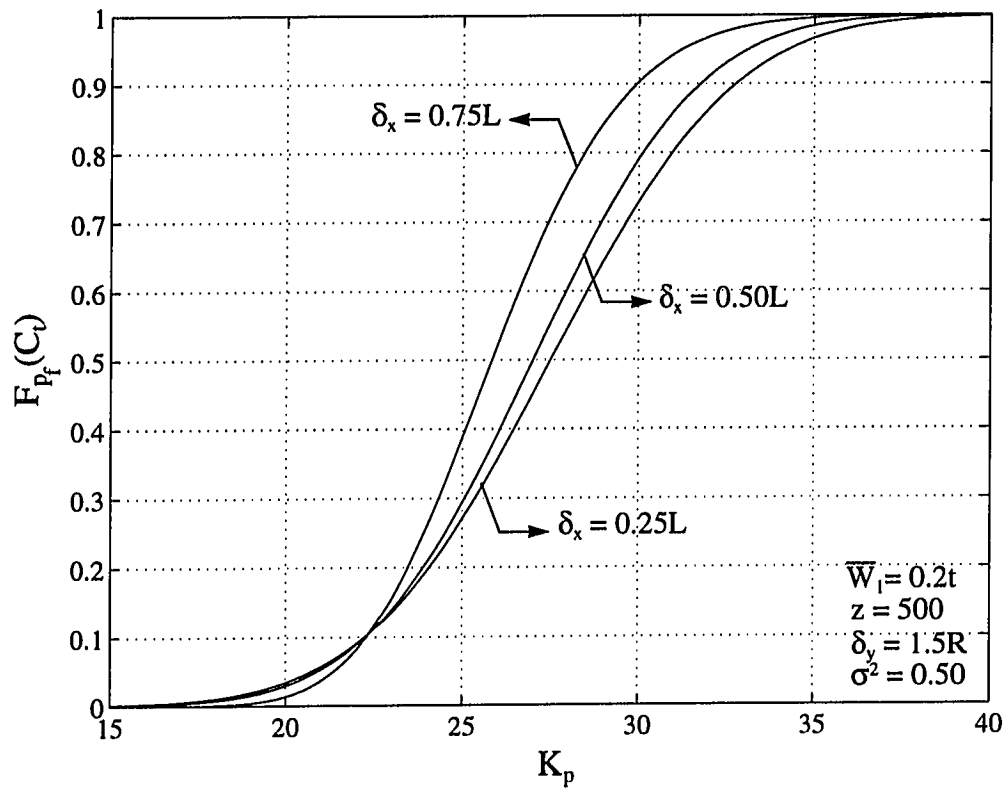


Figure 4.18 Cumulative distribution function for the buckling pressure of a clamped cylindrical shell for different values of the exponential correlation length in the axial direction.

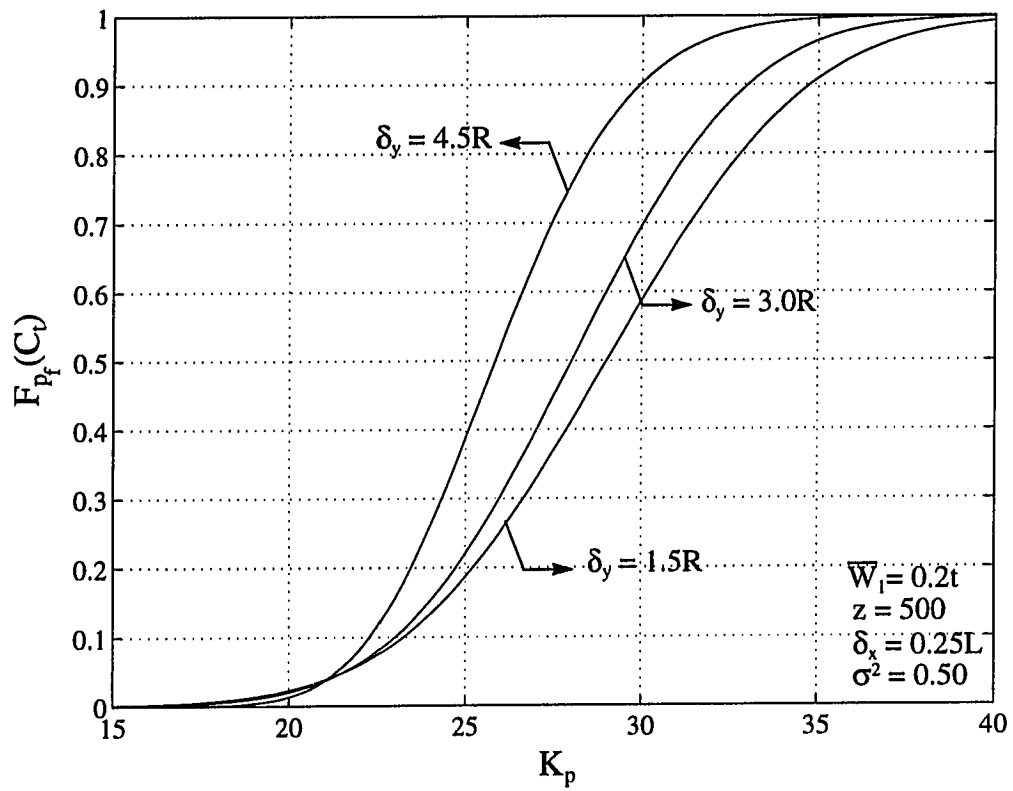


Figure 4.19 Cumulative distribution function for the buckling pressure of a clamped cylindrical shell for different values of the exponential correlation length in the circumferential direction.

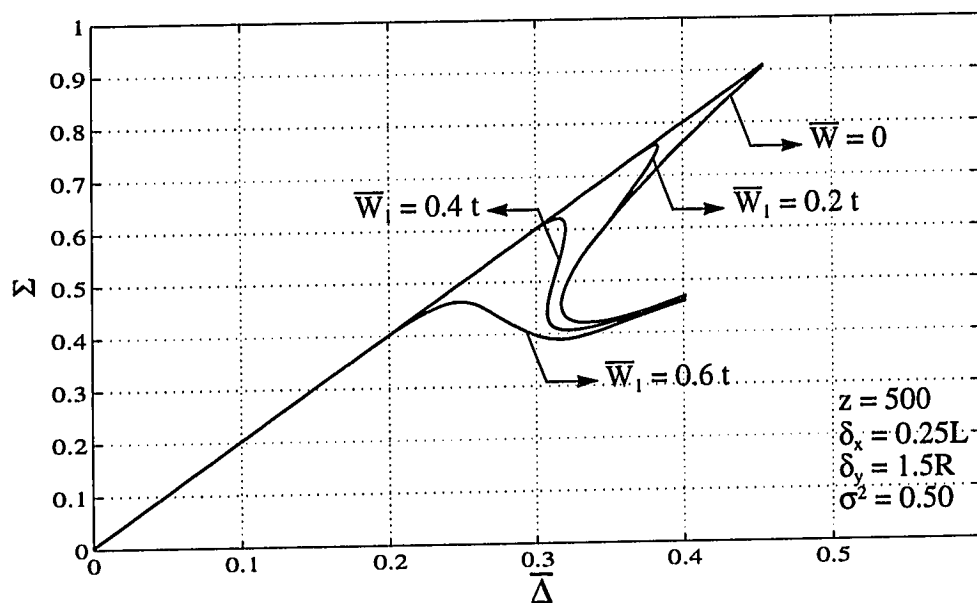


Figure 4.20 Effect of deterministic initial geometric imperfections on the typical postbuckling behavior of a clamped cylindrical shell under axial loading for $z = 500$.

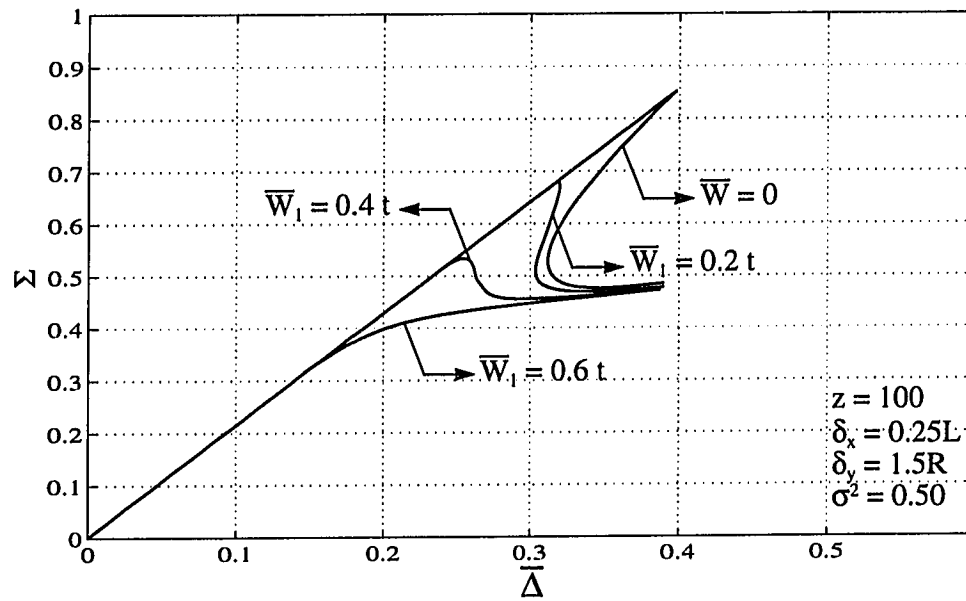


Figure 4.21 Effect of deterministic initial geometric imperfections on the typical postbuckling behavior of a clamped cylindrical shell under axial loading for $z = 100$.

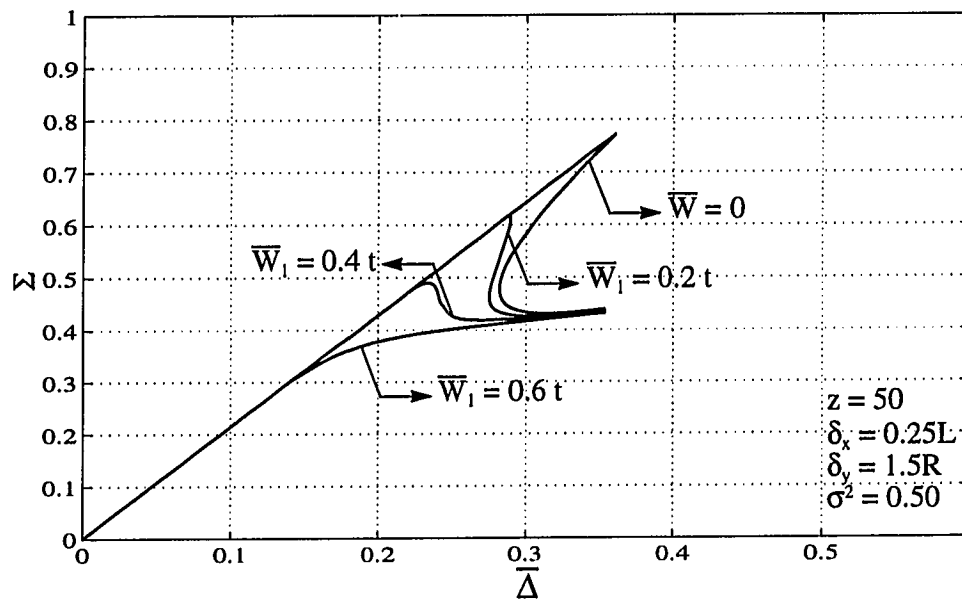


Figure 4.22 Effect of deterministic initial geometric imperfections on the typical postbuckling behavior of a clamped cylindrical shell under axial loading for $z = 50$.

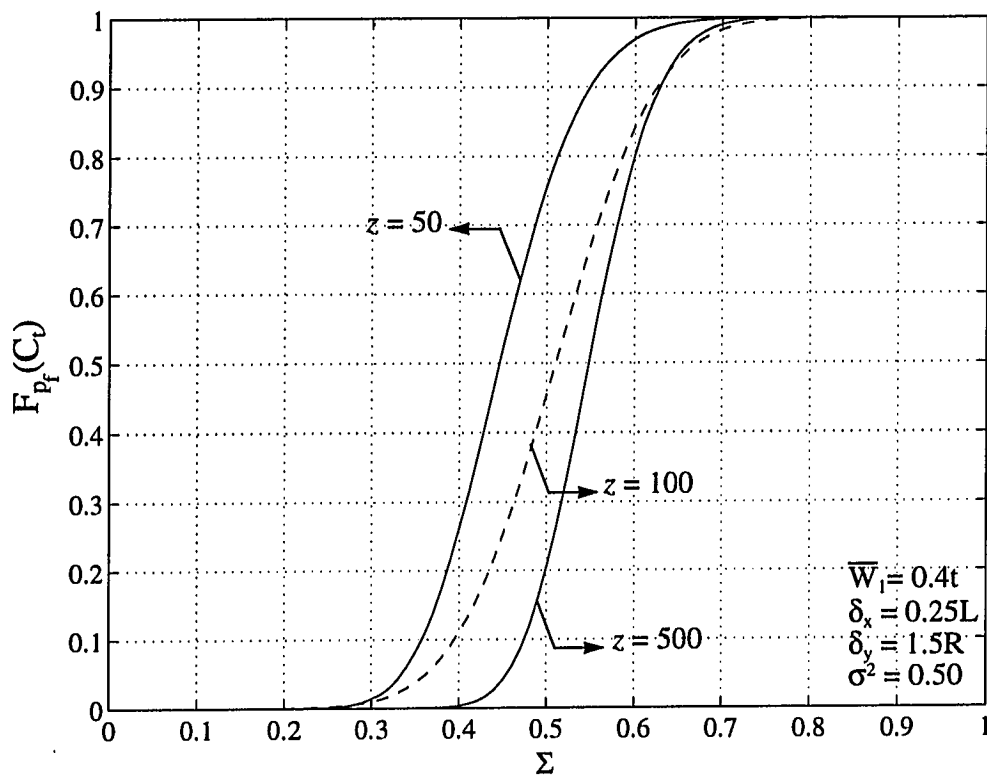


Figure 4.23 Cumulative distribution function for the buckling axial load of a clamped cylindrical shell for different geometric configurations under imperfection field $\bar{W}_1 = 0.4t$.

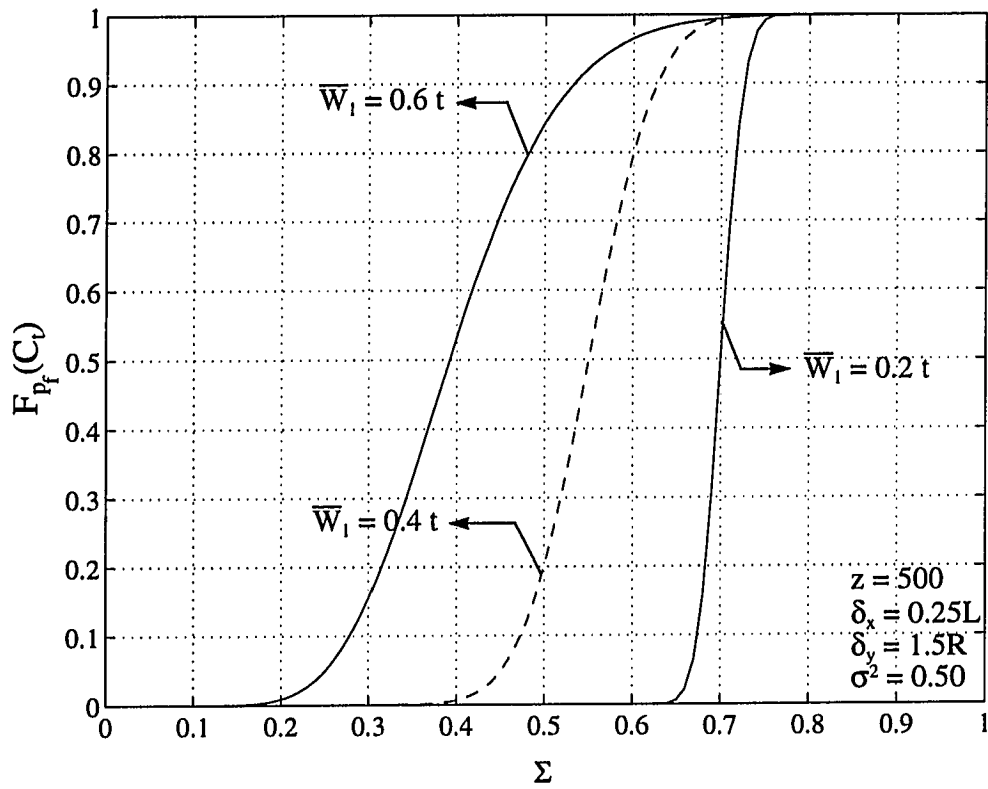


Figure 4.24 Cumulative distribution function for the buckling axial load of a clamped cylindrical shell for different amplitudes of the geometric imperfection configuration \bar{W}_1 .

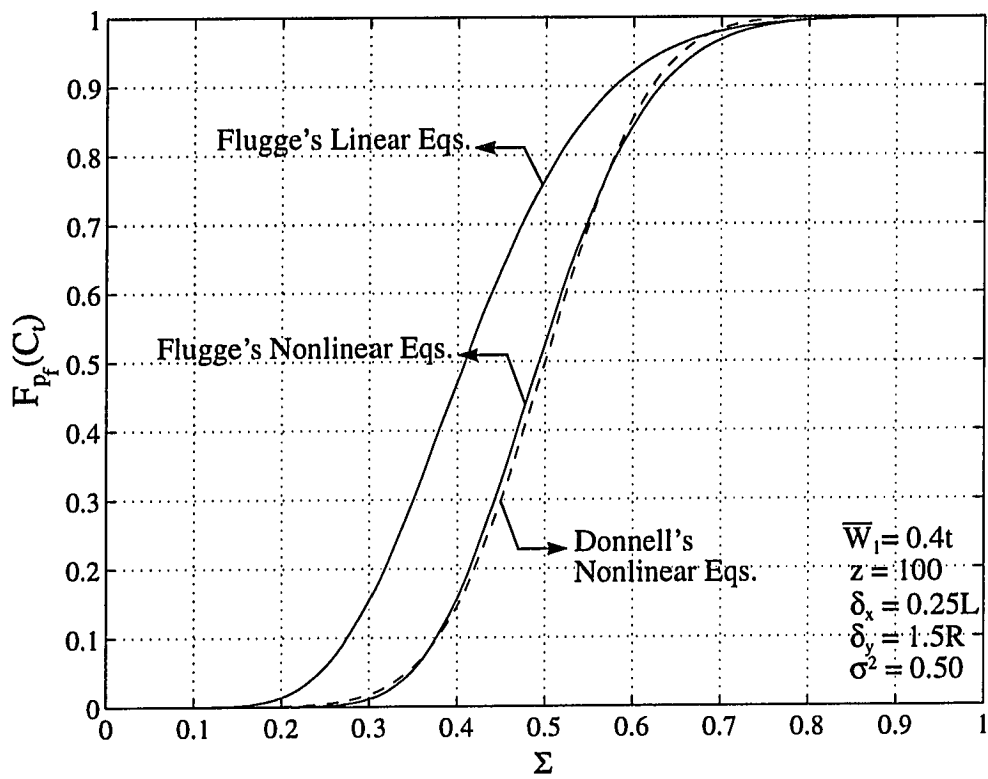


Figure 4.25 Cumulative distribution function for the buckling axial load of a clamped cylindrical shell for different methods of deterministic stability analysis.

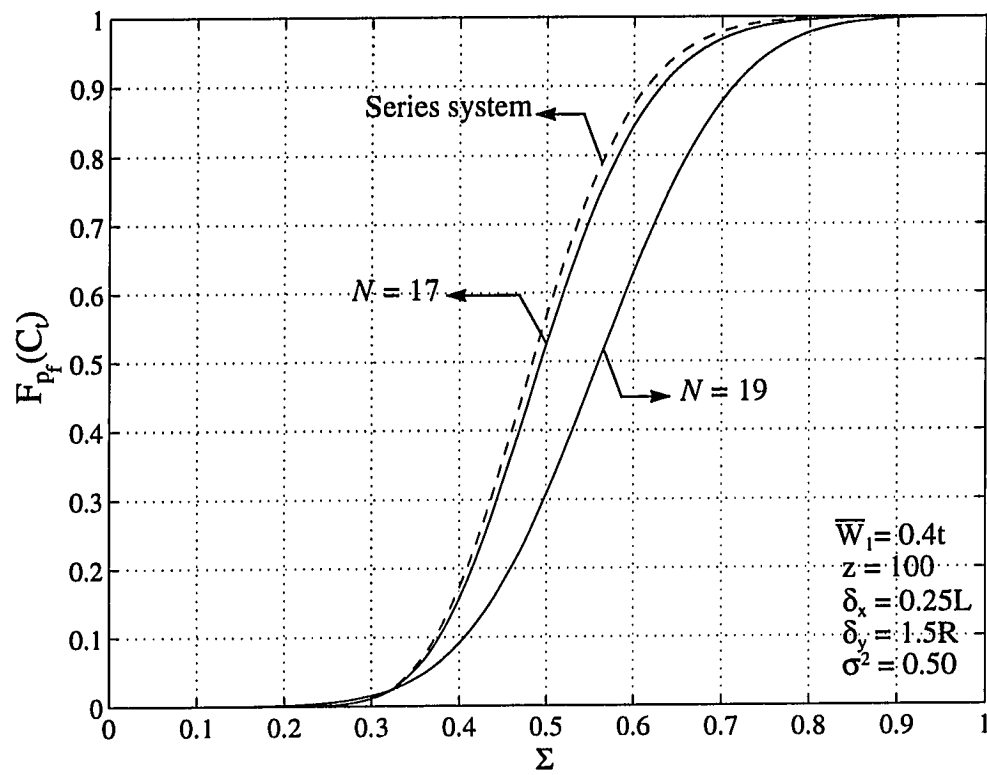


Figure 4.26 Cumulative distribution function for the buckling axial load of a clamped cylindrical shell for different values of N and for a series system.

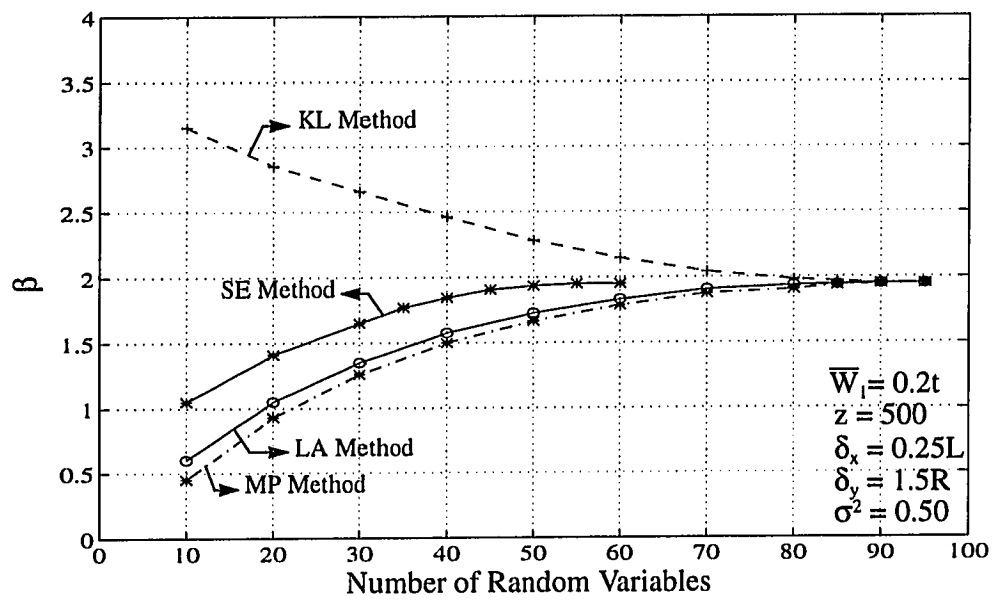


Figure 4.27 Rate of convergence of the reliability index for different discretizations methods for clamped ends cylindrical shell under axial loading.

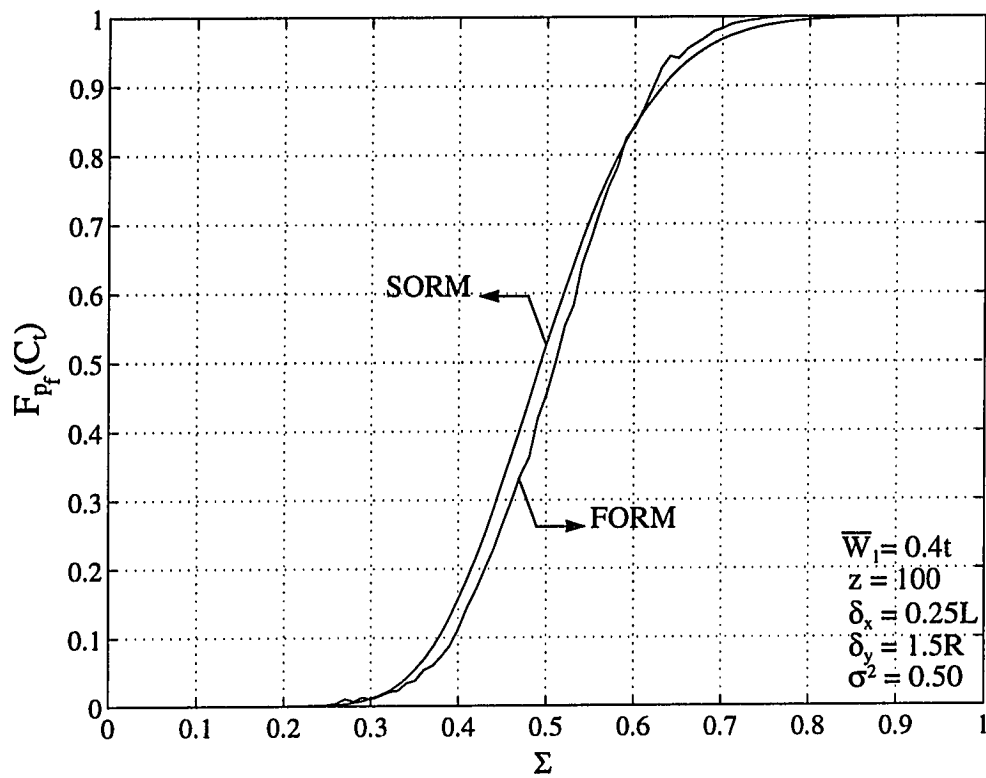


Figure 4.28 Effect of the reliability method used on the CDF for a clamped ends cylindrical shell under axial loading using SE method.

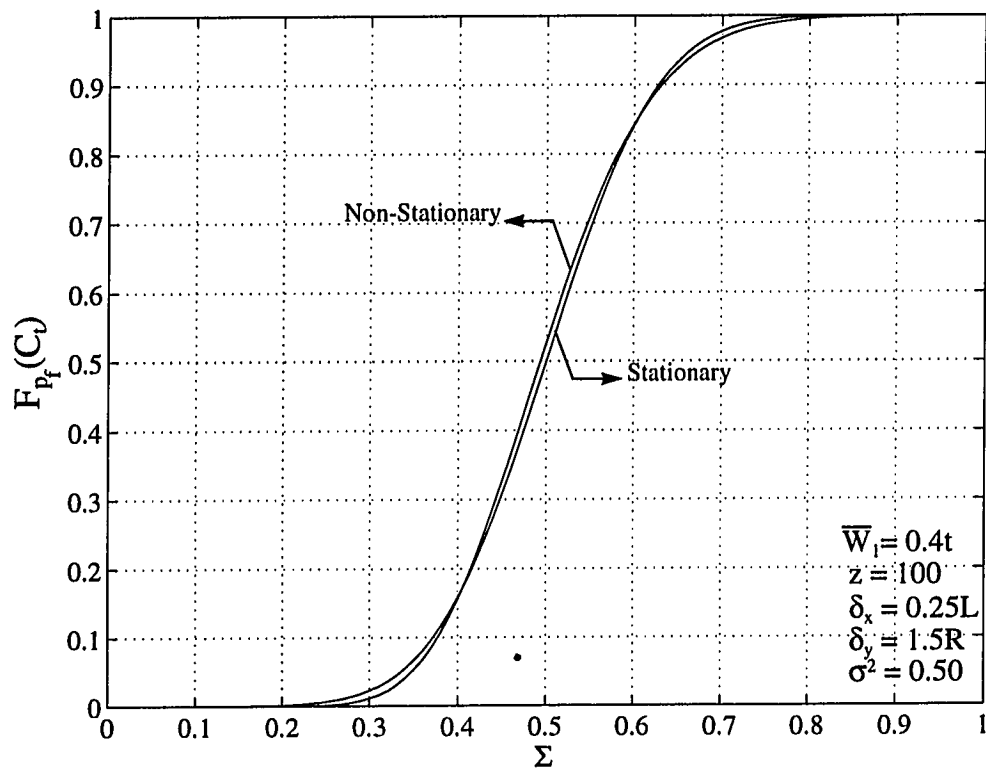


Figure 4.29 The effect of the non-stationarity of the autocorrelation coefficient function on the CDF for a clamped ends cylindrical shell under axial loading using KL method.

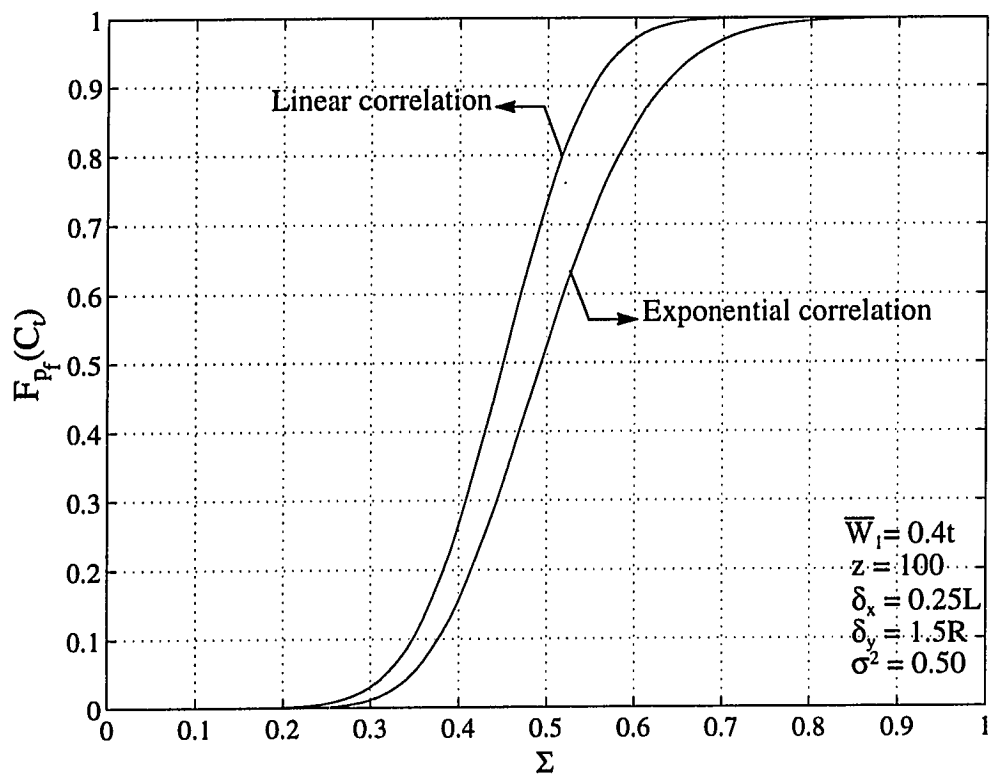


Figure 4.30 Cumulative distribution function for the buckling pressure of a clamped cylindrical shell for different autocorrelation coefficient functions.

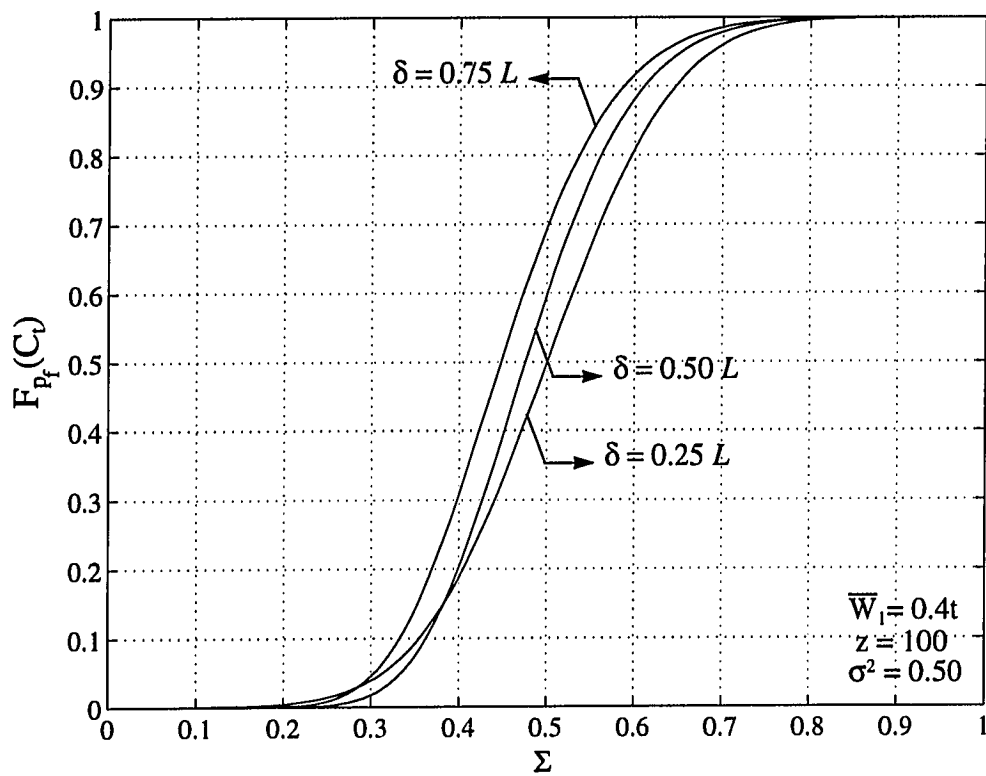


Figure 4.31 Cumulative distribution function for the buckling axial load of a clamped cylindrical shell for different values of the absolute exponential correlation length.

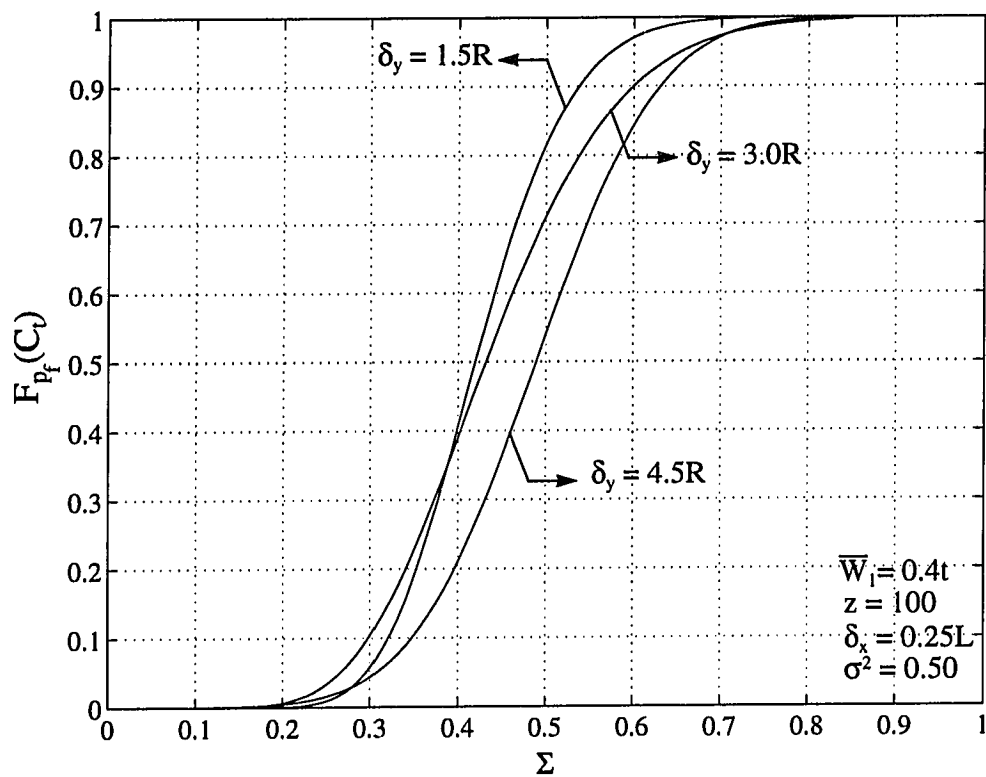


Figure 4.32 Cumulative distribution function for the buckling axial load of a clamped cylindrical shell for different values of the exponential correlation length in the circumferential direction.

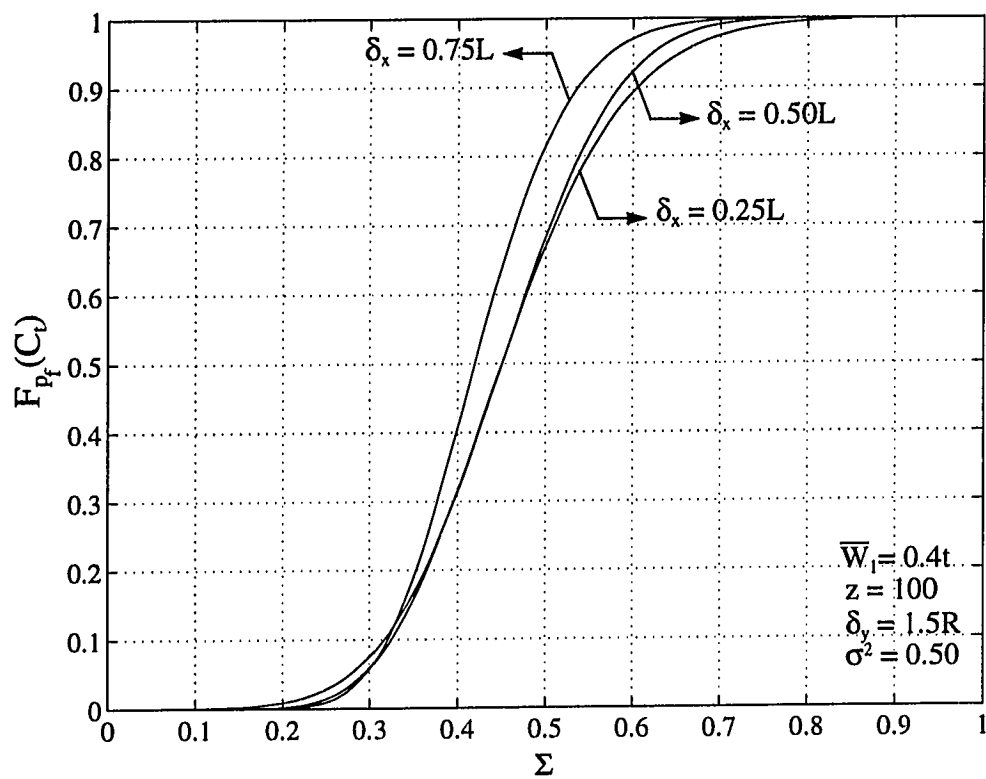


Figure 4.33 Cumulative distribution function for the buckling axial load of a clamped cylindrical shell for different values of the exponential correlation length in the axial direction.

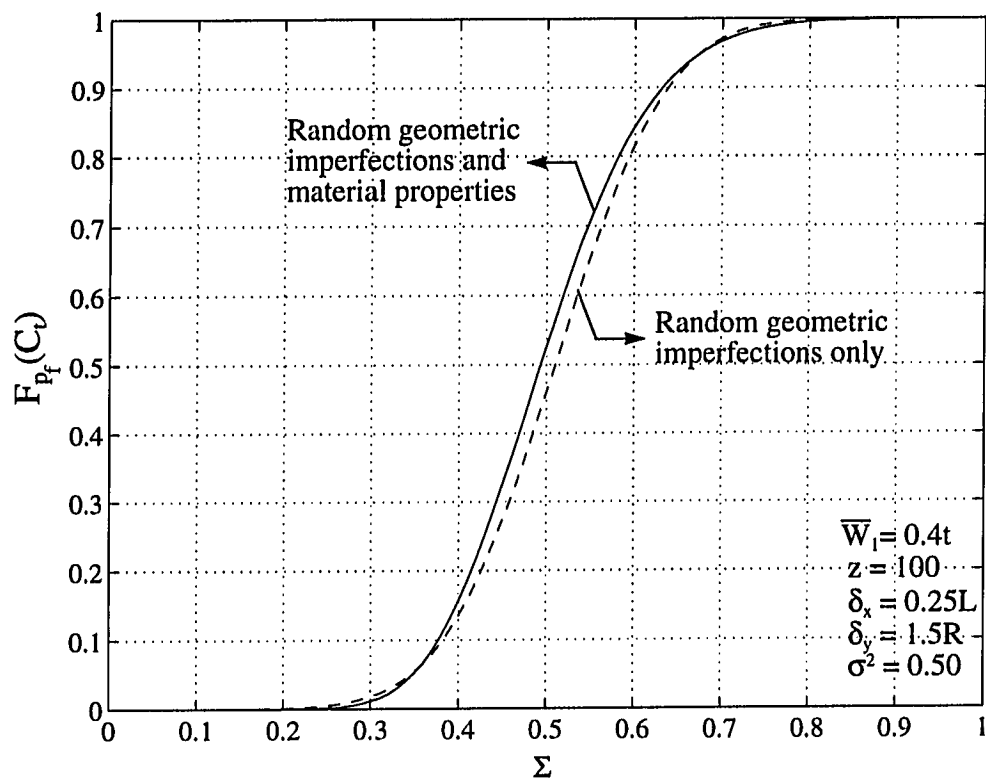


Figure 4.34 Effect of the randomness in the modulus of elasticity of the material of a clamped cylindrical shell on the buckling under axial loading.

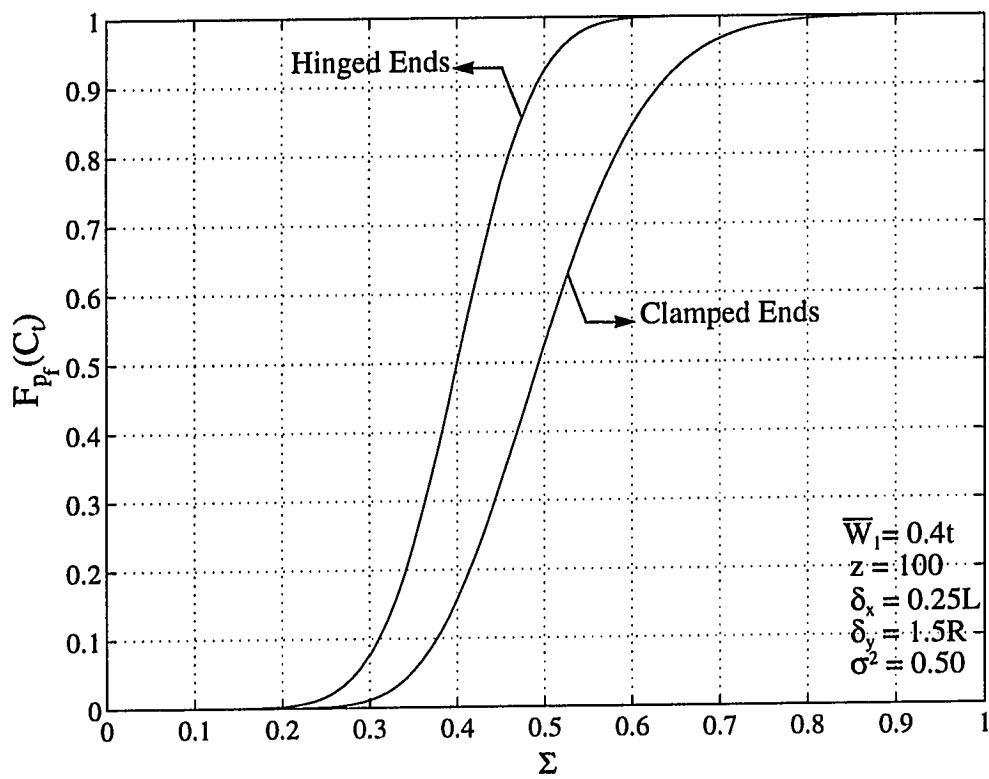


Figure 4.35 Cumulative distribution function for the buckling axial load of both clamped and hinged cylindrical shells under imperfection field $\bar{W}_1 = 0.4t$.

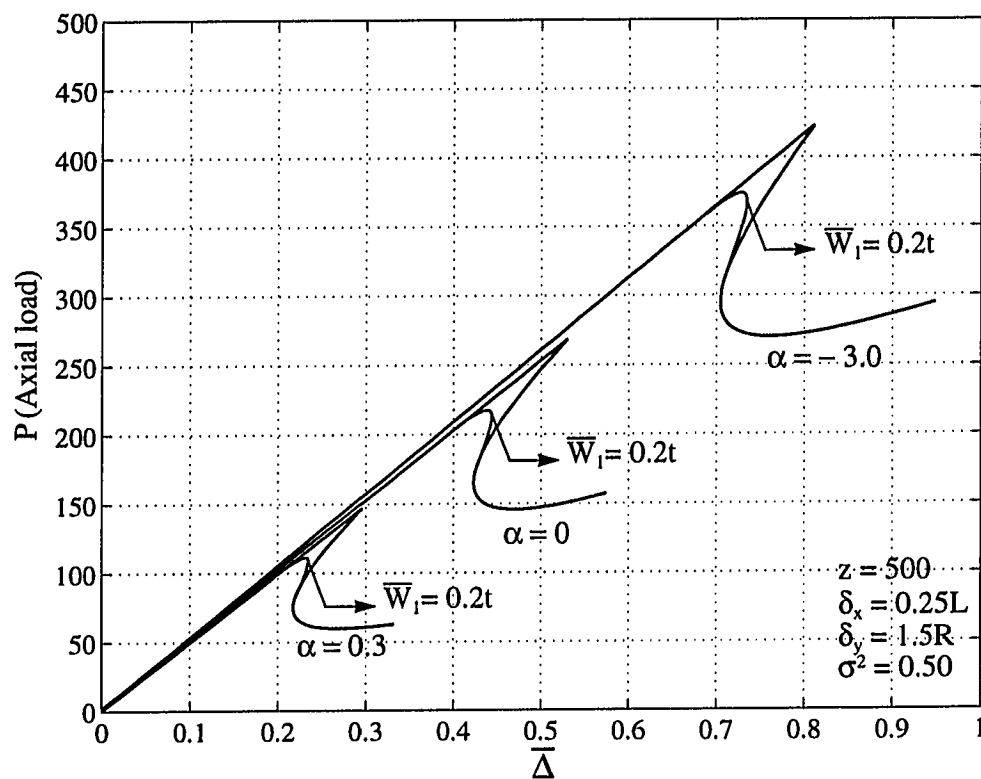


Figure 4.36 Effect of initial geometric imperfection field $\bar{W}_1 = 0.2t$ on the typical postbuckling behavior of a clamped cylindrical shell under combined axial and pressure loading for $z = 500$.

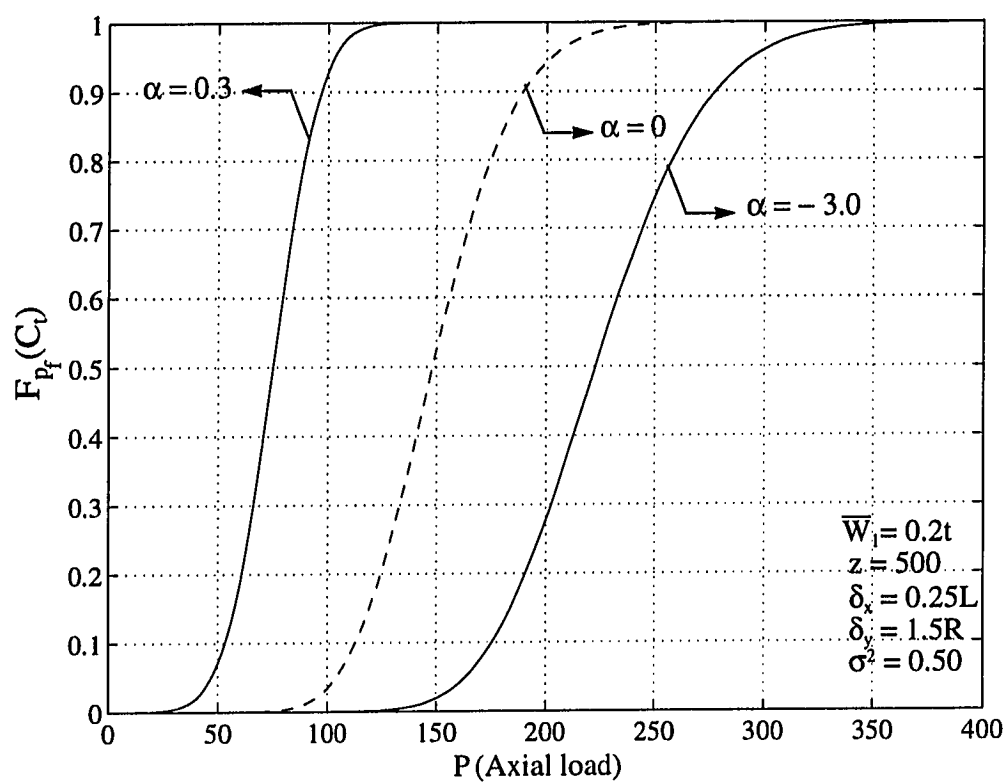


Figure 4.37 Cumulative distribution functions for the buckling axial load of a clamped cylindrical shell under various values of the hydrostatic pressure ratio.

Chapter 5

Summary and Conclusions

The buckling failure of shallow circular arches and cylindrical shells with random parameters has been studied by the methods of reliability analysis. Several important issues related to the development of adequate and computationally efficient models of engineering uncertainties were considered in this dissertation. The uncertain parameters considered included the initial geometric imperfections, material properties, and load distributions. A probabilistic approach for the spatial modeling of the random variables based on the use of one- and two-dimensional random fields was considered. Numerical calculations of the probability distribution for the buckling load has been carried out by the methods of FORM, SORM, and MCS with the aid of the deterministic nonlinear energy method. Results indicate that uncertainty in the random imperfections can have a significant effect on the probabilistic stability load.

In the present study, we first started by presenting the deterministic analysis methods for the instability of shallow arches and cylindrical shells. The buckling loads for different modes of instability under various loads and boundary conditions were obtained by nonlinear energy analysis. The mode of instability depends on a dimensionless geometric parameter. The initial geometric configuration and the imperfections distributions are the

main factors affecting the stability behavior and buckling modes of both arches and shells.

Characterization of the random buckling load has been treated as a problem in structural reliability theory. The initial imperfections have been modeled as random fields with known variances, mean functions, and autocorrelation coefficient functions over the arch and the shells. The random fields for the imperfection were discretized by the following methods: a) Midpoint (MP) method; b) Local averaging (LA) method; c) Karhunen-Loeve (KL) theorem; d) Series expansion (SE) method. In the first three of these methods, special calculations had to be taken to account for non-stationarity of the autocorrelation function due to end conditions. FORM and SORM have been used for evaluating the probability distributions and were compared to MCS in some cases. Numerical results have been presented for a number of examples to compare the convergence of the four discretization methods and to evaluate the effect of the non-stationarity. In the following sections, we list general conclusions of the work presented in the previous chapters.

5.1 Stability of Shallow Arches

For the arch case, the imperfection sensitivity with respect to the various uncertain parameters has been evaluated from consideration of the distribution of the buckling load for various values of the shallowness parameter λ . For higher values of λ , where asymmetric (bifurcation) buckling takes place, the arch showed more sensitivity regarding uncertainty in the geometric imperfection. On the other hand lower sensitivities were obtained for lower values of λ , where symmetric (limit load) buckling occurs.

The uncertain initial shape for the geometric imperfections, modeled by the mean

function of the random field, had a considerable effect on the buckling behavior. For an antisymmetric mean function, higher reductions in the bifurcation load were obtained compared with a symmetric function having the same maximum amplitude. Changes in the shape of the mean function did not affect the limit buckling load as much. Higher variance of the imperfections resulted, as expected, in wider distributions of the buckling load.

For the arch, the failure probability is relatively insensitive to the correlation length. Also, changes in the type of the autocorrelation function did not strongly affect the buckling behavior. The difference between including the effect of the non-stationarity of the autocorrelation function near the ends, and neglecting this effect is very small in this case.

5.2 Stability of Cylindrical Shells

Deterministic analysis of the buckling of cylindrical shells based on the use of nonlinear Donnell's equations showed to be in excellent agreement with the general shell theory for values of N higher than 3. The shells showed very comparable imperfection sensitivities in both cases of pressure and axial loading.

The buckling behavior was seen to be quite sensitive to the parameters defining the random field representing the geometrical imperfections. Higher reductions in the buckling loads were obtained when specifying the imperfection field with a mean function having the same N as that of the most critical buckling mode.

The effect of the correlation factors of the imperfections was quite large on the behavior of the shells. Generally, higher correlation resulted in lower buckling loads. The

increase in the correlation was modeled by either increasing the correlation length or changing from exponential to linear autocorrelation functions. Changes in the correlation length in the circumferential direction had larger effects on the buckling loads than comparable changes in the axial direction.

5.3 General Conclusions

It can be concluded that the Karhunen-Loeve (KL) method proves to be the most efficient method for random field discretization for cases where exact formulas are available for evaluating the eigenfunctions of the correlation kernel. The series expansion (SE) method is more efficient in cases where the KL method requires lengthy numerical analysis to evaluate the spectral decomposition of the field.

FORM and SORM results were obtained for all cases and were compared and tested against MCS results for many of the problems considered. Both FORM and SORM required a small fraction of the computational time needed for MCS. FORM results were obtained with the least processor time but showed high diversity from MCS in many occasions. Thus, FORM can be used only as a quick first approximation for the failure probability. SORM, on the other hand, for a little additional computational effort over FORM, proves to be in very good agreement with MCS. Hence, SORM can be recommended for obtaining good estimates of the failure probabilities.

In all cases, the uncertainty in the material properties, modeled in terms of a random field representing the modulus of elasticity, and the uncertainty in the loading distribution, were seen to be less important factors in affecting the buckling behavior compared with the geometrical uncertainties.

5.4 Applications and Future Research

The interface between complicated highly nonlinear deterministic solution methods and reliability theory techniques introduced in this study can basically be applied to any structural problem assuming it has a complete deterministic solution and the ability to be formulated in terms of a limit-state function. An extension of the current work to the problems of stability of stiffened circular cylindrical shells and to the snap-through buckling of shallow spherical caps is an immediate addition to the present research.

An important issue in the present study is the modeling of imperfections for design purposes. Data obtained from large numbers of samples is needed for a reliable representation of the imperfections with realistic parameters and distributions for the random field. The construction of a data bank with sufficient numbers of field measurements for different structures would be a step for a rigorous modeling of the imperfections. An example data bank for imperfections was given by Arbocz (1979) for some types of shell structures.

The techniques used in measurements of imperfections is also another open field for research. Advanced inspection methods together with efficient data interpretation programs would allow for obtaining reliable and realistic statistical characterization for structures.

Based on applying stochastic analysis methods to describe failure of structures under various types of imperfections, many limitations on quality control assessment can be introduced. Limits for the acceptable allowances in the imperfections in structural dimensions and configurations can be established based on probabilistic distribution

curves similar to those included in the present study.

The proposed methods could be viewed as generalized, computationally efficient, modeling techniques that can be extended to any structural component. Design procedures can be developed based on the mathematical modeling of engineering uncertainties. This allows more information to be incorporated in the design codes resulting in more economical designs with better safety margins. Thus, future research effort is needed to implement reliability based design procedures and inspection techniques to the same level at which analysis methods have reached.

Bibliography

- Allen, H. G. and Bulson, P. S. (1980), "Background to buckling," McGraw-Hill Book Company (UK) Limited, Great Britain.
- Amazigo, J. C. (1969), "Buckling under axial compression of long cylindrical shells with random axisymmetric imperfections," Quarterly of Applied Mechanics, Vol. 26, pp. 537-566.
- Ang, A. H.-S. and Cornell, C. A. (1974), "Reliability bases of structure safety and design," Journal of Structural division, ASCE, Vol. 100, pp. 1755-1769.
- Arbocz, J. and Abramovich, H. (1979), "The initial imperfection data bank at the Delft University of Technology," Report LR-290, Delft, The Netherlands.
- Arbocz, J. and Hol, J. M. A. M. (1991), "Collapse of axially loaded cylindrical shells with random imperfections," American Institute of Aeronautics and Astronautics Journal, Vol. 29, pp. 2247-2256.
- Augusti, G., Baratta, A. and Casciati, F. (1984), "Probabilistic methods in structural engineering," Chapman & Hall, London.
- Biezeno, C. B. and Grammel, R. (1939), "Technische Dynamik," Vol. 1, Julius Springer, Berlin.
- Bjerager, P. (1990), "On computational methods for structural reliability analysis," Struc-

- tural Safety, Vol. 9, pp. 79-96.
- Bolotin, V. V. (1962), "Statistical method in the nonlinear theory of elastic shells," NASA, TTF-85.
- Breitung, K. (1984), "Asymptotic approximation for multinormal integrals," Journal of Engineering Mechanics, ASCE, Vol. 110, pp. 357-366.
- Britvec, S. J. (1973), "The stability of elastic systems," Pergamon Press Inc.
- Budiansky, B. and Hutchinson, J. W. (1964), "Dynamic buckling of imperfection sensitive structures," Proceedings of the 11th IUTAM Congress, pp. 636-651.
- Budiansky, B. (1974), "Theory of buckling and postbuckling behavior of elastic structures," Advances in Applied Mechanics, Vol. 14, pp. 1-65.
- Conte, J. P., (1992), "Structural reliability theory and applications," Class Notes, CIVI524, Rice University, Houston, Texas.
- Der Kiureghian, A. and Ke, J.-B. (1985), "finite element based reliability analysis of frame structures," Proceedings of the Fourth International Conference on Structural Safety and Reliability, Vol. 1, Kobe, Japan, pp. 395-404.
- Der Kiureghian, A. and Ke, J.-B. (1988), "The stochastic finite element method in structural reliability," Probabilistic Engineering Mechanics, Vol. 3, pp. 83-91.
- Der Kiureghian, A. and Lin, H. S. H. (1987), "Second order reliability approximations," Journal of Engineering Mechanics, ASCE, Vol. 113, pp. 1208-1225.
- Der Kiureghian, A. and Liu, P. L. (1986), "Structural reliability under incomplete probability information," Journal of Engineering Mechanics Division, ASCE, Vol. 112, pp. 85-104.

- Dickie, J. F. and Broughton, P. (1971), "Stability criteria for shallow arches," Journal of the Engineering Mechanics Division, ASCE, VOL. 97, pp. 951-965.
- Ditlevsen, O. (1979), "Narrow reliability bounds for structural systems," Journal of Structural Mechanics, Vol 7, pp. 453-472.
- Donnell, L. H. (1933), "Stability of thin-walled tubes under torsion," NACA, TR-479.
- Elishakoff, I., van Manen, S., Vermeulen, P. G. and Arbocz, J. (1987), "First-order second-moment analysis of the buckling of shells with random imperfections," AIAA Journal, Vol. 25, pp. 1113-1117.
- Flugge, W. (1932), "Die stabilität der kreiszylinderschale," Ing.-Arch, Vol. 3, pp. 463-506.
- Flugge, W. (1973), "Stresses in shells," 2nd edition, Springer-Verlag, New York, N. Y.
- Fung, Y. C. and Kaplan, A. (1952), "Buckling of low arches and curved beams of small curvature," T. N. 2840, NACA, Washington, D. C.
- Ghanem, R. G. and Spanos, P. D. (1991a), "Spectral stochastic finite element formulation for reliability analysis," Journal of Engineering mechanics, ASCE, Vol. 117, pp. 2351-2373.
- Ghanem, R. G. and Spanos, P. D. (1991b), "Stochastic finite element: a spectral approach," Springer-Verlag, New York, N. Y.
- Gjelsvik, A. and Bodner, S. R. (1962), "Energy criterion and snap buckling of arches," Journal of the Engineering Mechanics Division, ASCE, Vol. 88, pp. 87-134.
- Hansen, J. S. and Roorda, J. (1974), "On a probabilistic stability theory for imperfection sensitive structures," International Journal of Solid Structures, Vol. 10, pp. 341-359.

- Hansen, J. S. (1977), "General random imperfections in the buckling of axially loaded cylindrical shells," *AIAA Journal*, Vol. 15, pp. 1250-1256.
- Hasofer, A. M. and Lind, C. N. (1974), "An exact invariant first-order reliability format," *Journal of Engineering Mechanics*, ASCE, Vol. 100, pp. 111-121.
- Huseyin, K. (1975), "Non-linear theory of elastic stability," Noordhoff International Publishing.
- Hutchinson, J. W. (1965), "Axial buckling of pressurized imperfect cylindrical shells," *AIAA Journal*, Vol. 3, pp. 1461-1466.
- Hutchinson, J. W. and Koiter W. T. (1970), "Postbuckling theory," *Applied Mechanics Reviews*, Vol. 23, pp. 1353-1366.
- Hyman, B. I. (1971), "Snap-through of shallow clamped spherical caps under uniform pressure," *International Journal of Non-linear Mechanics*, Vol. 6, pp. 55-67.
- Karman, T. V. and Tsien, H. S. (1941), "The buckling of thin cylindrical shells under axial compression," *Journal of Aeron. Soc.*, Vol. 8, pp. 303-312.
- Koiter, W. T. (1945), "On the stability of elastic equilibrium," Dissertation, Univ. of Delft, The Netherlands.
- Lawrence, M. (1987), "Basis random variables in finite element analysis," *International Journal of Numerical Methods in Engineering*, Vol. 24, pp. 1849-1863.
- Li, C.-C. and Der Kiureghian, A. (1993), "Optimal discretization of random fields," *Journal of Engineering Mechanics*, ASCE, Vol. 119, pp. 1136-1154.
- Liu, P.-L. and Der Kiureghian, A. (1986), "Optimization algorithms for structural reliability analysis," Technical report UCB/SESM-86/09, Department of Civil Engineering,

Division of structural Engineering and Structural Mechanics, University of California, Berkeley, CA.

Liu, P.-L. and Der Kiureghian, A. (1991), "Optimization algorithms for structural reliability," structural safety, Vol 9, pp. 161-177.

Liu, P.-L., Lin, H.-Z. and Der Kiureghian, A. (1989), "CALREL user manual," University of California, Berkeley, Department of Civil Engineering.

Love, A. E. H. (1888), "The small free vibrations and deformations of a thin elastic shell," Philosophical Transactions of the Royal Society of London, Vol. 179.

Love, A. E. H. (1927), "A treatise on the mathematical theory of elasticity," 4th ed., Cambridge.

Madsen, H. O., Krenk, S. and Lind, N. C. (1986), "Methods of structural safety," Prentice-Hall, Inc., Englewood Cliffs, N. J.

Masur, E. F. and Lo, D. L. C. (1972), "The shallow arch - general buckling, postbuckling, and imperfection analysis," Journal of Structural Mechanics, Vol. 1, pp. 91-112.

Melchers, R. E. (1987), "Structural reliability, analysis and prediction," Ellis Horwood Series in Civil Engineering, Structural Engineering Section, Ellis Horwood.

Nataf, A. (1962), "Détermination des distribution dont les marges sont données," Comptes Rendus de l'Academie des Sciences, Paris, France, Vol. 225, pp. 42-43.

Nordgren, R. P. (1993), "Theory of shells," Class Notes, CIVI519, Rice University, Houston, Texas.

Nordgren, R. P. (1994), "Structures stability," Class Notes, CIVI526, Rice University, Houston, Texas.

- Palassopoulos, G. (1995), "Efficient finite element analysis of imperfection-sensitive frames and arches with stochastic imperfection." Proceedings of the Computational Stochastic Mechanics Conference, Balkema, Rotterdam, pp. 461-467.
- Rackwitz, R. and Fiessler, B. (1978), "Structural reliability under combined load sequences," Computers and Structures, Vol. 9, pp. 489-494.
- Ravindra, M. K., Lind, N. C. and Siu, W. (1974) "Illustration of reliability-based design," Journal of Structural division, ASCE, Vol. 100, pp. 1789-1811.
- Roorda, J. (1965), "Stability of structures with small imperfections," Journal of the Engineering Mechanics Division, ASCE, Vol. 91, pp. 87-106.
- Roorda, J. (1969), "Some statistical aspects of the buckling of imperfection-sensitive structures," Journal of Mechanics and Physics of Solids, Vol. 17, pp. 341-359.
- Roorda, J. (1971), "Equivalent axisymmetric imperfections in axially compressed cylindrical shells," University of Waterloo, SMD report 87.
- Sankar, T. S. and Ariaratnam, S. T. (1971), "Snap-buckling of shell-type structures under stochastic loading," International Journal of Solids and Structures, Vol. 7, pp. 655-666.
- Schreyer, H. L. and Masur, E. F. (1966), "Buckling of shallow arches," Journal of the Engineering Mechanics Division, ASCE, VOL. 92, pp. 1-20.
- Schreyer, H. L. (1972), "The effect of initial imperfections on the buckling load of shallow circular arches," Journal of Applied Mechanics, Transactions of the ASME, pp. 445-450.

- Spanos, P. D. and Ghanem, R. (1989), "Stochastic finite element expansion for random media," *Journal of Engineering Mechanics*, ASCE, Vol. 115, pp 1035-1053.
- Tennyson, R. C., Muggeridge, D. B. and Caswell, R. D. (1971), "New design criteria for predicting buckling of cylindrical shells under axial compression," *Journal of Spacecraft and Rockets*, Vol. 8, pp. 1062-1067.
- Thompson, J. M. T. (1967), "Towards a general statistical theory of imperfection sensitivity in elastic postbuckling," *Journal of Mechanical Physics and Solids*, Vol. 15, pp. 413-417.
- Thompson, J. M. T. and Hunt, G. W. (1973), "A general theory of elastic stability," John Eiley & Sons.
- Timoshenko, S. P. and Goodier, J. N. (1951), "Theory of elasticity," 2nd edition, McGraw-hill Book Company, Inc., New York, N.Y.
- Timoshenko, S.P. and Woinowsky-Krieger, S. (1959), "Theory of plates and shells," 2nd edition, McGraw-hill Book Company, Inc., New York, N.Y.
- Tvedt, L. (1988), "Second order probability by an exact integral," *Proceedings of 2nd IFIP Conference on Reliability and Optimization of Structural Systems*, Springer-Verlag, Berlin, Germany, pp 377-384.
- Van Trees, H. L. (1968), "Detection, estimation and modulation theory," Part I, Wiley and Sons, Inc., New York, N.Y.
- Vanmarcke, E. H. (1983), "Random fields: analysis and synthesis," The MIT Press, Cambridge, Mass.
- Vanmarcke, E. H. and Grigoriu, M. (1983), "Stochastic finite element analysis of simple

beams," *Journal of Engineering Mechanics*, ASCE, Vol. 109, pp. 1203-1214.

Yamaki, N. (1984), "Elastic stability of circular cylindrical shells," North Holland, Amsterdam, The Netherlands.

Zhang, J. and Ellingwood, B. (1994), "Orthogonal series expansions of random fields in reliability analysis," *Journal of Engineering Mechanics*, ASCE, Vol. 120, pp. 2660-2677.

Appendix 1

Notation

The following symbols are used in this thesis:

X	The vector of basic random variables
$g(X)$	The limit-state function
n	The number of random variables
R	The resistance of a given structure
S	The load applied on a given structure
$P[...]$	The probability operator
C_i	A defined target value of a certain parameter
$C(X)$	The value of a parameter evaluated based on the randomness of the input variables
$f_X(x)$	The joint probability density function (PDF) of X
U	A vector of uncorrelated standard normal variates
$T(...)$	A linear one-to-one mapping
$G(U)$	The limit-state function in the standard normal space
u^*	The design point
β	The reliability index

FORM	First-order reliability method
SORM	Second-order reliability method
MCS	Monte Carlo simulation
FOSM	First-order second-moment reliability method
α^*	A unit normal vector at the design point
$\Phi(\dots)$	The standard normal cumulative distribution function
P_f	The probability of failure
$P_{f_{FORM}}$	The probability of failure approximated according to FORM
$P_{f_{SORM}}$	The probability of failure approximated according to SORM
κ_i	The principal curvatures of the fitting paraboloid at the design point
$\phi(\dots)$	The standard normal probability density function
∇	The gradient vector
$J_{u,x}$	The Jacobian of the transformation from the physical to the standard-normal space
γ	The unit gamma sensitivity vector
D	A diagonal matrix of the standard deviations of X
$I(x)$	A zero-one indicator function
$E[\dots]$	The expectation operator
\hat{P}_f	An estimate of the probability of failure based on MCS
N	Number of Monte Carlo simulations
β_L	A lower bound on the reliability index
β_U	An upper bound on the reliability index

P_L	A lower bound on the probability of failure
P_U	An upper bound on the probability of failure
$\nu(x)$	A multidimensional Gaussian random field
Ω	The domain in which a random field is defined
$\mu(x)$	The mean function of a random field
$\sigma^2(x)$	The variance function of a random field
$\rho(x, x')$	The autocorrelation coefficient function of a random field
$C(x, x')$	The covariance function of a random field
MP	Midpoint discretization method
LA	Local averaging discretization method
KL	Series expansion method based on the Karhunen-Loeve theorem
ξ_i	A set of independent standard normal variates
λ_i	The eigenvalues of the correlation kernel
$f_i(x)$	The eigenfunctions of the correlation kernel
SE	A general series expansion method
z_i	A vector of zero mean random variables
c_i	A vector of constant coefficients
$h_i(x)$	A complete set of orthogonal deterministic functions
κ	The change in the curvature of a structure under loading
ε	The elastic axial membrane strain
α	The polar angle coordinate measured from the center of the arch
R	The radius of the arch

u	The tangential displacement component
w	The radial displacement component
\bar{u}	The tangential component of the initial geometric imperfections
\bar{w}	The radial component of the initial geometric imperfections
H	The total energy of a structural system
E	The modulus of elasticity for the material of the structure
t	The thickness of the arch
b	The width of the arch
P	The total load acting on the arch
$\Omega(P,w)$	A loading function for the load applied on the arch
$\delta(\alpha)$	The Dirac delta symbolic function